MASTERARBEIT

Entwicklung und Evaluierung von Printing-Prozessen zur Erzeugung von leitfähigen Strukturen auf Si-Wafern

Markus HEINRICI

Zur Erlangung des akademischen Grades

Diplom-Ingenieur

Technische Universität Graz

Institut für Anorganische Chemie

Betreut von:

Ass.Prof. Dipl.-Ing. Dr.techn. Roland Fischer (TU Graz)

Dipl.-Ing. Dr.techn. Martin Mischitz (Infineon Technologies Austria AG)

Table of Contents

1. Introduction 1
2. Motivation 3
3. Printing of metallic Films 8
a. Selection of the optimal Printing technique 8
Inkjet-Printing 8
Stencil Printing 9
Screen Printing 11
Decision 11
b. Printing of the Paste 12
Process description 12
c. Drying 18
Shrinkage 18
Recommended Drying Procedure 18
Dilution – Varying the Solvent Content 20
4. Post-Treatment 24
a. Reduction with Hydrogen: 26
Patent situation [17] 27
Hydrogen plasma - TEPLA 27
Hydrogen plasma - MATTSON 29
Molecular hydrogen - Koyo 31
b. Reduction with Formic Acid: 33
Patent Situation [27] 34
Formic acid: - ATV Furnace 34
Results 38
c. Reduction with Carbon Monoxide: 41
Carbon monoxide - Koyo 41
d. Oxidation of the printed pastes 43

Atmospheric oxidation – DESPATCH furnace 43

Oxygen-Plasma – EKT 44

e. Wrap-up of the results 48

5. Process evaluation 50

a. Sheet resistivity 50

b. Film Thickness / Surface Topology 52

Optical Profilometers 52

Mechanical Profilometers 54

Scanning Electron Microscope (SEM) 56

c. Morphology / Porosity 57

Investigation of the Sample Morphology 57

Evaluation of the Reduction Process 58

Determining the porosity 59

d. Elemental composition 60

e. Adhesion 62

Results 62

f. Heat dissipation 64

6. Review and Outlook 66

7. Acknowledgements 67

8. Bibliography 68

9. Appendix: 72

Table of Figures

Picture 1: Thermal stress curve of ECD copper 4
Picture 2: Thermal stress curve of printed porous copper[1] 5
Picture 3: Porosity vs. resistivity........ 6
Picture 4: Porosity vs. stress[2] 6
Picture 5: Industrial inkjet printer 8
Picture 6: DEK printer assembly 13
Picture 7: Stencil, squeegee and copper paste in a DEK Horizon Printer during a printing session 14
Picture 8: Printed Wafer in shim 15
Picture 9: Screenshot of the CAD Design of the test-stencils 16
Picture 10: Typical drying procedure for standard CP-003 19
Picture 11: cracks due to residue solvent 19
Picture 12: 8Z169 (CP-003+ +1% CPD02) 50x........ 21
Picture 13: 8Z118 (CP-003+ +20% CPD02) 50x........ 22
Picture 14: Sample 27 (Standard CP-003) (mag. 1k) 23
Picture 15: Sample 118 (+20% CPD02) (mag. 5k)........ 23
Picture 16: Sample 169 (CP-003+ +1% CPD02) (mag. 1.8k) 23
Picture 17: Sample 169 (CP-003+ +1% CPD02) (mag. 450) 23
Picture 18: Sample 179 (CP-004) (mag. 1k)........ 23
Picture 19: Sample 169 (CP-003+ +1% CPD02) (mag. 5k)........ 23
Picture 20: Samples for the TEPLA trials before treatment 28
Picture 21: Samples for the TEPLA trials after treatment 28
Picture 22: Pictures of sample 2/5 Uncured obtained after TEPLA treatment........ 28
Picture 23: Mass spectrum of selected masses (Reduction of the laser cured samples) 30
Picture 24: Uncured sample after 30min at 300°C in forming gas........ 31
Picture 25: Wafers processed for 1.5h (17&13), 2.5h (24&23) and 3.5h (26&25) at 400°C in forming gas........ 32
Picture 26: Comparison between an uncured wafer (2), a wafer processed at 400°C in forming (23) gas and a wafer processed at 400°C in formic acid (16) 32
Picture 27: ATV furnace........ 35
Picture 28: cross section of an uncured (left) and a cured (right) sample 36
Picture 29: on top view of an uncured (left) and a cured (right) sample........ 36
Picture 30: Typical reduction process with Formic acid........ 37
Picture 31: 8Z20 and 8Z21 after 30min FA........ 38
Picture 32: Plot specific resistivity vs. time for different treatments of CP-003........ 39
Picture 33: Surface topology of sample 8Z135 (CP-004)........ 40
Picture 34: Surface if Sample CP-004, mag. 1000k........ 40
Picture 35: Surface of sample CP-004, mag. 235x........ 40
Picture 36: Printed wafer after 200°C 1h, air 43
Picture 40: Conductivity of the oxidized samples 45
Picture 37: Quartz wafer holder with test wafers inside the EKT 46
Picture 38: Comparison between a partially oxidized wafer before (left, 8Z166) after reduction with formic acid (right, 8Z154). 46
Picture 39: Previously reduced wafer after oxidation in O_2 Plasma 47
Picture 41: Comparison between different curing processes........ 48

Picture 42: Layer thickness of sample 8Z27, determined by SEM on different points of the wafer 50
Picture 43: RESMAP measurements on the central structure 51
Picture 44: top view of a surface profile acquired with an optical profilometer 53
Picture 45: side view of a surface profile acquired with an optical profilometer 53
Picture 46: line profile cut out of Picture 45 54
Picture 47: imaginary test structure 55
Picture 48: measurement of the test structure with a mechanical profilometer 55
Picture 49: measurement of the test structure with an optical profilometer 55
Picture 50: Determination of the sample thickness by SEM 56
Picture 51: Sample 8Z169 (mag. 1.8k) (Larger version of Picture 16) 57
Picture 52: SEM comparison between uncured, laser cured and formic acid cured samples 58
Picture 53: Sample 8Z23, cured for 2.5h at 400°C in forming gas 59
Picture 54: denotation of X-rays 60
Picture 55: X-ray spectrum 60
Picture 56: EDX spectrum of a lasercured + formic acid reduced sample 61
Picture 57: EDX Spectrum of a nitrogen annealed sample 61
Picture 58: DeFelsco PosiTest AT Adhesion Tester 63
Picture 59: samples after the pull-test 63
Picture 60: stamps ready for the pull-test 63
Picture 61: Schematic view of a polyheater device, taken from an internal presentation 64
Picture 62: 8Z169 cured (CP-003+ +1% CPD02) 235x 72
Picture 63: 8Z169 pre-dried (CP-003+ +1% CPD02) 235x 72
Picture 64: 8Z167 pre-dried (CP-003+ +2.5% CPD02) 235x 72
Picture 65: 8Z167 cured (CP-003+ +2.5% CPD02) 235x 72
Picture 66: 8Z117 pre-dried (CP-003+ +5% CPD02) 235x 72
Picture 67: 8Z117 cured (CP-003+ +5% CPD02) 235x 72
Picture 68: 8Z113 pre-dried (CP-003+ +7.5% CPD02) 235x 73
Picture 69: 8Z113 cured (CP-003+ +7.5% CPD02) 235x 73
Picture 70: 8Z115 cured (CP-003+ +10% CPD02) 235x 73
Picture 71: 8Z115 pre-dried (CP-003+ +10% CPD02) 235x 73
Picture 72: 8Z119 pre-dried (CP-003+ +20% CPD02) 235x 73
Picture 73: 8Z119 cured (CP-003+ +20% CPD02) 235x 73
Picture 74: 8Z167 (CP-003+ +2.5% CPD02) 50x 74
Picture 75: 8Z116 (CP-003+ +5% CPD02) 50x 74
Picture 76: 8Z112 (CP-003+ +7.5% CPD02) 50x 75
Picture 77: 8Z114 (CP-003+ +10% CPD02) 50x 75

1. Introduction

This work has been written in the course of an internship at Infineon Technologies Austria AG between March and October 2013. The main goal was to develop a process for the creation of thick conducting copper films. Due to its relatively low price and its high conductivity copper is an important material for the manufacturing of integrated circuits. Thick copper layers are desired for electrical contacts as well as for dissipation of heat in power semiconductors. The most common method for copper deposition is sputtering, which is a technique that uses ions (usually argon) which are accelerated towards a target consisting of the material to be deposited. The highly energetic ions erode the target and the released target atoms deposit on the wafer as well as on the walls of the chamber. The other main technology for copper deposition used in the semiconductor industry is electroplating (ECD, electrochemical deposition). Sputtered films are typically several hundred nanometers thick, electroplated layers can measure up to 10µm. One reason why thicker layers are not produced is that copper has a different thermal expansion coefficient α than silicon (α_{Cu} = 16.5 * 10^{-6} [K^{-1}], α_{Si} = 2.6 * 10^{-6} [K^{-1}]), which means that when the chip is heated, tensile and/or compressive forces between the copper and the silicon will sooner or later will cause the layer to delaminate or the chip to get cracks. When a whole wafer is coated with copper, this problem already emerges at low temperature changes as “wafer-bow”. The whole wafer is bent by the tensile/compressive forces the copper exerts on the silicon.

A team of Infineon engineers around Manfred Frank and Thomas Kunstmann has developed a physical process called “plasma dust” which bypasses this problem by using porous instead of dense copper. In this process the surface of copper micro particles is activated in nitrogen plasma, which anneals them together on the surface of a wafer. The particles form a porous structure and the porosity can be controlled by the process conditions. By moving the plasma torch over the wafer, stripes of porous copper can be generated. When many stripes are created right beside each other, large areas or even the whole wafer can be covered.

The main disadvantage of this process is that the equipment needed for it is yet just a prototype, which is still far away from series maturity. Also, the rather long process time for this single wafer process is limiting the throughput.

By the end of 2012 an alternative way of generating porous copper has been discovered: A British Company named Intrinsiq Materials Ltd. had developed a new screen print copper paste for the printed electronics industry that can be applied to flexible substrates like paper or PE. After drying,

this paste can be laser cured in order to become conductive. Martin Mischitz ordered some samples of this paste printed on silicon wafers, which showed similar behavior in the stress test (which is employed to measure the wafer-bow) to the layers created by plasma dust. SEM images have shown that the copper layer created by printing and annealing this paste is also porous and consists out of micro- and nanoparticles. The conductivity of the paste has yet to be increased, and the printing process has to be developed. The purpose of this work is to characterize the printing properties of the paste, develop a process flow (print, dry, cure, anneal) and evaluate the physical properties of the print results in order to show the principle applicability of this new process to new generations of Infineon microchips.

2. Motivation

The growing need for energy efficiency, which comes from rising oil prices and results in the increased use of alternative sources of energy creates new fields of application for power semiconductors. [1] Power semiconductors are microchips that have to switch large currents and voltages. Their history extends long before the invention of integrated circuits, when in 1920 Julius Lilienfeld described an electronic component that should switch large currents by exploiting a phenomenon that was later called the Field-effect. [2] The Bell Laboratories realized his ideas in 1947 with the invention of the point-contact transistor. A few months later they developed the bipolar junction transistor, which can be seen as the first power semiconductor, and which was the preferred device in the manufacturing of discrete and later also integrated circuits. [3] Examples for modern power semiconductors are IGBTs (insulated gate bipolar transistor), power MOSFETs (metal oxide semiconductor field effect transistor), power Diodes and thyristors. They are used in hybrid electric vehicles, power plants (like wind turbines, photovoltaic systems), breaking force recovery systems. It is estimated that more than 60% of all energy consumed in the United States flows through at least one power semiconductor. [4] It is due to this fact, that even small improvements in the efficiency of power semiconductors have a small impact on energy consumption.

Since its beginnings integrate circuit technology has been heading towards smaller sizes and denser packages. This can result in very large heat dissipation within small integrated circuit surface areas. In several power semiconductor technologies power fluxes in the magnitude of several hundred watts per square centimeter have been approached. [5] Together with increasing switching frequencies this challenges the heat sinks, which need to be improved in order to keep step with the ever increasing density of integrated circuits.

Typically, power modules are cooled through an external heat sink or cold plate, which is bolted to the module. A typical set up of a conventional IGBT module consists of the IGBT die, the die attach solder, a metal-clad ceramic substrate, substrate attach solder, metal or composite baseplate, thermal interface material (TIM), and the external heat sink. [6] The heat flow has to pass all these layers in order to be dissipated from the system through the backside. This setup cannot effectively cool devices with power dissipation densities exceeding 250-300W/cm^2. The front side of the chips is cooled with wire-bonded aluminum pads with thicknesses of several micrometers. This design has been optimized over time and has now come to a point, where new concepts are needed for further improvements. The next generation of Infineon IGBT Chips, the IGBT5, will be cooled by thick copper instead of aluminum on the front side. The typical operating temperature of IGBT chips has an upper

limit of about 150°C, above which its properties worsen dramatically, and the risk for chip failure is increased. The aim of a heat sink is thus to keep the temperature of the chip below the maximum temperature. Thin copper layers are not capable of incorporating the large amounts of heat generated in a current pulse, hence thicker copper needs to be employed.

As it has already been stated, conventional methods for copper metallization cannot be used for this purpose, since normal bulk copper applies too much mechanic stress on the chips during heat fluctuations. In order to avoid the mechanic stress of thick copper layers, porous layers are a good solution. The thermal stress curve of electrochemically deposited copper is shown in Picture 1, the corresponding curve of our printed layers in Picture 2. The stress in MPa is displayed on the ordinate, the temperature in °C on the abscissa. Tensile stress has a negative algebraic sign, compressive stress a positive one. (Note the different units on the ordinate!) The data presented here has been acquired by Manfred Schneegans with samples prepared by Intrinsiq. This data was obtained on a Flexus F2400, which actually measures the wafer bow by the deflection of a laser beam. The Stress can be calculated from the wafer bow.

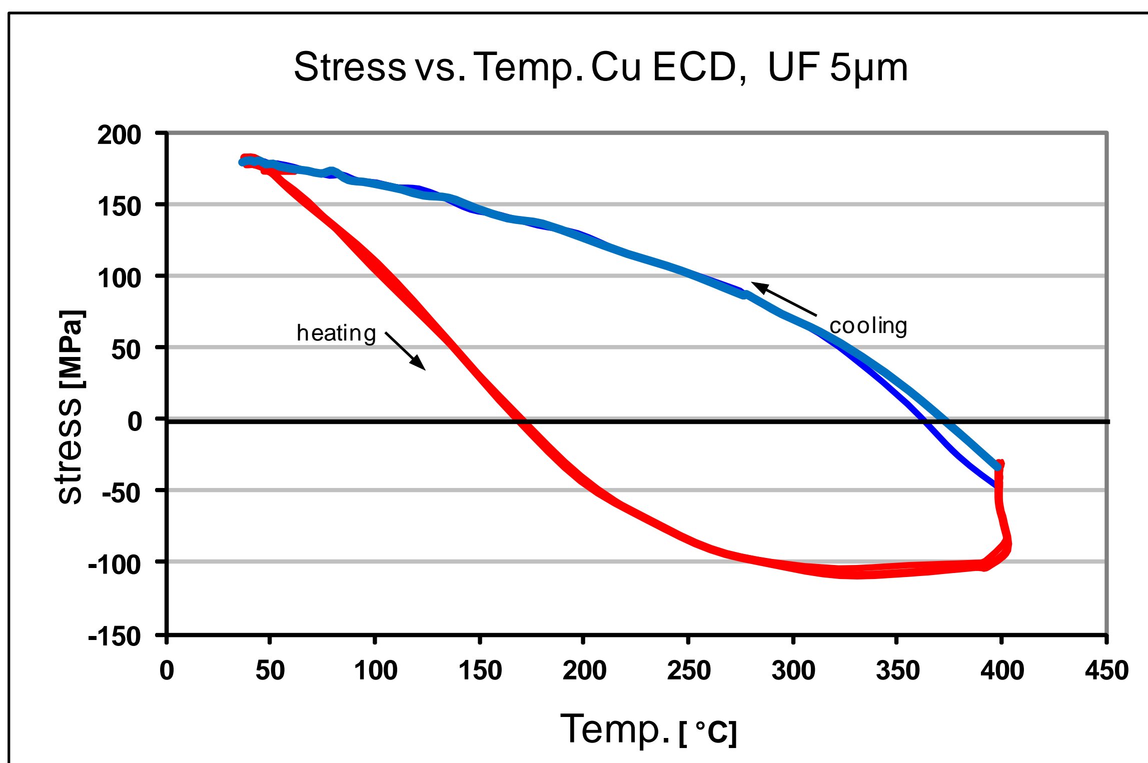

Picture 1: Thermal stress curve of ECD copper[1]

[1] Picture 1 and Picture 2 were taken from an internal report on this topic, performed by Manfred Schneegans.

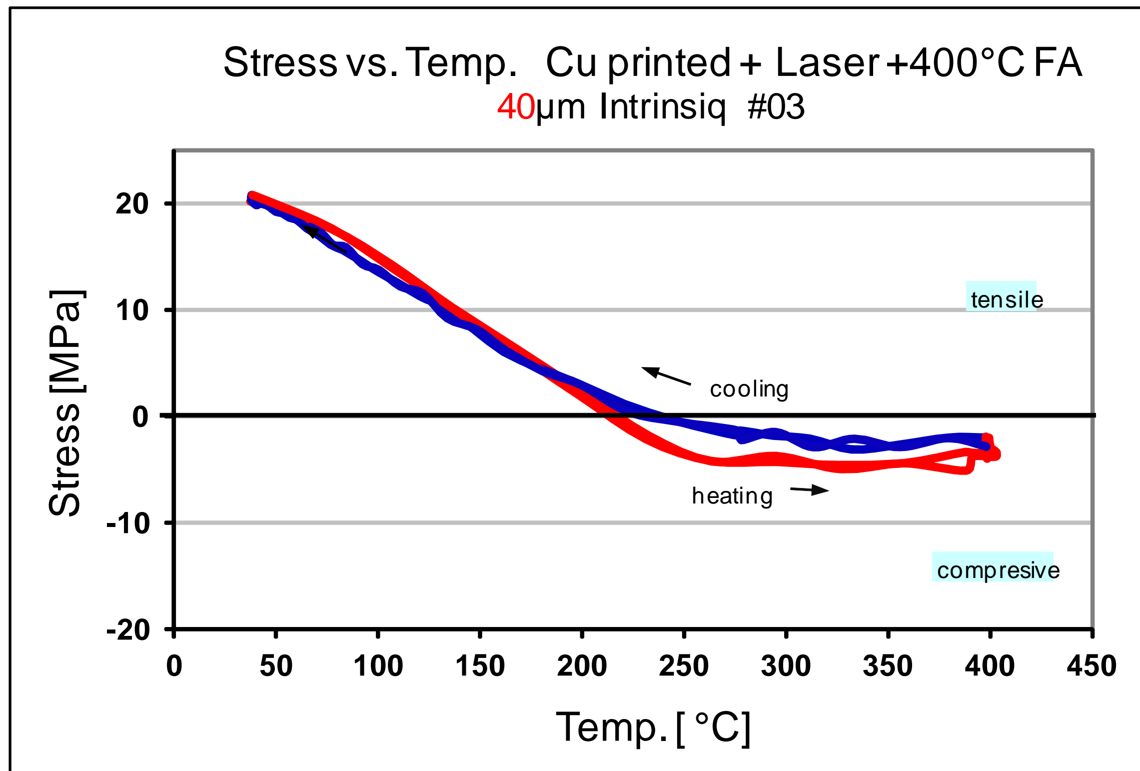

Picture 2: Thermal stress curve of printed porous copper[1]

The exact reason why this material shows a better behavior in the stress test than ECD copper is still controversially debated. Critics proposed that in fact what we see in the thermal stress curves is a delamination process. This can be disproved by performing a pull-test, as it has been done in the course of this work. Whatever the reason may be, the results from the thermo cycling test were promising.

Still, other very important properties have to be determined, for example: Can we achieve a better conductivity by changing process parameters? The electrical conductivity of the printed and reduced layers could be determined to be about 13-14µΩcm, bulk copper has about 1.7, ECD copper around 2 µΩcm. The thermal conductivity is rather difficult to measure, but it correlates with the electrical conductivity over the empirical Wiedemann-Franz law.

$$\frac{\kappa}{\sigma} = LT$$

Equation 1

σ ... electrical conductivity

λ ... thermal conductivity

L ... Lorentz number, a proportionality constant

T ... Temperature

A variation of the porosity of printed copper is mainly feasible by varying the particle size distribution of the paste, which is a matter of paste design. The material properties of copper layers with different porosities have already been investigated on material generated by the plasma dust method.

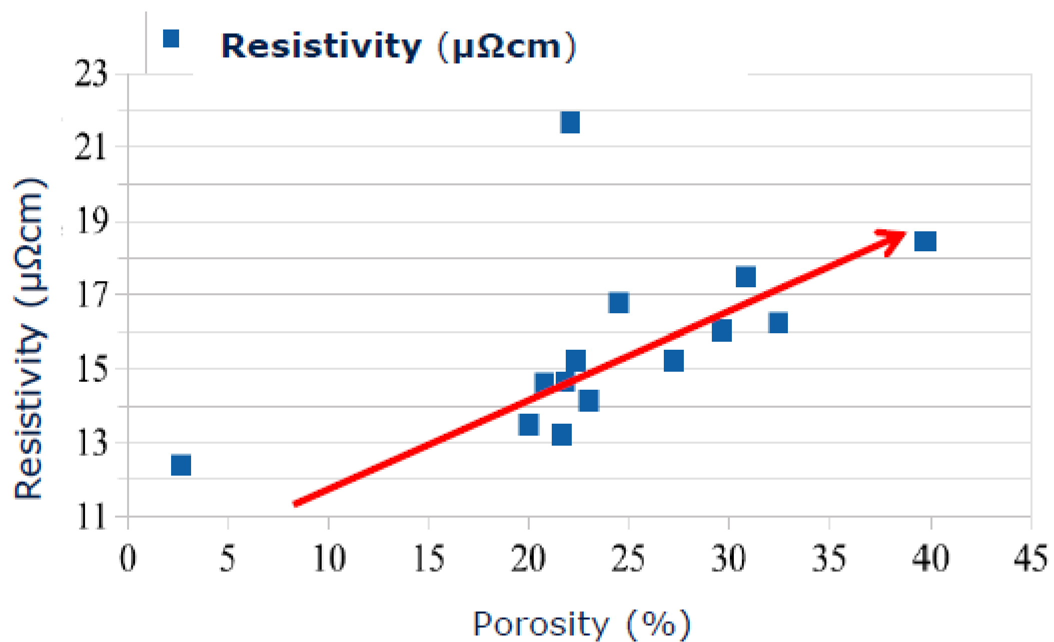

Picture 3: Porosity vs. resistivity[2]

The correlation between the porosity and the thermal stress can be seen in Picture 4.

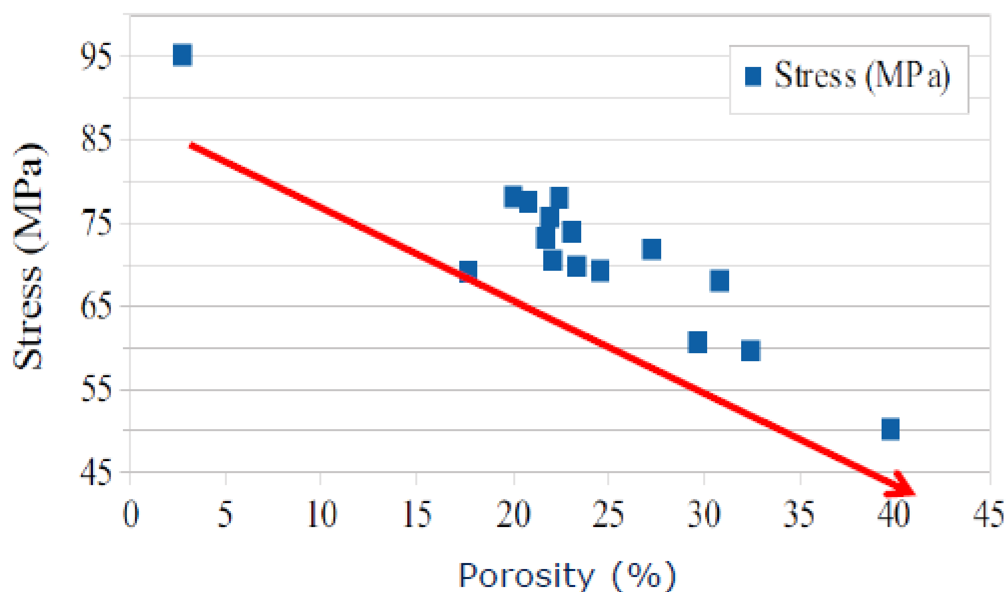

Picture 4: Porosity vs. stress[2]

[2] The diagram was taken from an internal report on plasma dust, presented by Thomas Kunstmann, Michael Krenzer and Manfred Frank.

The two displayed diagrams show, that there is a compromise to make when designing thick layers of copper. It is clear that one will never achieve the same conductivity with porous copper than there is in bulk copper. There are still many questions to answer regarding the printed copper, which are summarized in Table 1.

Conductivity / Stress	The demanded electric resistivity of the material depends on the application, but should not exceed 5µΩcm. As it has been shown in the previous diagrams, the resistivity is connected to the stress in an inverse relation. This means, that we have to find a way to generate copper layers which have the right porosity to fit the needs of our chip technologies.
Corrosion	Infineon microchips are used in many different areas in terms of technology and global region. Especially power semiconductors in tropical areas are often operated at harsh conditions and have to withstand corrosive environments (elevated temperatures, moisture). Can our printed copper pass the mandatory corrosion tests?
Process flow	**Structuring:** Printing has its limits, and it is not sure if the needed specifications for a productive process are within these limits. If not, then the printing needs to be combined with other structuring methods like lithography. Lithography could be applied before or after the reduction process. In any case, it needs to be determined whether our material can withstand the harsh conditions of a photoresist strip. Another possible structuring method is LDI (laser direct imaging). **Drying:** The paste contains a considerable amount of solvent, which needs to be removed from the system. This needs to be done without damaging the layers. Especially in very thick layers the drying step might become problematic. **Curing:** The dried paste does not have any conductivity and hence needs to be cured. A curing process must be developed which is capable of being integrated into a productive process. **Annealing:** The copper particles need to be annealed together in order to gain mechanical stability and the desired electrical properties. This step might be merged with the curing process.
Bonding / soldering	In front side metallization contacts are typically generated by wire bonding. If we want to offer a solution to the problem of missing heat sinks, we have to show that our material can be bonded. If it can't, we have to find out how we can modify it in order to make it "bondable". Other technologies are contacted by soldering the chip e.g. on a printed circuit board. Is soldering possible with printed copper?

Table 1: Questions to answer

Of course it won't be possible to cover all these topics in this master's thesis. This work will focus on providing fundamental data to enable further investigations.

3. Printing of metallic Films

a. Selection of the optimal Printing technique

The purpose of this work is to create layers of conductive material which are to be used on microchips. Microelectronics is characterized by a high degree of precision in manufacturing. Typical structure sizes are in the range of microns and submicrons, and chips are often not larger than a few millimeters. Hence the printing technique used should be capable of at least printing defined and homogeneous structures onto microchips without the danger of creating electrical shorts.

Inkjet-Printing

One printing technique is well known to most people from office applications: The Inkjet-printer, which is connected to a computer and prints documents on copy paper. In the industry, Inkjet-printing is a promising technique with many advantages. Compared to other techniques, it is fast, flexible and material conserving. *“The process essentially involves the ejection of a fixed quantity of ink in a chamber, from a nozzle through a sudden, quasi-adiabatic reduction of the chamber volume via piezoelectric action. A chamber filled with liquid is contracted in response to application of an external voltage. This sudden reduction sets up a shockwave in the liquid, which causes a liquid drop to eject from the nozzle. (…) The ejected drop falls under action of gravity and air resistance until it impinges on the substrate, spreads under momentum acquired in the motion, and surface tension aided flow along the surface. The drop then dries through solvent evaporation.“* [7] In industrial applications the substrates can vary from textiles over polymers to metals or glass. The inks, which consist out of particles dispersed in a solvent, can be used to generate various structures with all kinds of purposes, depending on the characteristics of the ink.

Picture 5: Industrial inkjet printer

Inks usually have low viscosities, typically 8-15cP [8] and contain metallic nanoparticles or metal-organic precursors. The films produced by this technique have thicknesses of up to 15µm, typically 1-5µm. One major advantage of inkjet-printing over other printing techniques like stencil- or screen-printing is that different shapes can be printed without the need for new equipment. On the other hand, the

printing process is more time consuming than in the other mentioned techniques. This is important in mass production, where the same pattern needs to be printed onto many pieces. A good example where inkjet-printing is used in mass production are expiring dates and lot numbers on food cans and PET-bottles. In the electronics industries, inkjet-printing is mainly used for the creation of conducting lines and electrodes, for example on solar cells [9] or chip cards (RFID antennas) [10]. As conductive material, silver has yet been the most important metal to be used in inkjet printing, since it has a good conductivity and is stable to oxidation. The main disadvantage of silver is its high price, which is why there are efforts to substitute it by copper, which is also a very good conductor, but is very vulnerable against oxidation by atmospheric oxygen. This problem already appears during the fabrication of the nanoparticles, where the creation of the oxide layer on the particles is inevitable in ambient atmosphere because it is thermodynamically more stable than metallic copper. [11] The formation of this oxide layer has two negative effects: The electrical resistivity of the created sheets is increased and the annealing temperature is raised.

Typical volumes of Inkjet-drops are 5-30pl (pikoliters), which generate orbital structures on the substrate with a diameter of about 40-100µm, depending on ink and substrate.

Stencil Printing

Compared to inkjet-printing which began to emerge during the 1950s, stencil printing is a dinosaur: The first use of this technique dates back to 10,000 BC when humans used their hands as stencil to create cave paintings. In 15th century Europe stencil printing was used to color old master prints. The advantage of this printing technique was the possibility of mass production, which made it attractive for rather cheap everyday life articles like play cards. The main disadvantage is that it is not flexible since every desired change in the printing pattern has to be achieved by modifying the stencil. Common materials of the stencils used to be wood and metal, nowadays also paper and plastic stencils are in use, always depending on the application. In industrial applications mainly metallic materials are in use, because they have a better forming stability, longer life time and better cleaning properties.

In order to maintain a well-defined printing pattern the paste has to be removed from the recesses of the stencil between the prints. Remaining paste would decrease the quality of the prints. Modern industrial stencil printers like those used in this work have integrated cleaning programs which use a cleaning agent and paper towels to wipe off the back side of the stencil. The cleaning program can be adapted to the particular needs of the process, especially the properties of the paste together with the stencil.

The stencils used in this work consisted of stainless steel or hard nickel, which were laser processed or electroformed. The precision of the stencil etch of course has a significant influence on the printing quality. The stencils are mounted onto an aluminum or steel frame which applies a tensile force on the stencil. This tensile force, which is required to stabilize the stencil, restricts the minimum thickness of the metal to about 50µm. The maximum thickness of a stencil is not restricted in a useful range.

Besides the stencil many other printing parameters influence the quality of the print: The squeegee is usually a steel blade, but can also be made of rubber or plastic. Steel can handle higher printing pressures and generally has a longer life time. Plastic squeegees are needed in screen printing when screens made of polymer are used. A metal squeegee could damage the screen and reduce its lifetime. The shape of the squeegee can also vary: simple blades can be used for small structures; thicker squeegees like half round rods which have a higher rigidity can be used for very large structures. The angle between the squeegee and the stencil can be varied from 90° down to below 45°. The angle has direct influence on the density of the printed layers. Squeegees with small angles will press the paste into the recesses of the stencil, while large angle ones will rather wipe off any excess of the paste.

Those “hardware” parameters have to be modified by changing the equipment. Additionally, parameters like the print speed, the print pressure, the number of prints and the separation speed after the print can be changed over the printer software. The goal is always to find the right settings for a particular system consisting out of the printer, the squeegee, the stencil and the paste. The influences of some parameters are displayed in Table 2.

Print Parameter	Effect of Print Parameter on Print Volume	
	Screen Printing	**Stencil Printing**
Squeegee Durometer	Typically 70-80, Increased durometer decreases print volume	Typically 90, Increased durometer increases print volume
Squeegee Pressure	Typically 50 N, Increased pressure increases print volume	Typically 0 N, Increased pressure decreases print volume
Attack Angle	Typically 45°, Increased angle decreases print volume	Typically > 45°
Stroke Speed	Increased speed decreases print volume	Increased speed decreases print volume
Snap-off Distance	Typically 1-2 mm, Increased snapp-off can increase or decrease print volume	Typically 0 mm (on contact printing)

Table 2: Influence of Print Parameter on Print volume, table taken from literature [12]

In stencil print high viscosity pastes with a high solid content are used. For example, typical solid contents of stencil print pastes for thick film metallization range between 80-90% [12]. Additionally those pastes usually contain solvent, binder material and several other additives. The binders are monomers, which polymerize during the drying or curing step after the application and have to maintain forming stability to the printed structure. Various additives are used to improve the properties of the paste, for instance the adhesion to substrates or drying characteristics, porosity of the cured films and so on. The use of metallic pastes in stencil printing is common in the production of printed circuit boards, where components are mounted on the boards by printed solder paste. [13]

Screen Printing

Screen printing is much a like stencil printing. In fact, often even the same machines are used. At Infineon, two DEK Horizon 02i printers are used, one being configured for screen, the other for stencil printing. Screens are mounted in the same metal frame as stencils, which apply tensile force on them to keep them in place. The difference between a screen and a stencil is that where there is a recess in the stencil, there is a mesh in the screen. Screen printing requires rather lower viscosity pastes than stencil printing, because the paste is pressed through this thin mesh of plastic or metal and has to disperse afterwards to create a continuous layer. The thickness of this layer is determined by the properties of the mesh and the paste. Thick wires in the mesh will create thick layers, and pastes with low viscosities will disperse over a larger area and hence form thinner layers. Also, the mesh of the screen limits the maximum grain size of the paste.

In the electronics industry, the main products made by screen printing are printed circuit boards (PCBs) and contacts for solar cells [14]. The pastes have much higher viscosities than inks, usually several thousand cP.

Decision

The right printing technique is always depending on the material that is to be printed. All pastes and Inks used in this thesis were received from Intrinsiq Materials Ltd., who put much effort into developing the paste to fit Infineon’s needs. Most of the trials were performed with the paste “Copper Printing Paste – Intrinsic CP-003”, which is a close variation of the commercially available CP-002. According to its datasheet, the CP-002 has a viscosity of 10-30Pa.S (Bohlin CVO 100 at 25°C) and a solid content of 82-90%. [15] The paste consists of nano and micro particles of copper, as well as metal organic precursors and solvent. It is designed for screen printing, but can also be used for

stencil print. According to Intrinsiq, the particles in the paste are protected against oxidation by a special polymer, which is decomposed upon the recommended laser treatment and generates a reducing atmosphere.

On the basis of CP-003 Intrinsiq developed the CP-004, which should have a decreased specific resistivity due to a lower porosity. The viscosity of this paste was not determined, but it was much more viscous than the CP-003.

In order to optimize the printing properties towards our needs we received a sample of high concentrated CP-003 (from here on called CP-003+) and the respective solvent (CPD02), which is actually a mixture of Ethylene Glycol (80%) and Diacetone Alcohol (20%) [16]. By adding roughly 5 wt.% solvent to the CP-003+ one can gain the viscosity of the standard CP-003.

For further modification of the paste and/or the printed structures, we received the copper ink "Copper Ink Jet Printing Ink CI-002", which contains copper nanoparticles in organic solvents.

The datasheets of the two commercial products, CP-002 and CI-002 can be found in the appendix.

We decided to perform our trials with a stencil printer. This gave us the ability to work with a wide range of viscosities, where screen printing would have set an upper limit. Also, stencil printing can generate smaller structures, because high viscosity pastes do not disperse that much on the substrate, compared to lower viscosity screen printing pastes. Nevertheless, screen printing might still be an option if the structuring of the pattern is done lithographically.

b. Printing of the Paste

Process description

The paste was printed on 8" and 6" standard dummy wafers, manufactured by the "Covalent Silicon Corporation". The wafers are 725 ± 25µm thick and were covered in house with 150nm TiW and 150nm Cu by sputtering.

The paste was printed on a DEK Horizon industrial printer manufactured by DEK Printing Machines Ltd. For the structuring, metal stencils were used in a variety of thicknesses, ranging from 50-200µm. The vast majority of the prints were performed with a "half-round" squeegee, which is basically a metal rod with a flat side, which generates very homogeneous film thicknesses even if the whole wafer is to be covered by the paste.

The Printer is connected to an automatic Wafer handler, which takes the wafers out of a cassette and places them in the middle of a shim. The whole assembly is displayed in Picture 6. The shim is a sheet of metal with roughly the thickness of the wafer (always being some microns thinner) with a wafer-sized (202mm) hole in the middle. (Picture 8) Its purpose is to assists the wafer during the print, so that there is less step height between the chuck and the wafer. The chuck is located below the wafer and the shim. It is basically a plate with cut-out trenches, where vacuum is applied that holds both the wafer and the shim in place. This whole assembly, chuck, shim and wafer, is automatically moved into the printer, where it is brought in contact with the stencil.

Picture 6: DEK printer assembly

There are markings on the shim and on the stencil, sometimes also on the wafer. These markings are used to adjust the position of the assembly to the stencil in order to control the position of the printed pattern on the substrate. This adjustment is performed once manually with integrated cameras and is saved for every further print in a stencil-specific file, which also contains the print parameters.

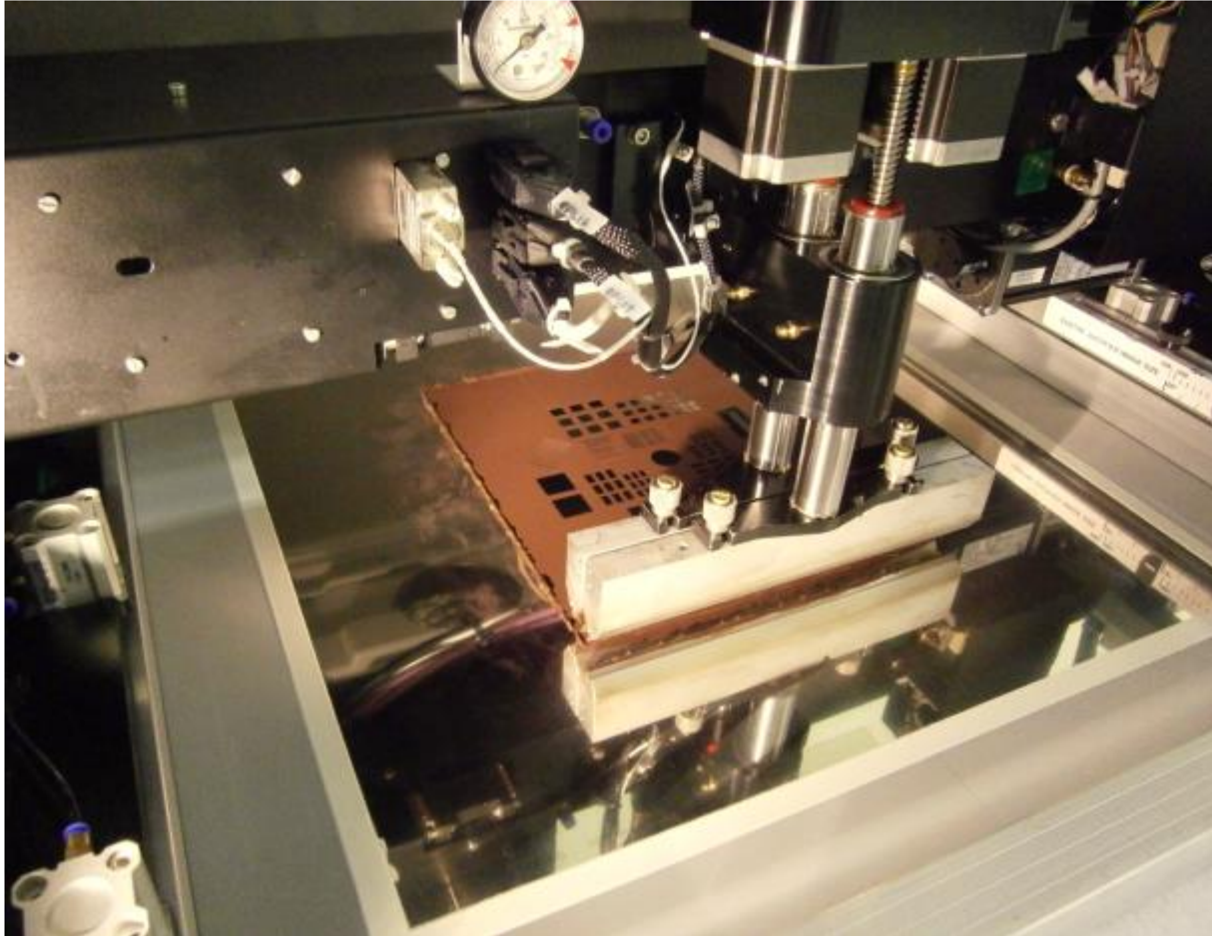

Picture 7: Stencil, squeegee and copper paste in a DEK Horizon Printer during a printing session

The printing parameters can be chosen in the printer software. The most important parameters to vary were:

- printing speed (how fast does the squeegee slide over the stencil, unit: mm/s)
- contact pressure (how strong is the squeegee pressed onto the stencil, unit: kg)
- number of runs (how often is the squeegee driven over the stencil during one print)
- separation speed (how fast is the squeegee separated from the stencil after the print (unit: mm/s)
- backside cleaning procedure (wet with solvent, dry, vacuum)
- Shim to Stencil distance

All those parameters have influence on the precision of the print and might also change the material properties of the printed structures.

The first samples were printed with a 200µm stencil which generates test structures of different size and shape. The influence of different parameters on the print quality was tested in a series of prints. The most obvious problem that occurred was that solvent was bleeding out of the printed pattern,

which carried copper particles in it. This effect can be diminished by using less solvent in the paste. Also the backside-cleaning steps contributed to this effect, since the solvent used in the cleaning procedure diffused into the paste and lowered its viscosity. As an overall result of the first tests, some standard print parameters were determined, with which all further prints were performed unless stated differently. The parameters were:

- Printing speed: 10mm/s
- Contact Pressure: 2kg
- Number of runs: 1
- Separation speed: 2mm/s
- Backside cleaning procedure: 3 times dry wipe
- Shim to stencil distance[3]: 3.2mm

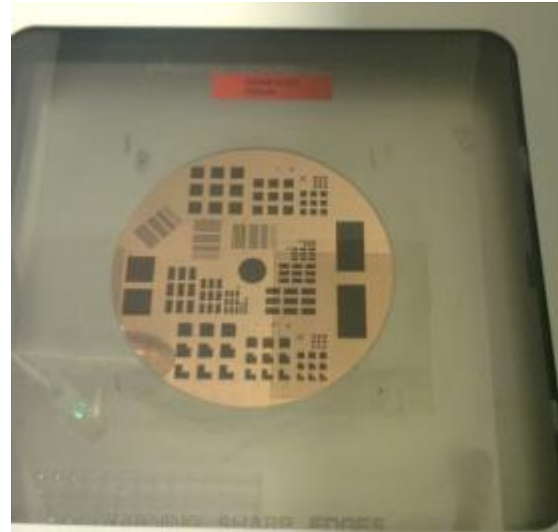

Picture 8: Printed Wafer in shim

For economic reasons, the printing speed should be set to the maximum value at which the structures are filled completely. The squeegee pushes the paste over the stencil, which causes the paste to “roll” forward. When the paste rolls over a hole in the stencil, it flows into it. The time it needs to fill the hole depends on its viscosity. Low viscosity pastes can flow faster into the holes and hence can handle higher print speeds. Highly viscous pastes often need to be pressed with force into the openings, and hence the print pressure has to be increased and the print speed needs to be reduced. Also, such pastes often cannot fill the openings within one run. A second run, on the other hand, might reduce the printing quality, since the stencil is always lifted a bit in front of the squeegee and in a second run paste that is already in the openings can run between the stencil and the substrate. Hence, we tried to work with one run and in case of highly viscous pastes decreased the print speed and increased the pressure. The shim to stencil distance was chosen in a way, that the wafer touches the stencil, but does not deform it. This is one of two possible setups. In the other one, there is a defined gap between the stencil and the wafer. This is only suitable for pastes with a higher viscosity, since low viscosity pastes would run in the gap directly after the squeegee has moved on. This technique is sometimes used when printing solder pastes. The separation speed can have an influence on the quality of the print, although we did not notice any difference between high and low separation speed (0.1 and 2mm/s were tested).

[3] This parameter is called “Leiterplattendicke” in the printer software and is no absolute value. This means, that the distance between the shim and the wafer is not actually 3.2mm, but the system needs to be set to this value in order to touch the wafer (0mm distance).

After the print is finished and the wafer assembly is pulled out of the printer automatically, the wafer can either be returned to its slot in the cassette, or it can be passed on to a reflow furnace. This is a continuous system, where the wafer is carried by a conveyor through discrete temperature stages. The stages are separated from each other by an intense stream of Nitrogen gas. The whole furnace is operated under Nitrogen overpressure in order to keep Oxygen out of the system. This oven might be of use in order to improve the printing results of our samples, since a quick pre-drying step can fixate the printed patterns and prevent solvent bleeding. The suitability of this process was not tested due to a lack of time.

Generally spoken, the optimization of the print quality was not a focus of this work. The prints were primarily performed to generate samples for material characterization.

The test pattern for the stencil was designed in CAD. Two stencils were manufactured by DEK, one being 50µm and the other 100µm thick. They were labeled T9999-050-1D-ST11 and T9999-100-1D-ST11 respectively. Most prints were performed with the 50µm version. A screenshot of the CAD Design can be seen in Picture 9.

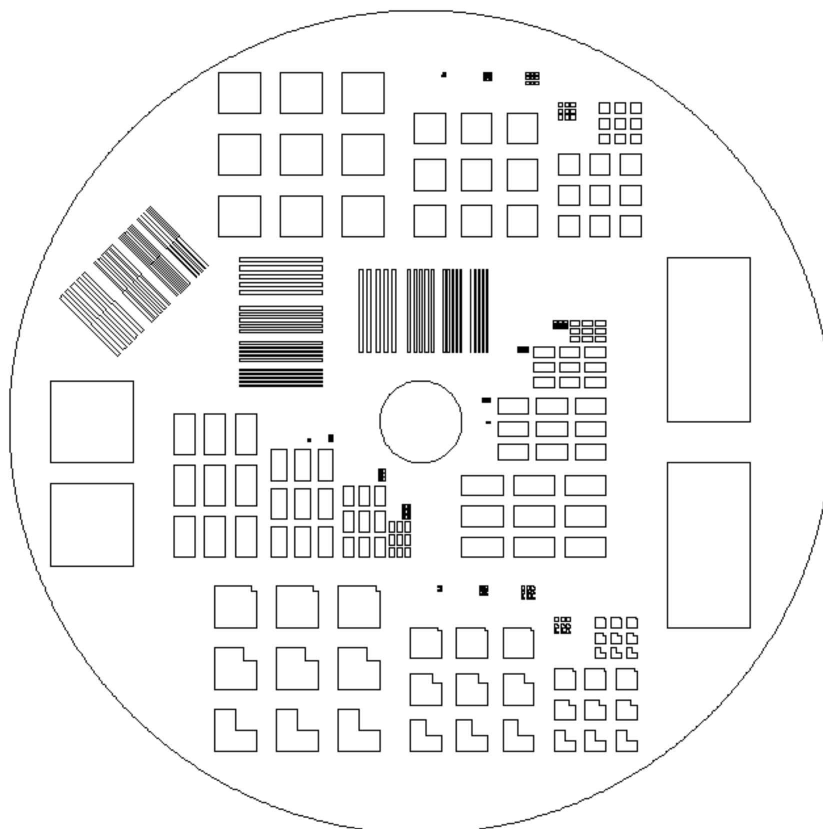

Picture 9: Screenshot of the CAD Design of the test-stencils

It consists of squares and rectangles in different sizes and shapes, the largest being 20x20mm and 20x40mm. The smallest structures are squares with 250µm edge length. These geometric shapes will be the most likely ones to be used in productive processes. The circular shape in the middle of the stencil has a diameter of 20mm and is used for the resistivity measurements. Also, the profilometric data was acquired on this structure in order to calculate correct values for the specific resistivity.

Depending on the solvent content of the paste 1-2g of paste (wet) were printed through the 50µm stencil, and 2-4g through the 100µm one. Compared to the weight of the wafer (~53g) this is not much. In order to determine the drying characteristics of the paste, some wafers were printed with a full-face stencil. This stencil has a 196mm large hole in it, which covers the complete wafer except a 2mm rim with paste. Of this design, also two stencils were used, again 50 and 100µm thick.

The stencils are strained in a metal frame, which forms the stencil assembly, which is inserted into the printer.

In a further stage of this project, the Copper ink CI-002 might also come in the focus of interest. This ink needs to be printed with an inkjet printer. At Infineon Villach, there is a Roth&Rau Pixdro IP410 industrial inkjet printer (Picture 5) used for several productive processes, as well as ongoing research projects. This printer is suitable for handling the CI-002 ink and could use it either to generate new conducting structures or to overprint existing ones, thus modifying their properties.

c. *Drying*

Shrinkage

The pastes used in our experiments have a solvent content of around 10% of the total mass. This solvent causes our printed structures to shrink upon drying. The standard formulation of the CP-003 paste shrinks down to about 50-60% of its wet thickness. Patterns printed with a 50µm stencil usually have a dry thickness of 25-30µm. We observed this value to increase over time, 3 Months after the can containing the paste was opened the first time, the viscosity had increased noticeably and the printed structures were up to 42µm thick. At this point, the structures had cracks of several 100µm length in their surface after drying. Several approaches have been tried to avoid these cracks by appropriate drying conditions in order to be able to keep the low solvent content. The low solvent content is desirable, because it reduces the effects of solvent bleeding, improves the aspect ratio (which is the proportion of a structures width to its height) and enables thicker layers to be printed with the same stencil. Also, varying the solvent content can be a convenient way to achieve a desired layer thickness without the need of buying a new stencil. Hence, the problems with the cracks need to be solved in order to establish a range of possible solvent contents instead of just one optimum.

Recommended Drying Procedure

Intrinsiq Materials Ltd. recommends drying its pastes for 15-30mins at 50°C. [15] Additionally we were informed that applying vacuum to the oven should prevent crack formation during the curing process. The paste is usually printed on flexible substrates like paper, PET, polyimide as well as ceramic and FR4 (glass supported epoxy laminate). The layer thickness on these substrates is typically 20µm. [15] For our purpose, 20µm is the lowest thickness we want to achieve, and layers of 50-100µm strength are desired. Here, the drying procedure gets more complicated, as the volume to surface ratio increases.

Intrinsiq could not recommend an exact gas pressure as they made their trials in an evacuated furnace without a manometer. We used a SR0700 furnace manufactured by ATV Technologie GmbH which can evacuate its chamber down to 2mbar. A typical drying procedure which has been used for most of the samples in this thesis is displayed in Picture 10. It consists of ten repeated steps of evacuating (30 seconds, end pressure about 25-30mbar), holding the pressure (1 minute) and purging nitrogen into the system (30 seconds, up to atmospheric pressure). The Temperature of this step was typically 60°C, also 90°C were tested. The standard paste CP-003 could be dried without cracks appearing. After three months and several openings of the can, the paste could no longer be dried crack free. Although no cracks could be detected after the drying, they occurred during the curing process indicating that there was residue solvent in the system (see Picture 11).

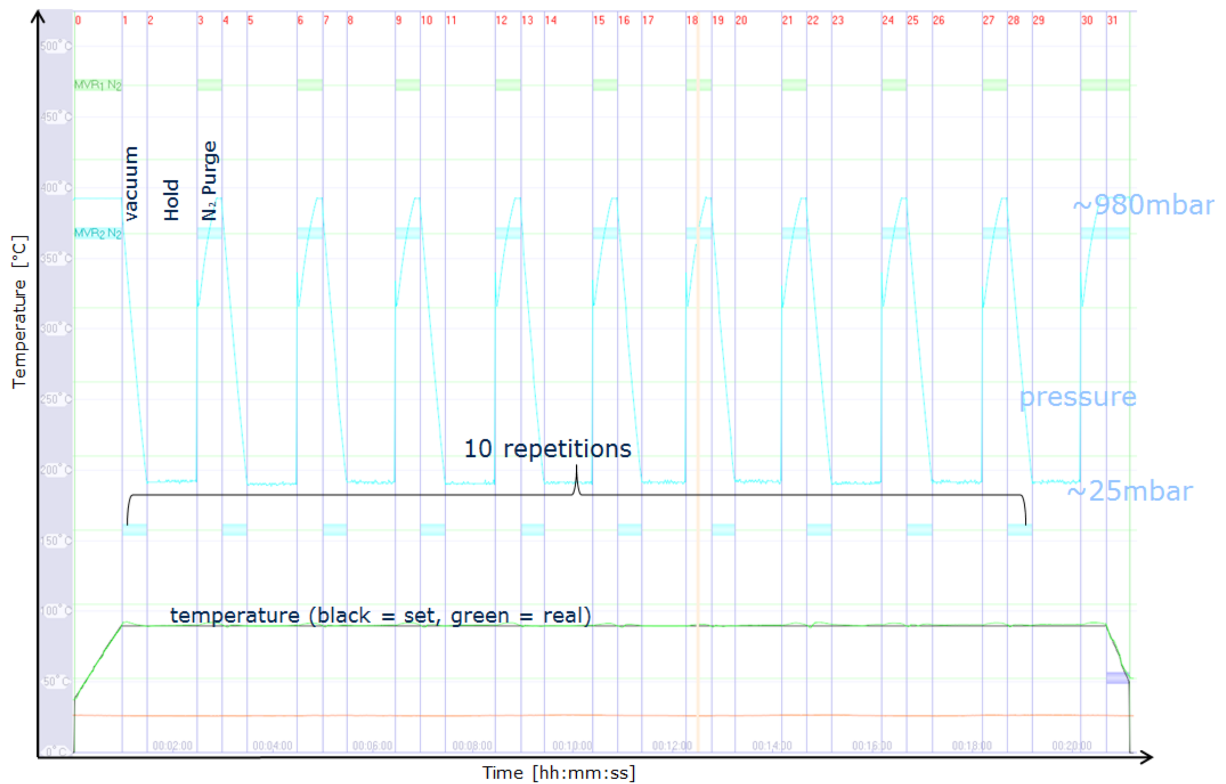

Picture 10: Typical drying procedure for standard CP-003

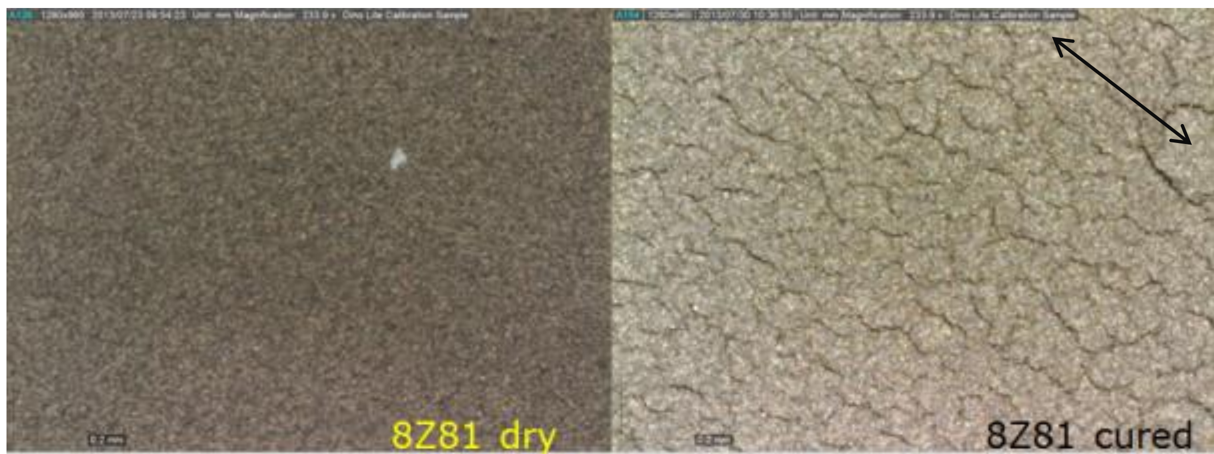

Picture 11: cracks due to residue solvent

The black arrow in Picture 11 indicates the direction of the print. As it can be seen, the movement of the squeegee determines the preferred orientation of the cracks. Several drying procedures were tested in order to avoid these cracks, but the initial CP-003 received in March 2013 could not be dried crack free with any of them, if no additional solvent was added. Also the paste CP-004, which is a variation of the CP-003 and was designed to achieve a better conductivity showed cracks, as it featured a much higher viscosity comparable to the CP-003 in August. Unfortunately, no viscometer is available at the Infineon site, so no figures can be presented here.

During our trials it could not be confirmed that the drying procedure had any influence on the formation of cracks at all. In fact, a comparison of similar wafers (same print parameters, same lot), of which some were dried prior to curing and others were cured immediately after the print[4] showed no influence on either of the relevant parameters (crack formation, resistivity). This is interesting, because after pre-drying step there is definitely residue solvent in the layers, as can be proven by weighing the samples after each step. Also, the solvent can be seen as film covering the chamber of the ATV furnace after the drying step. If the reduction with formic acid is performed immediately after the drying step, the solvent adhering on the walls of the chamber will turn brown and sticky. It is yet to determine if the drying step is necessary, because even though there could not be proven any influence on relevant material properties, the contamination of furnace equipment with organic solvents might not be acceptable in a productive process.

Dilution – Varying the Solvent Content

As it has been already stated, the variation of the solvent content by diluting a concentrated version of the paste (CP-003+) with the proper diluent (CPD02) might be important for further applications. Therefore, 6 different concentrations of the paste were created by addition of 1%, 2.5%, 5%, 7.5%, 10% and 20% (weight percent) of CPD02 (Batch Number: QNA 5939) to the Paste CP-003+ (Batch Number: QNA 5896). The diluent was stirred into the paste with a glass stir rod. It was taken care that no air bubbles were trapped inside the paste. The samples were printed onto wafers using the stencil T9999-050-1D-ST11 (50µm stencil thickness) with the standard print settings. Between prints with different paste dilutions, the stencil as well as the squeegee was thoroughly cleaned and dried. The so gained wafers were pre-dried (30min at 60°C in N_2) and reduced in formic acid for 15 minutes at 450°C. The surfaces of the samples were investigated with a USB microscope. The pictures obtained can be found in the Appendix. (Picture 63 - Picture 73) It can be seen that dilutions below 5% added solvent lead to cracks in the surface upon curing. What is interesting is that all samples regardless of their grade of dilution showed large pores or holes in their surface. These pores seem to be an entity of the CP-003+, because the standard paste CP-003 never had such holes in the surface.

Whether these cracks and holes pose a problem or not cannot be determined yet. It is probable that in a productive process the printed layers will receive a post treatment, either to seal the surface in order to bond wires on it, or to further modify its properties. If that was the case, the mentioned surface defects would be filled during this post treatment. Nevertheless, the cracks did not seem to

[4] A pre-drying step of 30min/60°C in N2 was performed on all the wafers so that they could be transported without sticking to the wafer box.

influence the specific resistivity of the samples, which are listed in Table 3 and lie between 12 and 15 µΩcm.

Sample	Dilution	Thickness [µm]	Spec. Resistivity [µΩcm]
8Z169	+1% CPD02	35	14,34
8Z167	+2,5% CPD02	25	13,38
8Z116	+5% CPD02	26	12,63
8Z112	+7,5% CPD02	26	13,35
8Z114	+10% CPD02	22	12,56
8Z118	+20% CPD02	18	14,03

Table 3: Specific resistivity of the diluted CP-003+ samples

Another important aspect of this experiment was the printability of the diluted pastes. By adding 5% solvent to the CP-003+ we obtained a paste that had roughly the viscosity of the standard CP-003 paste. This paste showed the already known solvent bleed which led to a broadening of the printed structures and to a decrease in the aspect ratio. The pastes with 1% and 2.5% added solvent did not show any solvent bleed at all. (Picture 12)

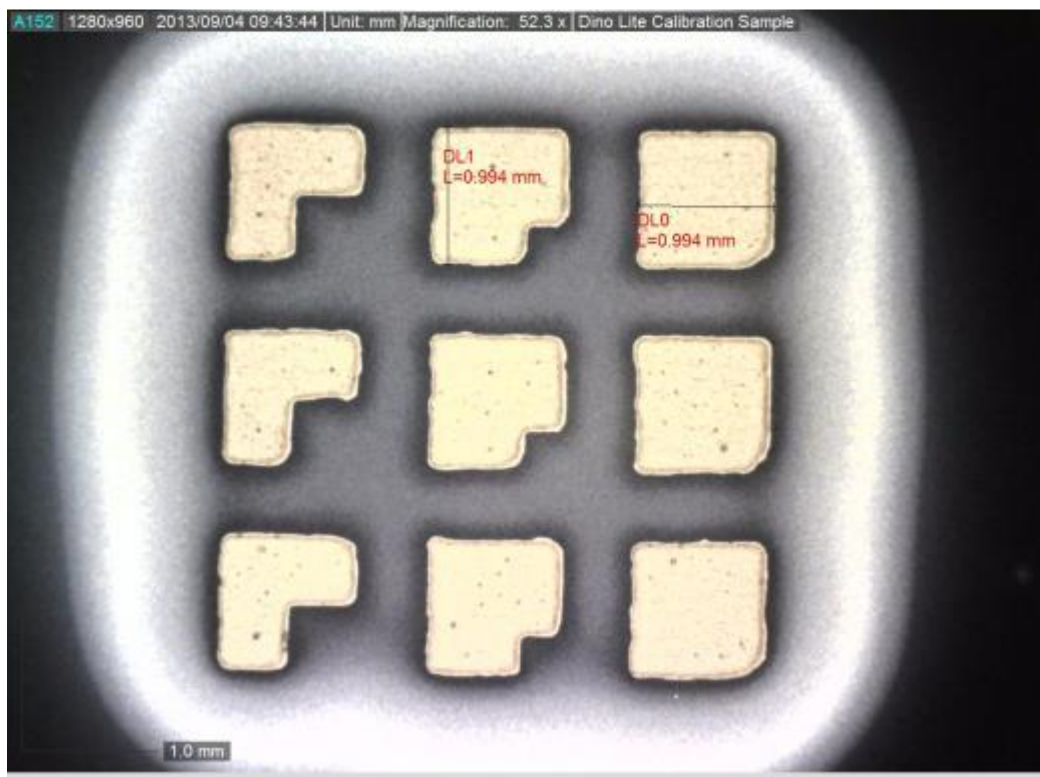

Picture 12: 8Z169 (CP-003+ +1% CPD02) 50x

The structures printed with the strongest dilution (+20%) lost their defined shape and completely dispersed over a large area. (Picture 74) The images of the intermediate dilutions can also be found in the Appendix. (Picture 74 - Picture 77)

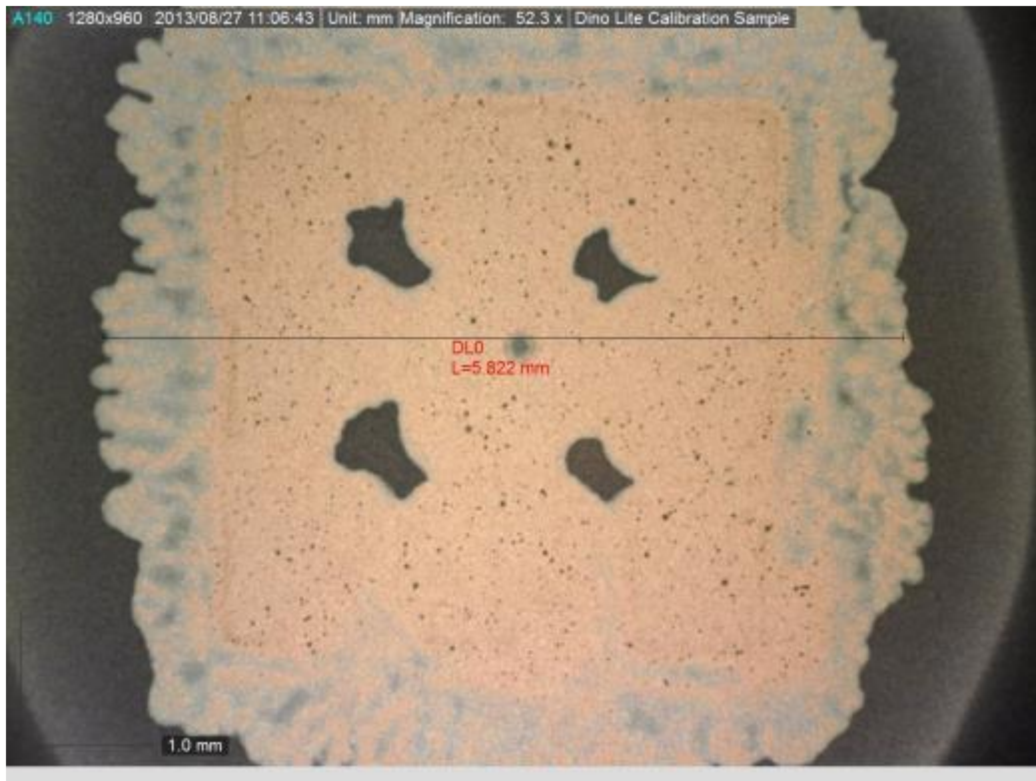

Picture 13: 8Z118 (CP-003+ +20% CPD02) 50x

SEM Pictures did not show any influence of the grade of dilution on the morphology of the layers. The particles are of the same size and have a smooth surface. (Picture 15 and Picture 19) No nano particle agglomerates are visible, as it was to expect from the good conductivity values. One thing that came up during the SEM investigations is that the CP-003+ forms interesting, spherical copper structures of up to 40µm diameter on top of its layers. (Picture 17) This effect has previously been observed on samples of the CP-004 (Picture 18), but not on the standard CP-003 (Picture 14). This observation somewhat questions the results of the physical data obtained by the trials with the diluted CP003+, as it is no longer sure that it is the exact same system as the CP-003.

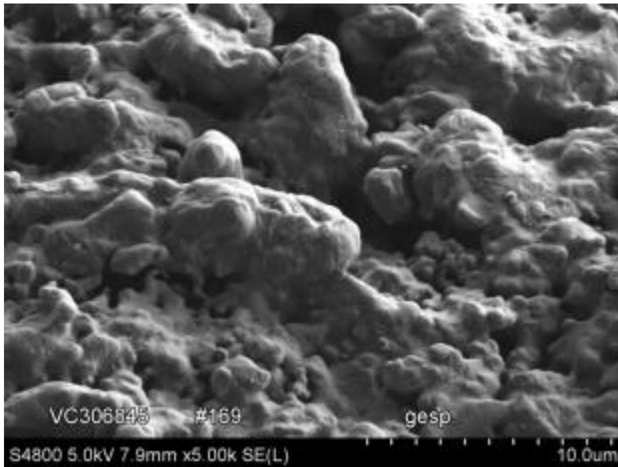

Picture 19: Sample 169 (CP-003+ +1% CPD02) (mag. 5k)

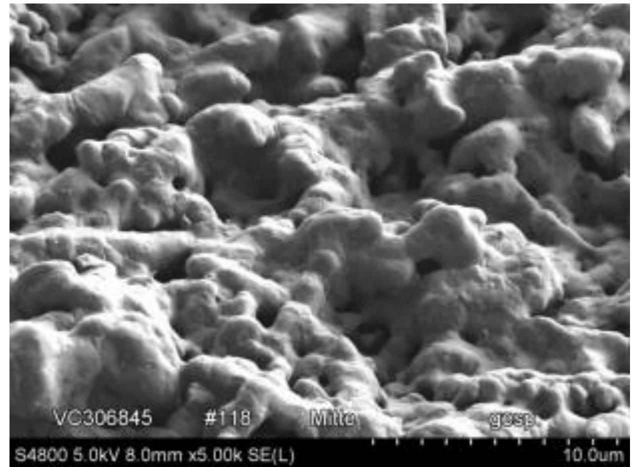

Picture 15: Sample 118 (+20% CPD02) (mag. 5k)

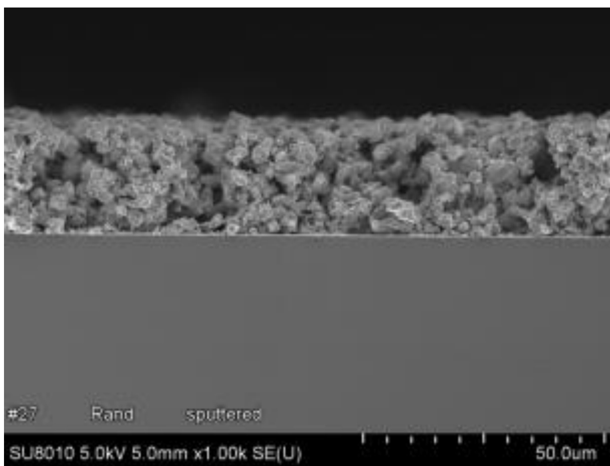

Picture 14: Sample 27 (Standard CP-003) (mag. 1k)

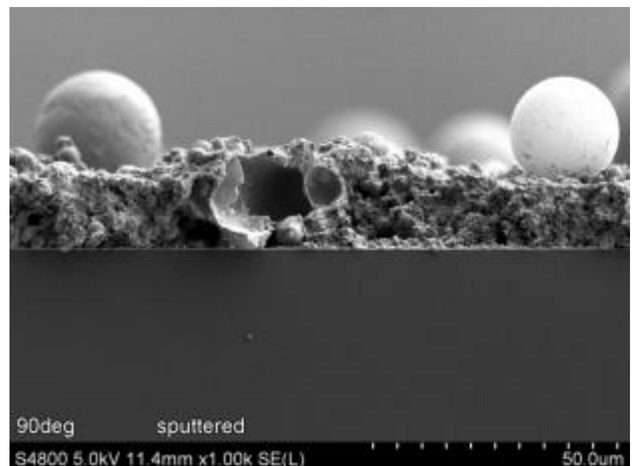

Picture 18: Sample 179 (CP-004) (mag. 1k)

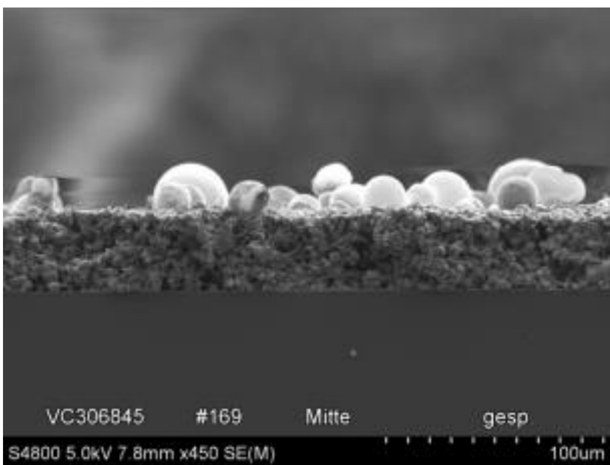

Picture 17: Sample 169 (CP-003+ +1% CPD02) (mag. 450)

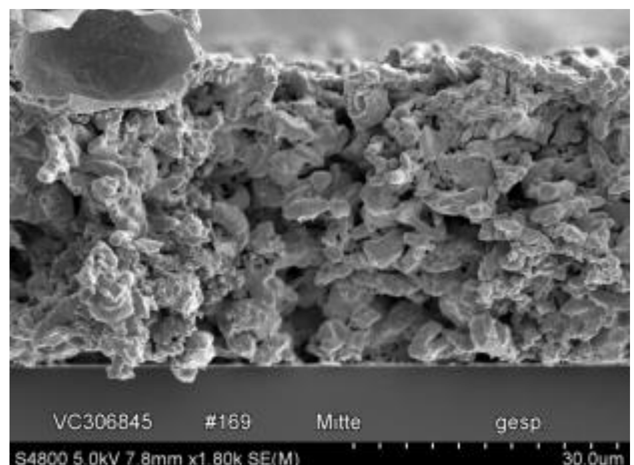

Picture 16: Sample 169 (CP-003+ +1% CPD02) (mag. 1.8k)

4. Post-Treatment

„God made the solids, but the surfaces were the work of the devil.“
Wolfgang Pauli, Physicist (1900 – 1958)

The printed pastes need to be further processed upon drying: After the standard pre-drying step (30 minutes at 60°C in N_2) the conductivity of the layers cannot be measured, since the needles of the RESMAP machine (resistivity measurement according to the 4-point method) push right through the soft copper paste layer and actually measure the copper seed layer below. After an annealing step (for example 15min at 400°C in N_2), the resistivity can be measured, but is far above the desired values. This might have two reasons: The annealing was not finished completely, and/or the material is not actual copper but copper oxide. If the second possibility is the case, the paste would need to be reduced in order to become conductive. The reduction of copper oxide is an important step in the semiconductor industry. Since the invention of the first copper interconnects by IBM in 1997, copper started to succeed aluminum for its lower specific resistance (1.7 µΩcm vs. 3.1 µΩcm) and higher current carrying capacity. [17] [18] Copper readily reacts with atmospheric oxygen and forms a brown-black copper oxide, which hinders the bulk from getting further oxidized. Cu_2O is a p-type semiconductor due to copper vacancies and has a reported band gap of 2.0-2.6 eV, depending on the source. [19], [20], [21], [22] CuO is also a p-type semiconductor with a reported band gap of 1.2-2.1 eV. [20], [21], [22] The electrical resistivity of copper oxide films has been determined to be between 11 mΩcm and 300 Ωcm, depending on the oxygen content. [23] Hence, the oxidized copper surfaces need to be reduced in order to create good contacts.

In recent years, much effort was put in the development of copper nanoparticles for use in inks and pastes in order to print antennas and circuits on various substrates. One huge problem of these techniques is that the nanoparticles are usually all covered by a copper oxide layer, which increases the resistance of the printed layers. Although the thickness of this oxide layer can be more or less controlled [11], there is still the need to reduce the remaining oxide on the surface of the particles in order to achieve a good conductivity.

As it can be seen from the activation energies (Equation 3 and Equation 4), the reduction of Cu(II) oxide has faster kinetics than the reduction of Cu(I) oxide. This can be a problem, especially when nanoparticles are used to build up copper layers. In order to obtain a continuous layer, nanoparticles need to be sintered together. During this sintering step, a partial reduction of CuO to Cu_2O can occur, as showed in Equation 2 [24].

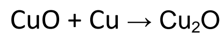

$$CuO + Cu \rightarrow Cu_2O$$ **Equation 2**

This can also happen due to a shortage of hydrogen in the reducing step. [25] Since the formation of Cu(I) oxide results in a slower reduction rate which means a longer process time, it is undesired and should be avoided. Hence, the sintering of copper oxide nanoparticles should always be combined with the reduction step.

In macroscopic systems, CuO is the thermodynamically most stable form of copper in ambient atmosphere. However, in copper nanoparticles, it has been found that Cu_2O is more stable, so that the copper core is covered by a rather large shell of Cu_2O, which again is covered by a very thin shell of CuO. [22] Hence, an oxidation step prior to the reduction might be a way of lowering the activation energy and accelerating the process when nanoparticles are used.

The reduction of the copper paste turned out to be quite a hurdle to overcome. The supplier of the paste recommended a laser curing procedure, during which the layer should be cured. The laser should decompose a polymer layer, that protects the nano- and micro particles from oxidation as well as agglomeration, and the decomposition product of that polymer should have reductive properties, so that a conductive layer of metallic copper should be formed. We received some samples, which had been printed and cured by the supplier with this method, but found the conductivity to be insufficient. Also, the laser could only cure in a linear direction, which means that larger structures like ours needed to be processed with a grid of laser lines. This process seemed to be inapplicable for our purpose.

It is important to emphasize that these experiments should one day lead to a productive process. Hence, we tried to limit our trials to productive equipment (or similar) and use only chemicals that could also be used in the fab. In terms of reducing agents this limits us to hydrogen, carbon monoxide and formic acid.

a. Reduction with Hydrogen:

The exposure to hydrogen under appropriate conditions is the best evaluated way to obtain metallic copper. This option can be divided into two variants: Using molecular hydrogen and using atomic hydrogen. The reduction of copper oxide with molecular hydrogen calls for higher temperatures than that with atomic hydrogen [25], but less sophisticated equipment is needed. Atomic hydrogen needs to be generated by a plasma [26] or decomposition of hydrogen containing chemicals like formic acid or methanol [27]. The main advantage of atomic hydrogen, i.e. hydrogen in the *status nascendi*, is its higher reactivity towards reduction.

The high reactivity is desired for obvious reasons, but there is also another important fact that requires a fast reduction: Hydrogen – especially atomic hydrogen – readily diffuses into and through the copper oxide and can be chemisorbed on the copper atoms. There it forms a “hydride-like layer”, which has a higher resistivity than metallic copper. The kinetics of the copper oxide reduction need to exceed those of the hydrogen diffusion in order to achieve a well conducting layer, which is the case at temperatures above 150°C. At temperatures above 350°C, the highly active surface of the reduced copper readily reacts with all kinds of contaminations, and hence the optimal temperature range – according to literature – is between 150 and 350°C. [26]

On the other hand, the presence of an incubation period before the reduction indicates the importance of the hydrogen diffusion into the copper oxide. The length of this incubation period strongly depends on the temperature, which likely could be due to the enhanced diffusion rates of hydrogen. The presence of even small amounts of water or oxygen in the hydrogen gas leads to a prolongation of this induction period and needs to be eliminated. On the other hand, the preliminary treatment with dry air is reported to lead to an increase of the reduction rate. [28] This might be due to the oxidation of Cu(I) oxide to Cu(II) oxide.

The reduction of copper oxide to copper by hydrogen results in the formation of water, following Equation 3 and Equation 4 [25].

$$CuO + H_2 \rightarrow Cu^0 + H_2O \qquad E_a = 14{,}5\ kcal/mol \qquad \textbf{Equation 3}$$

$$Cu_2O + H_2 \rightarrow 2\ Cu^0 + H_2O \qquad E_a = 27{,}4\ kcal/mol \qquad \textbf{Equation 4}$$

This water needs to be removed from the system in order to avoid the establishment of an equilibrium, which would lead to incomplete reduction of the oxides.

The reduction process seems to be localized at the interface between the metallic copper and the copper oxide layer [25]. According to literature, the addition of metallic copper to the copper oxide prior to the process accelerated the rate of reduction, which lead previous researchers to the

assumption that the reaction is autocatalytic [28]. Those results were contradicted by other researchers, who could not reproduce these results, and suggested that the autocatalytic nature of the reaction is due to the formation of cracks in the oxide, caused by the newly formed copper, which increases the active area available for the reaction. [29]

Patent situation [17]

The company Applied Materials Inc., located in California, US, claims to have developed a process for the reduction of Cu(I)- and Cu(II) oxide films by using a radio frequency (RF) plasma containing hydrogen and nitrogen at relatively low temperatures. The reduction takes place in a CVD or PECVD (plasma enhanced CVD) chamber. Ammonia is used as a reducing agent and reacts with the Cu_2O according to Equation 5.

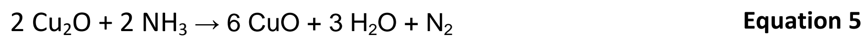

$$2\ Cu_2O + 2\ NH_3 \rightarrow 6\ CuO + 3\ H_2O + N_2 \qquad \textbf{Equation 5}$$

The plasma provides the energy to dissociate the ammonia molecules to nitrogen and hydrogen in the *status nascendi*. The pressure of the process ranges between 1 and 9 mtorr, the RF power between 100 and 1000W and the sample surface temperature between 100 and 450°C. The gas flow of the reducing agent should be between 100 and 1000 sccm. This process has been developed for surface cleaning of copper layers, so a relatively short timeframe of 5-60 seconds is stated. By extending this timeframe, the reduction of thicker oxide layers might also be possible.

Hydrogen plasma - TEPLA

The first trials were performed on uncured samples that we received from the supplier. Our first clue was to reduce them in a Tepla Microwave-Plasma machine, which could generate nitrogen and hydrogen plasma. The machine consists of a chamber, which can accommodate two batches of wafers, which are surrounded by the coils that generate the RF waves. The trials were performed in Week 11 of 2013 under the supervision of Joachim Hirschler, who is the responsible Process Engineer for the machine. Two copper-printed pieces of a wafer which we had received as samples by Intrinsiq, both vacuum dried, one laser cured, were processed for up to one hour in 100% Hydrogen plasma. The power of the RF generator was set to 900W, the flow of hydrogen into the chamber was 200sccm. During the process, the pressure of in the chamber was kept constant at 0.8mbar, the maximum temperature reached was 113°C after 1h. The Resistivity of the laser cured sample could be lowered from 61 to 47µΩcm, while the annealing of the uncured sample was not successful: the pins from the RESMAP machine (automated 4-Point-Measurement) pushed through the copper paste and measured the resistivity of the underlying copper seed layer.

The results of the TEPLA trials can be seen in Picture 20 and Picture 21, which show the uncured sample to the left and the laser cured sample to the right. During the plasma treatment, a mat ring around the printed areas was generated. The samples were analyzed in a PLU_2300 optical profiler to investigate the nature of this effect. The results of this investigation are displayed in Picture 22.

Picture 20: Samples for the TEPLA trials before treatment

Picture 21: Samples for the TEPLA trials after treatment

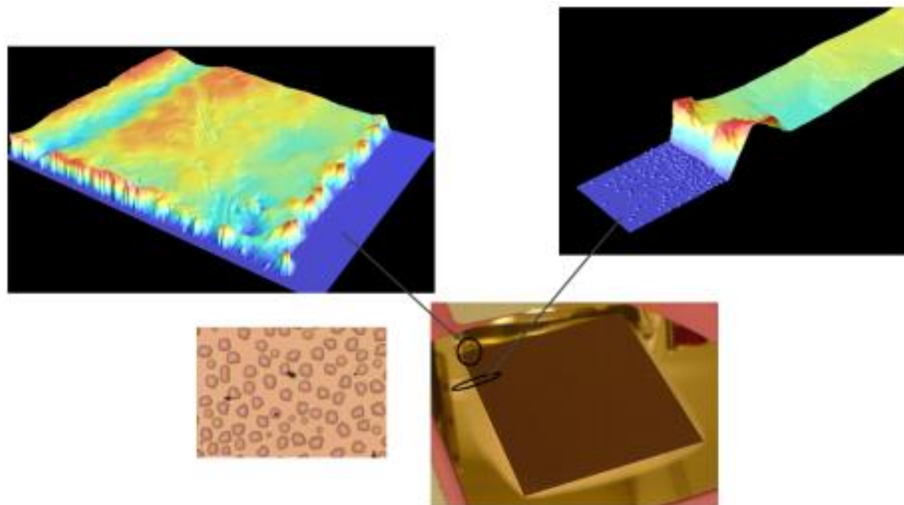

Picture 22: Pictures of sample 2/5 Uncured obtained after TEPLA treatment

The reason for the bad performance of the TEPLA process might lie in its relatively low temperature: The machine does not contain heating coils, hence the whole temperature increase during the process is generated by the RF coils. That way, the hydrogen plasma cannot reach the minimum temperature needed for proper reduction, which is about 150°C. [26] The resistivity of "Sample 2/5 – Uncured" could not be measured because the layer was still too soft, which means that the RESMAP measured the copper seed layer beneath. The resistivity of Sample 2/2 Curing Process 1 was decreased from 76 to 74µΩcm, which probably is due to statistic scatter. The thickness of the samples was not measured but obtained from a report from Intrinsiq.

Hydrogen plasma - MATTSON

Since the Tepla machine could not reach the necessary temperature, the next trials were performed on a Mattson Aspen-II plasma etching machine. In this machine, the wafers are put on a heated metal plate, which can reach temperatures of up to 290°C, which according to literature should be sufficient for the reduction. A plasma torch with ICP (inductively coupled plasma) was aligned over the wafers in about 20cm distance. The power of the plasma torch was set to 800W. The pressure in the chamber during the process was 1.1 Torr, the gas flow through the torch was 900 sccm forming gas, consisting of 4% hydrogen in nitrogen. The chamber consists of a large heater plate and two plasma torches, so that two wafers can be processed simultaneously. The machine was operated by Joachim Hirschler and Josef Schellander. The process was monitored by a Transpector-2 RGA (residue gas analysis) mass spectrometer from the company Inficon, which was operated by Gerhard Findenig and Herbert Preiml.

This particular Mattson is configured to handle 6" Wafers, so we could neither use the uncured sample pieces which we received from our paste supplier, nor could we use the 8" wafers we had yet printed. Hence, we reduced 6" glass wafers that had already been laser cured by the supplier, and we used 6" glass wafers on which we applied a copper layer with a squeegee by hand.

The mass spectrometer detected masses in the range of 1-50 AMU and was used to monitor the evolution of water, which is the reduction product of copper oxide with hydrogen. Picture 23 shows the mass spectrum of the reduction of the two laser cured samples, which were reduced simultaneously. The Transpector-2 machine is operated with the software TWare32. This program has an unconventional definition of ppm (parts per million): In this program, one has to choose a mass signal to which all the other signals are referenced to. This mass is set to be 10^6 ppm (100%). Usually, 10^6 ppm is the sum of all the signals, so that every signal is a partial quantity of this total

signal. The mass chosen for the picture below was argon (40), which is expected to be constant over the measurement.

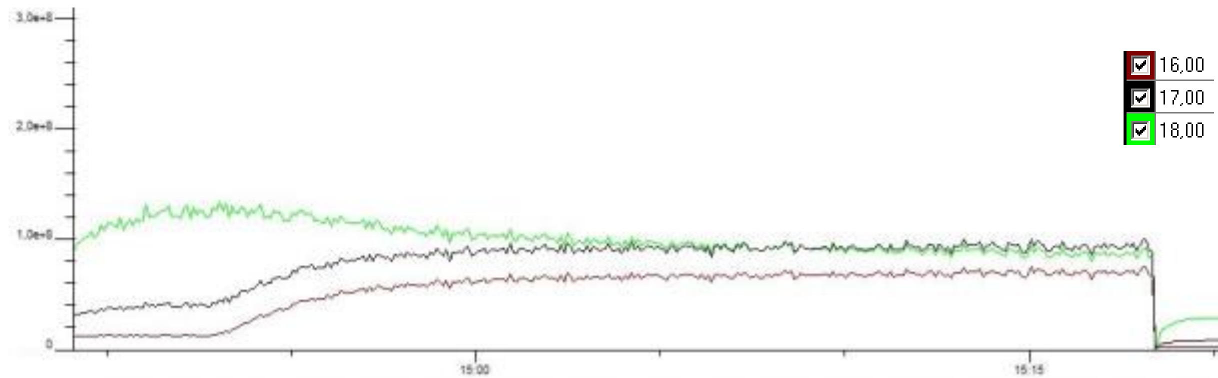

Picture 23: Mass spectrum of selected masses (Reduction of the laser cured samples)

During the process, we only monitored the green line, which represents the mass 18 (H_2O). As the peak vanishes after 10 minutes, we assumed the reduction to be over and canceled the experiment after 30min. Later we found the signals at mass 16 and 17 to be at an elevated level, and concluded that the water gained from the reduction is ionized in the hydrogen plasma. Hence, the "water"-signal is the sum of the signals 16, 17 and 18, which was still at an elevated level when we aborted the experiment. The resistivities of the previously laser cured samples are displayed in

Table 4. They can only be compared with each other and should not be seen as absolute values, since the thicknesses of the layers were not measured but only taken from an Intrinsiq report.

Sample Number	**3**	**4**	**5**	**6**
Before Mattson	41	32	47	42
After Mattson	33	26	52	46

Table 4: Conductivity of the processed samples in µΩcm

The samples 3 and 4 were printed on a glass wafer; the samples 5 and 6 were printed on a glass wafer coated with polysilicon.

It might be possible to reduce our samples in an Aspen-II plasma etching machine, but due to the unfavorable requirements of this machine[5] we did not perform any further experiments.

[5] Since the machine is used for production in the Front End, copper contamination must be avoided at all cost. Hence, after the experiment, my dear colleague Josef Schellander had to clean the whole process chamber thoroughly and process several ANKO Wafers ("Anlagenkontrolle", equipment check) in order to ensure that no copper contamination has occurred.
Additionally, the mass spectrometer was attached to the machine only for this experiment. Further tests would have required the participation of 4 Infineon process engineers.

Molecular hydrogen - Koyo

At the Infineon site in Villach, Molecular hydrogen is used in a 4% mixture with nitrogen as forming gas. This gas is used in plasma etchers, as well as in ovens and probably other machines. The reduction of thin native oxide layers on copper can be and is performed in an oven from the manufacturer Koyo Thermo Systems Co. Ltd. This oven can be operated at temperatures up to 700°C (cleaning program) and seems suitable for our trials.

In a first trial, pieces of a wafer, which carried an uncured layer of copper paste, were placed on a Taiko-Ring Wafer and treated at 300°C for 30 and 60 minutes. The sheet resistivity could be measured afterwards, which indicated that the copper paste had been sintered. Still, the color of the samples was brown, and the conductivity was unsatisfactory.

Picture 24: Uncured sample after 30min at 300°C in forming gas

In a next step, full-face printed 8” Wafers were processed at 400°C for 1.5, 2.5 and 3.5 hours. At each temperature two wafers were processed. As it can be seen in Picture 25, there is no visible difference in the color of the wafers. The specific resistivity of the copper deposits during the oven process did not correlate with the process time, as it can be seen in Table 5.[6]

Prozess Time	**90min**		**150min**		**210min**	
Sample #	13	17	23	24	25	26
spec. Resist. [µΩcm]	21	40	27	28	30	29

Table 5: mass loss and spec. resistivity of the samples processed in forming gas at 400°C

[6] It is important to mention that these values include a high degree of uncertainty: The specific resistivity is the product of the (measured) sheet resistivity and the film thickness. The film thickness could NOT be measured at the points were the resistivity was measured, but was determined by REM in the middle and on the edge of the wafer. Hence, the presented values are only estimations and can only be compared to one and another, but not to other values gained from other experiments. Further details are stated in the “Process evaluation” section.

Picture 26 shows one of the wafers reduced in course of the Koyo-oven process compared to an uncured wafer and a wafer that had been reduced by formic acid (details in the respective chapter). It can be seen that wafer 23 had been reduced incompletely. Since a prolongation of the process does not result in an improvement of the specific resistance, and higher temperatures cannot are inapplicable, the reduction in molecular hydrogen is not an option.

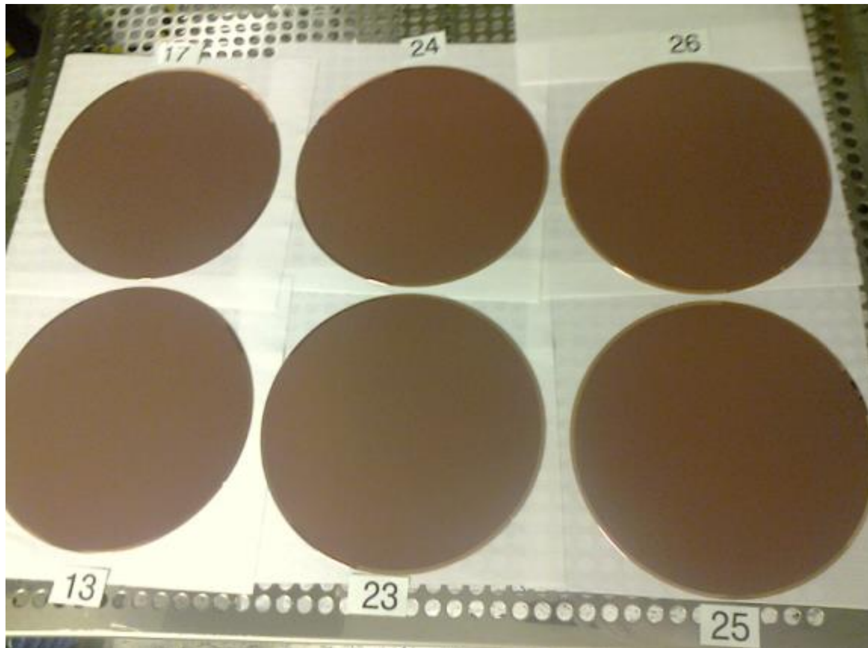

Picture 25: Wafers processed for 1.5h (17&13), 2.5h (24&23) and 3.5h (26&25) at 400°C in forming gas

Picture 26: Comparison between an uncured wafer (2), a wafer processed at 400°C in forming (23) gas and a wafer processed at 400°C in formic acid (16)

b. *Reduction with Formic Acid:*

Formic acid is an interesting reducing agent for copper oxide, since it is liquid and hence can be easily stored. Its boiling point is 101°C [30], so it can easily be vaporized and brought into a reduction chamber. Above 150°C, formic acid decomposes either to hydrogen and carbon dioxide, or to water and carbon monoxide.

$HCOOH \rightarrow H_2 + CO_2$ **Equation 6**

$HCOOH \rightarrow H_2O + CO$ **Equation 7**

In the presence of copper or other transition metals, formic acid may adsorb to the metal surface, which will then act as a catalyst for the decomposition. [31], [32]

$HCOOH_{(g)} \rightarrow HCOOH_{(ads)}$ **Equation 8**

$HCOOH_{(ads)} \rightarrow HCOO_{(ads)} + H_{(ads)}$ **Equation 9**

$HCOO_{(ads)} \rightarrow CO_{2(g)} + H_{(ads)}$ **Equation 10**

$2\,H_{(ads)} \rightarrow H_{2(g)}$ **Equation 11**

$HCOOH_{(ads)} \rightarrow CO_{(ads)} + H_2O_{(gas)}$ **Equation 12**

These reactions might also be valid for CuO and Cu_2O. [33] The absorbed species can react with the Oxygen from the copper oxides to H_2O and CO_2 respectively, and hence reduce the oxides to metallic copper. The ratio between H_2O and H_2 formed by the decomposition of formic acid has been determined on ruthenium to be 56:44. The reaction model for this reaction is shown in Scheme 1.

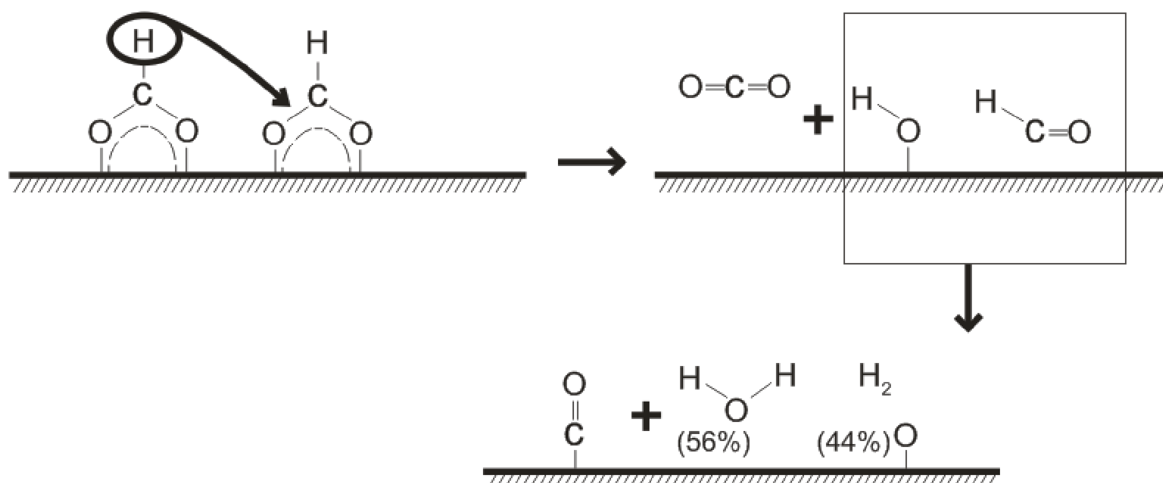

Scheme 1 – Model for the adsorption of Formic acid on Ru(001) according to literature [34].

The details of this reaction have not yet been studied [33], but there are already commercial applications, as it is reviewed in detail below.

Patent Situation [27]

The Korean company Samsung claims to have found a way to achieve a good conductivity (below 5 µΩcm) by treating a layer of copper oxide nanoparticles with a mixture of formic acid and alcohol at 200°C. Formic acid is not stable at temperatures above 150°C and decomposes to carbon dioxide and hydrogen. This hydrogen in the *status nascendi* is very reactive and readily reduces the copper oxide. However, "*the* (formic) *acid also reacts with reduced copper particles which are further etched"*. These particles can be transported to other areas of the wafer and be adhered there, where they can cause problems. In order to eliminate this problem, C1-C3 alcohol (methanol, ethanol or isopropyl alcohol) is added.

The sintering step should be performed in not more than 15 minutes. The reason for this is that copper is very sensitive to even small amounts of oxygen and is readily oxidized, especially at elevated temperatures. The optimal conditions for the sintering and reduction of copper nanoparticles in formic acid have been found to be 15min at 200°C (for 25nm particles).

Formic acid: - ATV Furnace

Formic acid is a powerful reducing agent, as it has been pointed out in a previous chapter of this work. Formic acid can be inserted into an oven by bubbling nitrogen through a flask containing the acid and carry the gas flow into the oven chamber. At Infineon Villach, this setup is attached to an "IR Vacuum Reflow Table Top System SRO700" built by ATV Technologie GmbH, displayed in Picture 27. The oven can easily generate the temperature needed for the decomposition of formic acid (150°C) as well as the highest temperature of interest for our process (400°C). The sample is placed either on a heater plate, which is heated by IR lamps located beneath the plate, or directly on the IR lamps. The machine has three independent thermocouples to control the temperature in the furnace: TC1 is the main temperature control, which controls the power of the IR lamps. It is located in the heater plate, but can be placed directly on the wafer in case the heater plate is not in use. TC2 is a thinner thermocouple, which is very flexible and can be placed on a particular site of the wafer in order to control the temperature there. TC3 is the safety thermocouple, which is also located in the heater plate and shuts down the oven if a critical temperature limit is reached.

Picture 27: ATV furnace

The system also consists of a vacuum pump, which can evacuate the chamber down to about 2mbar. The evacuation of the system is necessary before every process in order to remove oxygen. After the evacuation, the system is purged with dry nitrogen.

The sample can be inserted into the oven right after the print, without an intermediate drying step, but since the printing is performed in the clean room and the samples need to be transported to the oven, a pre-drying step at 60°C for 30min is performed inside the cleanroom.

The changes of the sample morphology have been studied by SEM. Picture 28 and Picture 29 show the cross section and the surface of an uncured 8” sample 22 (left) and a cured 8” sample 27. It can be seen that the micro particles of the uncured sample are covered with nanoparticles, which are vanished (molten) after the curing process. Sample 27 had been dried in an oven at atmospheric pressure and 45°C for 2h and cured in formic acid for 1h at 400°C (380°C surface temperature). The reduction of the copper oxide as well as the annealing process generate layers with a specific resistivity of about 13-14µΩcm for the Intrinsiq paste CP-003.

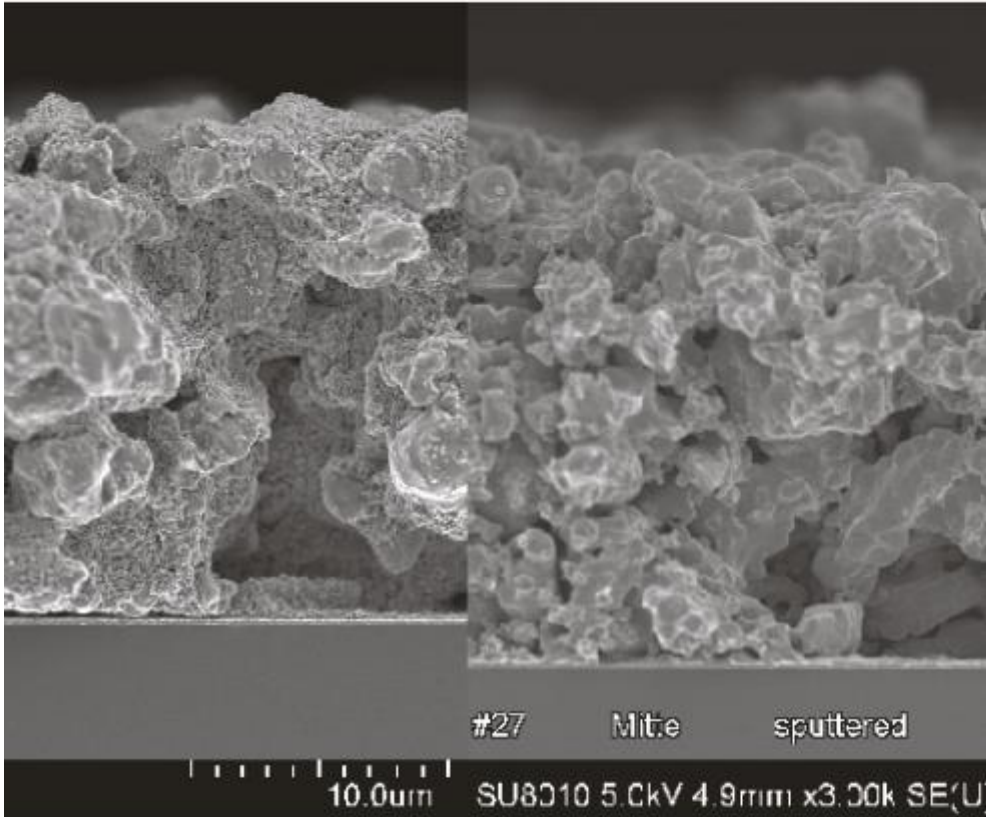

Picture 28: cross section of an uncured (left) and a cured (right) sample

Picture 29: on top view of an uncured (left) and a cured (right) sample

A typical reduction program can be seen in Picture 30. At first, it is important to remove the air from the chamber. Therefore, an initial vacuum step evacuates the chamber down to about 25-30mbar, which is then filled with dry nitrogen up to atmospheric pressure. A second vacuum step removes the nitrogen, and the nitrogen/formic acid mixture is pumped into the chamber with a rate of about 2.8 standard liters per minute. The mixture is generated in a so called “bubbler”, which contains the formic acid at room temperature. Nitrogen is blown through the bubbler and carries the fumes of the formic acid into the furnace. According to the manufacturer of the oven, this flow rate of nitrogen delivers 0.185g/min formic acid.[7]

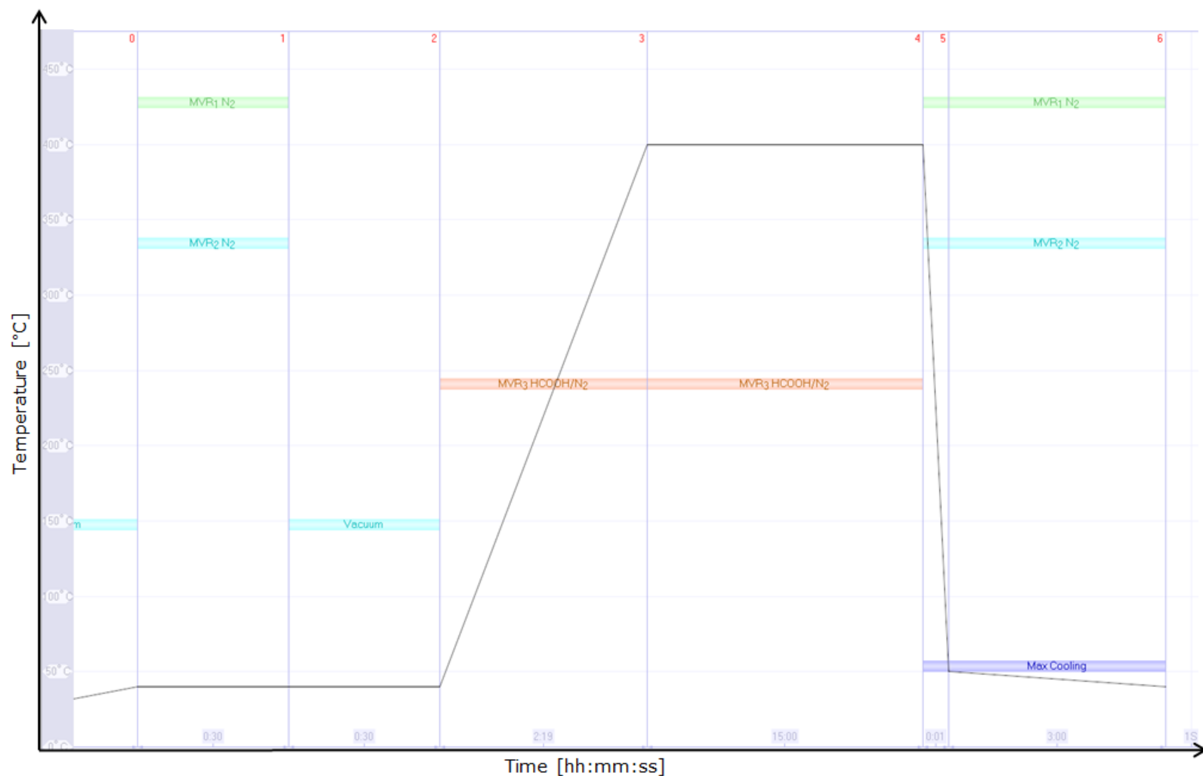

Picture 30: Typical reduction process with Formic acid

Note that the formic acid enters the system while the furnace is still at 50°C. When the system is first ramped up to 400°C under nitrogen and the formic acid enters the system at this elevated temperature, no further reduction seems to occur, which can be seen on the color of the samples as well as on their specific resistivity. Sample 8Z20 and 8Z21 were printed with CP-003 through a 50µm stencil. They were both pre-dried at 60°C for 30 minutes under nitrogen atmosphere and then reduced for 30 minutes at 400°C under formic acid without an intermediate drying step. The formic acid was pumped into the furnace at 50°C (8Z21) and at 400°C (8Z20). The specific resistivity of 8Z20

[7] Information received from Siegfried Kowalsky, sales/support manager at ATV Technologie GmbH on July, 23rd 2013 via Email.

was determined to be 25 μΩcm, that of 8Z21 15 μΩcm. The color of the samples can be compared in Picture 31.

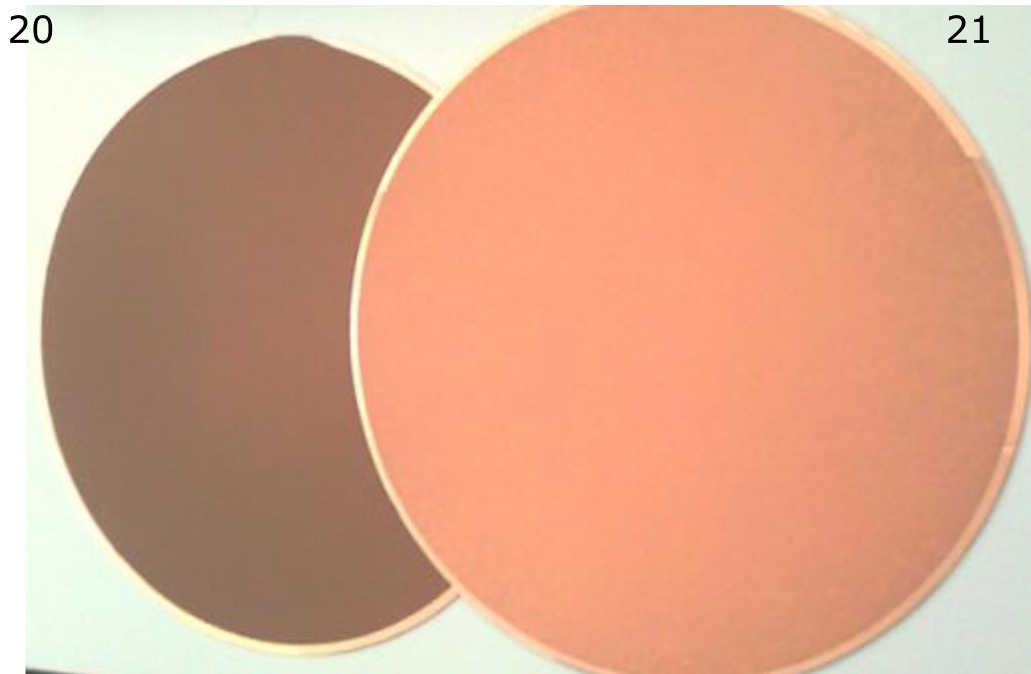

Picture 31: 8Z20 and 8Z21 after 30min FA

At temperatures below 200°C the formic acid can reach the surface of the sample without prior disproportionation and might generate copper formate.[8] This reaction can only be postulated and was not evaluated during this thesis. At 200°C, Copper(II) formate is rapidly decomposed to metallic copper, carbon dioxide and formic acid. [35] These copper nuclei on the surface might be the starting point for the autocatalytic reduction of copper oxide, which had been postulated by other authors. [28] Another theory is that it is the acid that attacks the coating of the particles and enables the reduction with the carbon monoxide. Which one of these theories is correct or if there is another reason for the described effect could not be determined.

Results

The resistivity of the standard paste CP-003 could be determined to be **13-15μΩcm** when being reduced with formic acid at 450°C for 15-30 minutes. The resistivity depends on the temperature of the reduction process (annealing) and surely on the time of the annealing/reduction step. Picture 32 shows the influence of the annealing temperature and time on the specific resistivity of the layers. The shown data was obtained from only one sample per data point, so the spread of the results cannot be estimated. It is probable that the value 450°C / 45 minutes is an outlier. Also it might be

[8] According to the furnace manual, published by ATV Technologie GmbH.

the case that the difference in the resistivities of each series is actually nothing more than statistic scatter, meaning that the maximum time needed for proper reduction/annealing is already exceeded. Further studies will be performed with a shorter timescale in order to show the time dependence of the annealing process. What is indeed noticeable is that lower temperatures always lead to higher resistivities, even after longer treatments. Still, speculations about the reason for this effect should be suspended until a larger data pool is available.

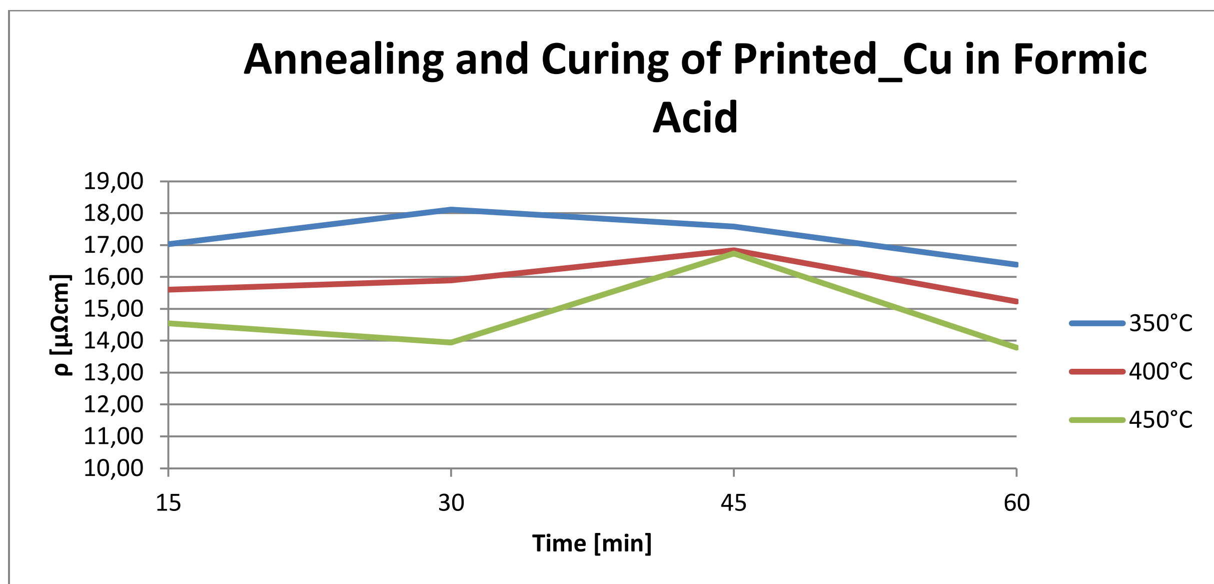

Picture 32: Plot specific resistivity vs. time for different treatments of CP-003

The diluted samples of the CP-003+ had around the same resistivity as the standard CP-003. The paste CP-004, which was specifically designed for us in order to achieve layers with a better conductivity did not show any improvements: In fact, without dilution the reduced layers were cluttered with deep cracks sometimes even extending all the way down to the copper seed layer, which resulted in higher specific resistivities than the crack-free standard paste. (Picture 35 and Picture 44)

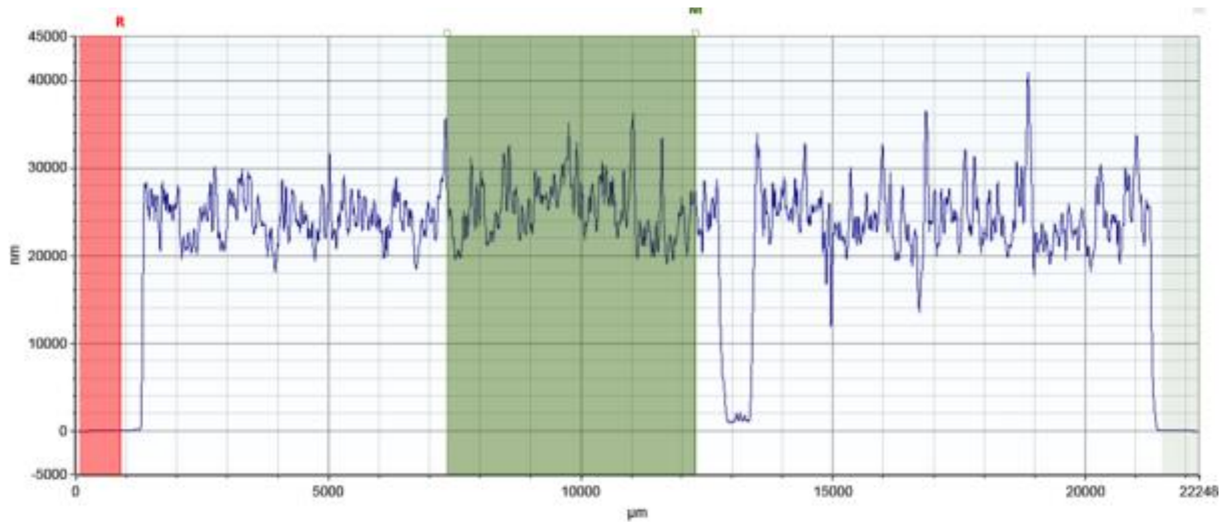

Picture 33: Surface topology of sample 8Z135 (CP-004)[9]

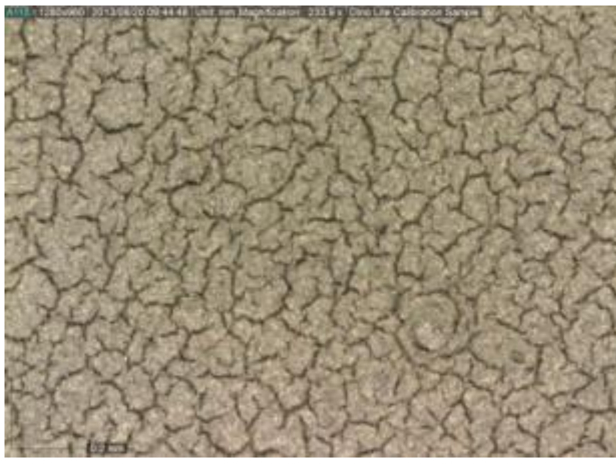

Picture 35: Surface of sample CP-004, mag. 235x

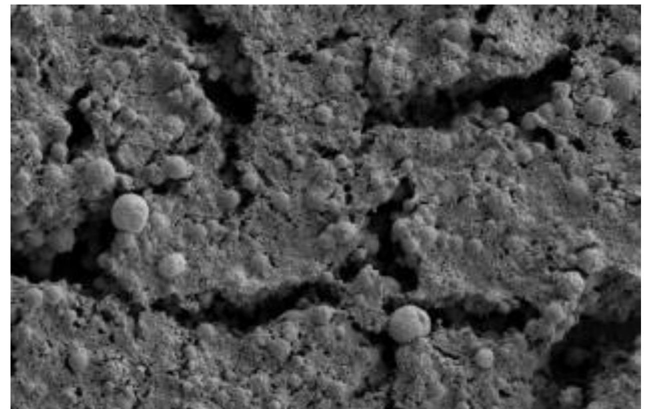

Picture 34: Surface if Sample CP-004, mag. 1000k

The best obtained resistivity with a diluted CP-004 (which still had cracks in it) was **19µΩcm** with sample 8Z190. (Standard print parameters, CP-004 + 10% CPD02, reduced 15minutes at 450°C in formic acid)

[9] The mechanical profilometer cannot resolve the deepness of the cracks, which is due to the thickness of the needle and its angle to the sample.

c. *Reduction with Carbon Monoxide:*

Literature on the reduction of copper oxide with carbon monoxide was first published in 1879. [36] In principal, the reaction equation can be written as the following:

$Cu_xO_y + CO \rightarrow Cu_xO_{y-1} + CO_2$ **Equation 13**

Carbon monoxide is widely used as a reducing agent for metal oxides. It is easily generated by burning coal under high pressure, where Carbon monoxide is the preferred reaction product of the Boudouards reaction.

$CO_2 + C \leftrightarrow 2\ CO$ **Equation 14**

In general, carbon monoxide is considered a stronger reducing agent than hydrogen. [37] Similar to the reduction of Copper oxide with hydrogen, at low temperatures (<125°C) an incubation period exists. Also the reduction with Carbon monoxide is said to be autocatalytic. The reaction is less vulnerable to small amounts of oxygen in the gas than the reduction with hydrogen, since the adsorption of Carbon monoxide on copper is much stronger than that of hydrogen, and hence the CO molecule cannot be replaced by oxygen at the active sites of the reduction. Also, the reaction proceeds at higher rates at lower temperatures compared to hydrogen. [38]

Carbon monoxide - Koyo

Although the formic acid process delivered good results, the process is not optimal for mass production: A formic acid bubbler is no standard equipment and needs regular maintenance (refilling). Also, since formic acid at high temperatures is decomposed to carbon monoxide which then acts as the reducing agent, it might be beneficial to use the gas itself instead. For our trials the Koyo8C furnace, which had already been used in the forming gas trials, was modified. A 7.5 liter carbon monoxide flask was connected to the gas inlet, which had previously been used to deliver forming gas. In a first trial we tried to quantify the benefits of carbon monoxide over formic acid. Therefore, we processed three lots of wafers with different programs: Each program starts at 100°C (machine specific); 50 standard liters of Nitrogen and 5 standard liters of carbon monoxide per minute are pumped into the chamber before the start of the temperature ramp. The temperature was raised with 5°C per minute. Lot 1 should show if carbon monoxide can reduce our layers at lower temperatures than formic acid. The plateau step of this program was 5 minutes at 300°C. After that, an annealing step (1h at 400°C, inert atmosphere) was performed. Lot 2 was processed just like lot 1, except the plateau step was 30 minutes long. Lot 3 should simulate the standard formic acid process with carbon monoxide as reducing agent. Therefore, the plateau time was set to 30 minutes and the

temperature to 400°C. To our surprise, the results of the three programs were all the same, with specific resistivities being between 40 and 54µΩcm. The samples did not differ in color, which was similar to the color of the wafers processed in forming gas.

In a second run, three more lots were processed with different settings: Lot 4 should ramp like usual (5°C/min) up to 400°C with a higher carbon monoxide concentration (50 standard liters per minute total gas flow with a mixture of nitrogen : carbon monoxide 1:1). The same gas flow, CO concentration and temperature are kept for 30 minutes. Lot 5 is a exact copy of lot 4, except the total gas flow is 10 instead of 50 liters per minute (again a 1:1 mixture). Lot 6 has the same temperature profile like lot 4 and 5, but uses the same gas flow and mixture as lot 1-3 (50 l/min N2, 5 l/min CO). A summary of the different settings is listed in Table 6. Some of the wafers processed in the first run (lot 1-3) were also processed in the second run. The results were comparable to those of the first run, except one wafer (8Z98) which was also part of the first run and improved from 43 to 34µΩcm. Besides the different reducing agent the ramp rate is one of the main differences between the two processes (Koyo and ATV). The ramp rate might as well be an important factor, which should be confirmed by further tests.

Up to now, the reduction with formic acid is the only working reduction process for our printed copper layers. As it has been stated earlier, formic acid decomposes at high temperatures into carbon monoxide and water. It seems obvious that carbon monoxide is the actual reducing agent in the formic acid process, and the question arises why the direct treatment with carbon monoxide does not lead to comparable or even better results. Since the flow rate and the concentration of carbon monoxide in the Koyo furnace is higher than in the ATV furnace, we would have expected better results. Instead, it seems as if the whole process is not possible without prior treatment with formic acid in a non-decomposed state. It is still unclear whether it is the acidity that attacks a protective layer on the particles and by doing that enables the attack of carbon monoxide, or if the formic acid forms copper formats, which decompose at higher temperatures and then catalyze the reduction.

At this very point, the statement cited in the beginning of this chapter proves to be true: The reduction of copper oxide (like the oxidized copper seed layer) proceeds with a divine elegance, as it can be observed through the window of the ATV furnace, but as soon as any surfactants come into play, like it is the case with the paste, developing a production process becomes a nightmare.

The search for a more economic reduction process will go on, but it will not be covered in this thesis.

d. *Oxidation of the printed pastes*

The oxidation of the generated structures might be important for the further process development. One possible way to achieve a better resolution is to etch the generated structures (or full-face printed wafers) through a photoresist mask. After this step, the mask would have to be removed, which is often done with Oxygen-Plasma. Therefore, we wanted to know how our system behaves under oxidizing conditions.

Atmospheric oxidation – DESPATCH furnace

The easiest way to oxidize our wafers is atmospheric oxidation in a furnace. In line, the DESPATCH furnace that has already been in use for pre-drying and drying our samples can be used for this purpose by simply not using the nitrogen inlet. Samples were dried for 5 minutes at 100 and 150°C under air without visibly being oxidized. After 200°C for 10 minutes, the copper seed layer turned blue, although the printed areas as well as some millimeters of copper seed layer that surrounded our structures remained unharmed. (Picture 36)

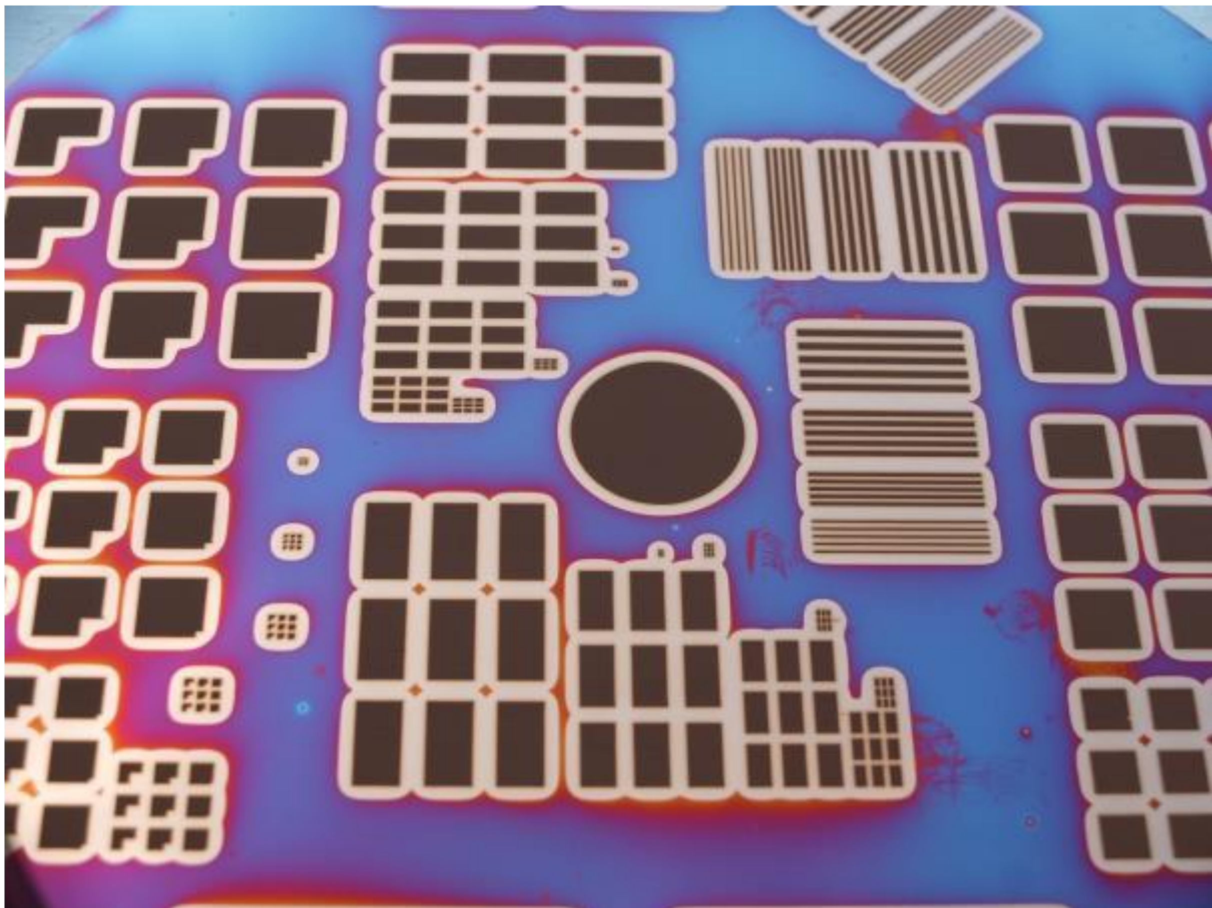

Picture 36: Printed wafer after 200°C 1h, air

It seems obvious that something in the paste protects the surface from getting oxidized. It has been mentioned in chapter 3 that the particles in the paste are protected against oxidation. The nature of this protective layer has not been revealed to us by Intrinsiq. From the appearance of the wafer seen in Picture 36, it seems as if this protective layer is bleeding out of the printed structures after the print and protects the neighboring copper seed layer as well as the printed structures. It might be possible, that this protective layer also hinders the reducing agent from reaching the copper oxide surface and hence hinders the reduction.

Further studies were performed in oxygen plasma, what can also be seen as a step towards a productive process.

Oxygen-Plasma – EKT

Usually, the EKT machine (EKT is the abbreviation for “EInkammertunnel”, one chamber tunnel) is used for plasma etching of photoresists. Like the TEPLA machine, it generates radio frequency waves to ignite the plasma. A typical etching process consists of the evacuation of the chamber, filling it with nitrogen, heating by igniting nitrogen plasma, inserting oxygen and etching the photoresists with oxygen plasma. The oxygen plasma step usually takes from 10-40 minutes, the RF power ranges from 500-1000W.

For this trial we used structured wafers that had been pre-dried but not sintered, as well as one wafer that had been reduced in formic acid. The wafers were placed in a quartz wafer holder with one slot empty between two wafers, which is the standard procedure to gain a better homogeneity. The assembly can be seen in Picture 38. The wafers were processed with a LAB process (“Lackablöseprozess”) which is designed to strip photoresists.

The process consists of an evacuation step ($p < 0.5$Torr), followed by a oxygen purge (1300sccm until 1Torr is reached). After this step the oxygen plasma is ignited with a RF power of 1000W. The oxygen plasma oxidizes the wafers for 20 minutes (1300sccm, 1000mTorr). During this step the temperature rises up to near 120°C. After this procedure the chamber is evacuated again below 0.1Torr and purged with oxygen (400sccm) in order to cool it down.

The first wafer was homogenously oxidized: The copper seed layer had turned greenish and reddish, the printed copper pads were brown to black. The other wafers were only partially oxidized: The oxidation proceeded from the edge to the center of the wafers. The edge was grey in color, turned blue and red when approaching the center, and the center itself seemed completely unharmed by the plasma. The oxidation on the first wafer and on the edge of the others was so intense, that the

copper seed layer began to delaminate from the TiW-barrier. This is of course due to the fact that the incorporation of oxygen into the copper caused an expansion in the layer which resulted in ruptures.

Interestingly, the previously reduced wafer (15min 450°C formic acid) did not seem to be as oxidized as the others (Picture 40). The printed pads could not be oxidized at all, and the pads were again surrounded by an area of not or less oxidized copper. The resistivity of these pads increased from 13.5 to 14.1µΩcm, which might be in the range of statistic scattering. Whatever the nature of the protective layer on the pads is, it could not be removed by the formic acid reduction.

One of the oxidized wafers was reduced with the standard reduction procedure (15 minutes, 450°C). The resistivity measurement revealed that the previous oxidation did not interfere with the subsequent reduction: a resistivity of 14.5µΩcm was measured. Again it is emphasized that these values are well in the range of the statistic scatter. The two processes are graphically illustrated in Picture 37.

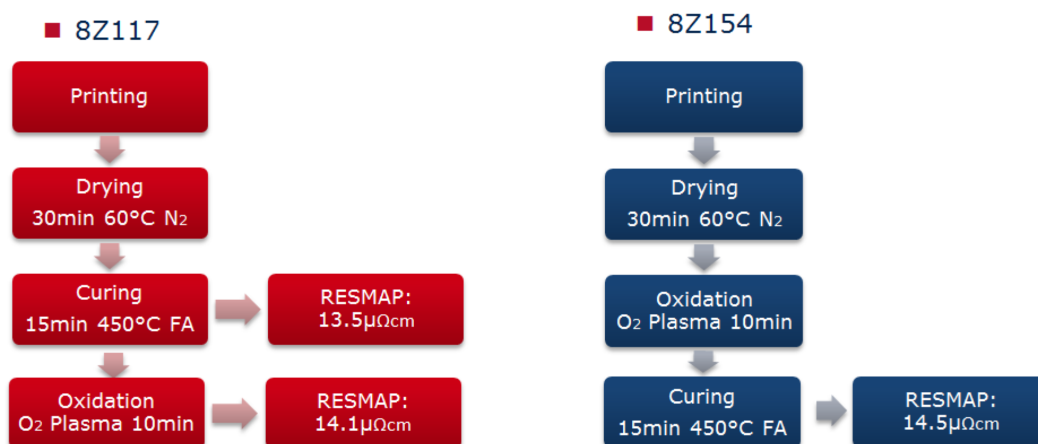

Picture 37: Conductivity of the oxidized samples

In order to gain a better understanding of the oxidation characteristics of the printed paste, further tests will inevitable. For the moment, one important intermediate target could be reached by showing that the oxidation neither destroys our structures, nor does it hinder the subsequent reduction.

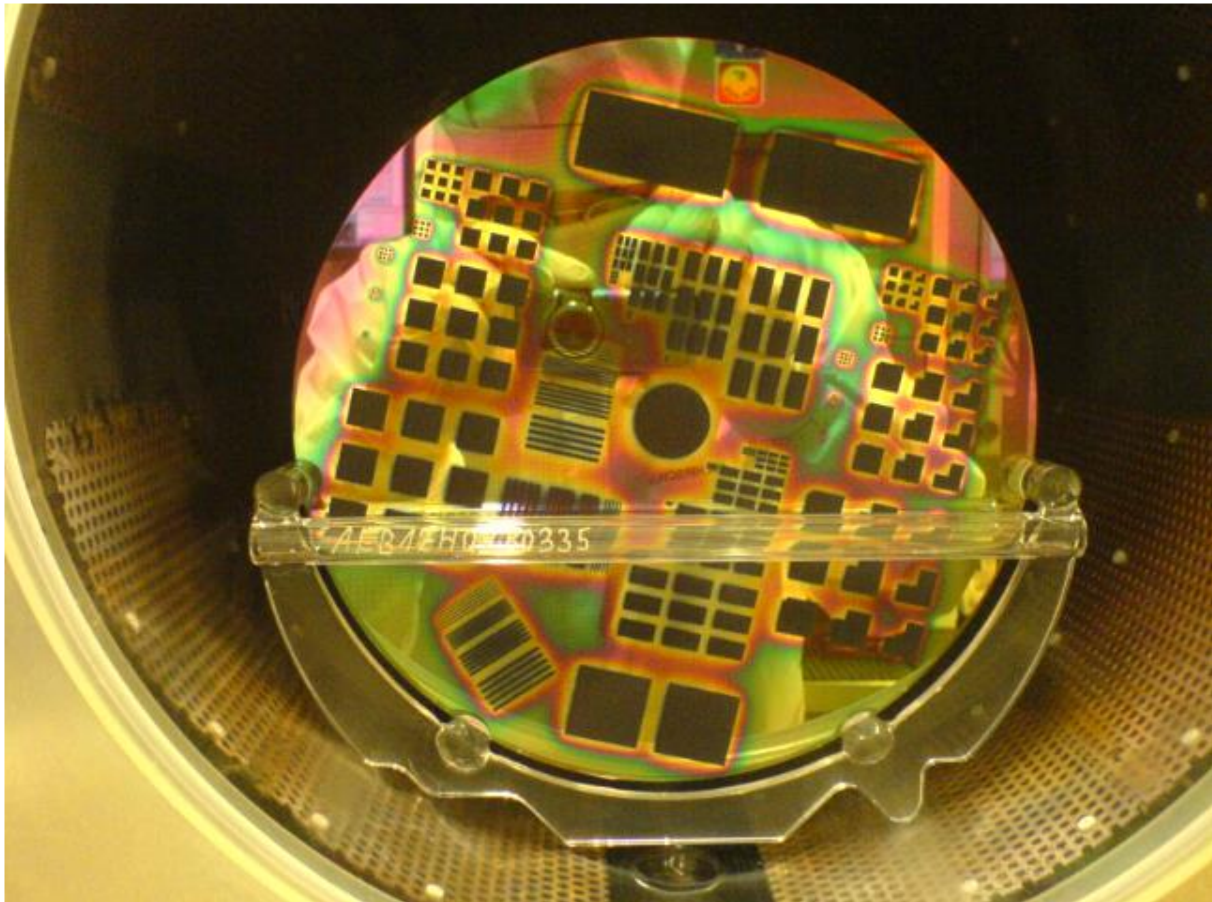

Picture 38: Quartz wafer holder with test wafers inside the EKT

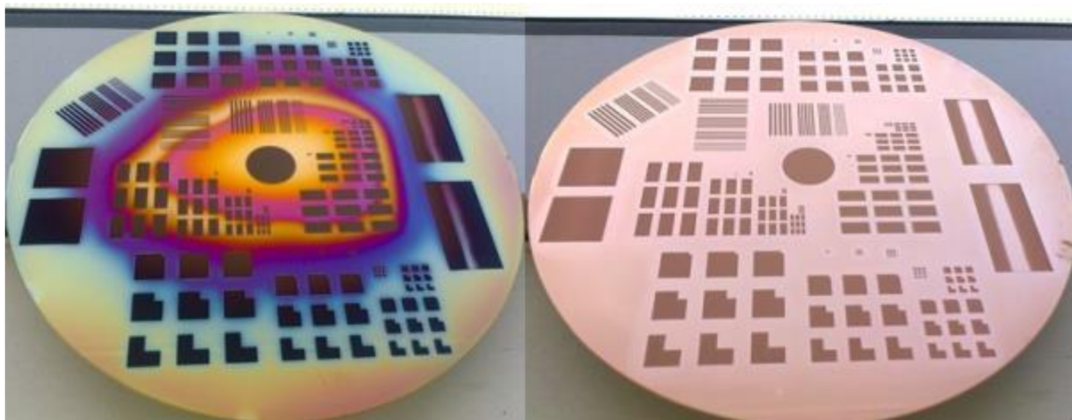

Picture 39: Comparison between a partially oxidized wafer before (left, 8Z166) after reduction with formic acid (right, 8Z154).

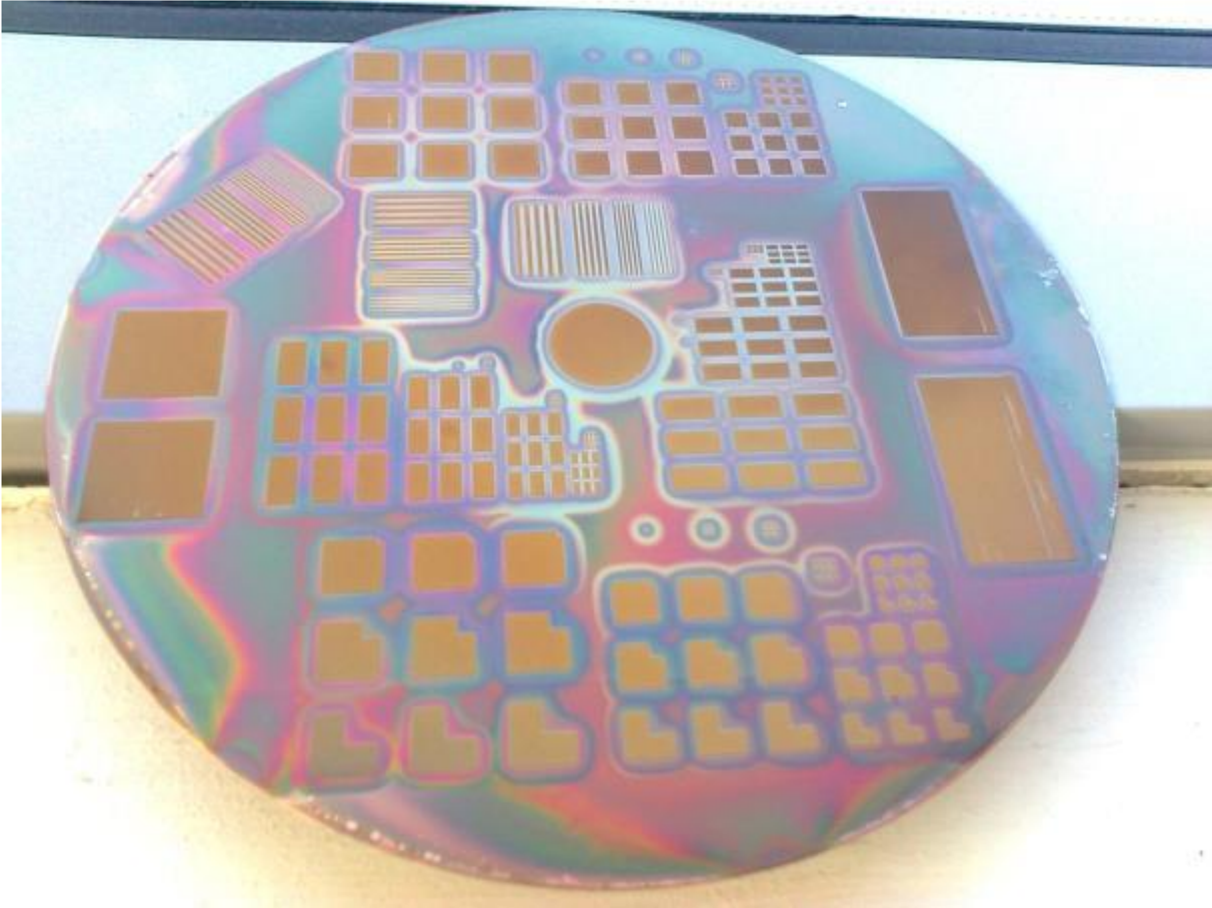

Picture 40: Previously reduced wafer after oxidation in O_2 Plasma

e. *Wrap-up of the results*

The different conductivities obtained by the methods are summarized in Picture 41. An explanation to the different processes is given in Table 6. The horizontal red line marks the desired resistivity of 5µΩcm. The samples processed in the TEPLA and in the Mattson are not displayed because of the poor quality of the results and the lack of comparability to the other samples.

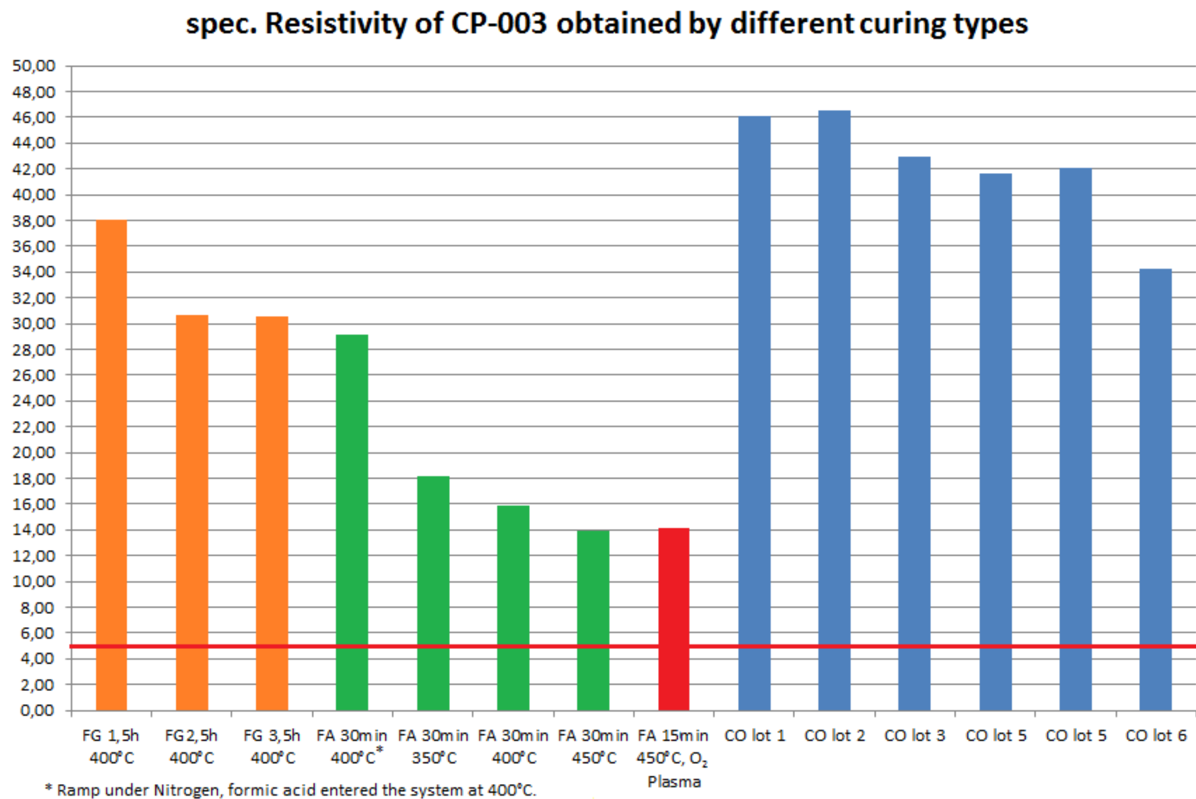

Picture 41: Comparison between different curing processes

	Gas	Ramp	Plateau
FG 1.5h 400°C	H_2in N_2 4%, 52 l/min	5°C/min	**90min 400°**
FG 2.5h 400°C	H_2in N_2 4%, 52 l/min	5°C/min	**150min 400°**
FG 3.5h 400°C	H_2in N_2 4%, 52 l/min	5°C/min	**210min 400°**
FA 30min 400°C	FA in N_2 6.5% 2,8 l/min	**150°C/min N_2**	30min 400°C
FA 30min 350°C	FA in N_2 6.5% 2,8 l/min	150°C/min FA	**30min 350°C**
FA 30min 400°C	FA in N_2 6.5% 2,8 l/min	150°C/min FA	**30min 400°C**
FA 30min 450°C	FA in N_2 6.5% 2,8 l/min	150°C/min FA	**30min 450°C**
FA 15min 450°C, O2 Plasma	FA in N_2 6.5% 2,8 l/min	150°C/min FA	**15min 450°C**

CO lot 1	CO/N_2 10:1, 55 l/min	5°C/min	**5min 300°C**
CO lot 2	CO/N_2 10:1, 55 l/min	5°C/min	**60min 400°C**
CO lot 3	CO/N_2 10:1, 55 l/min	5°C/min	**30min 400°C**
CO lot 4	**CO/N_2 1:1, 50 l/min**	5°C/min	30min 400°C
CO lot 5	**CO/N_2 1:1, 10 l/min**	5°C/min	30min 400°C
CO lot 6	CO/N_2 10:1, 55 l/min	**10°C/min**	30min 400°C

Table 6: Details to the reduction process settings

5. Process evaluation

a. *Sheet resistivity*

The sheet resistivity was measured by using a RESMAP machine. This machine employs the four-point method, which is a technique that eliminates the inner resistivity of the cables in the measuring apparatus and hence is capable of determining very small resistivities.

The measurement setup goes the following: Four needles are placed in line and with a known distance to each other on a homogeneous surface. A current is applied to the outer two needles, and the voltage drop is measured between the inner two. With knowledge of the distance between the needles, one can calculate the sheet resistivity of the layer.

In our case, the machine calculated the values and delivered the results in Ohms per square. (This "unit" is identical to Ohm. The "per square" is often added to emphasize that the sheet resistivity is meant. As a symbol, $\Omega_{\square}$ is used to abbreviate the sheet resistivity.) The RESMAP is usually used to determine the sheet thickness, which can be calculated from the sheet resistivity when the specific resistivity of the material is known.

We used the RESMAP to characterize every printed wafer. For a proper calculation of the specific resistivity knowledge of the exact thickness of the layers is crucial. Wafers that were printed with a full-face stencil had a poor homogeneity. (Picture 6)

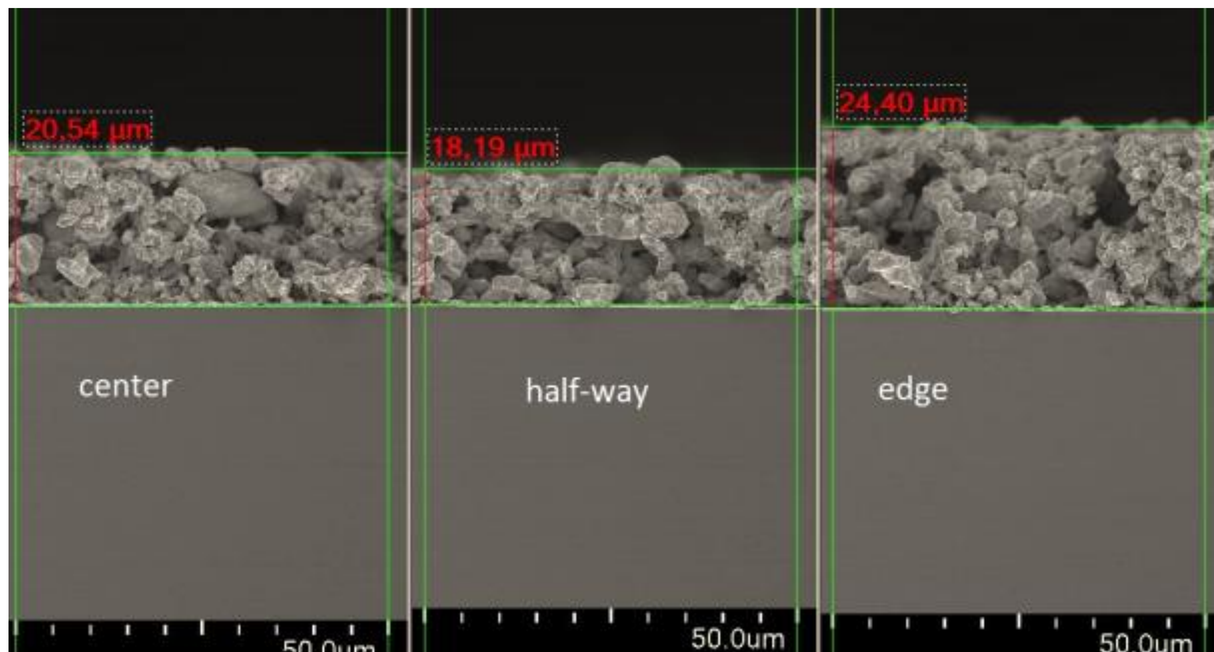

Picture 42: Layer thickness of sample 8Z27, determined by SEM on different points of the wafer

Hence, the specific resistivity calculated for full-face wafers can only be regarded as proximity. Structured wafers contained a circular structure in the center. The resistivity was measured at five points in this structure, namely in the center and at four points surrounding the center in a distance of 7.5 millimeters with a 90° angle between each other.

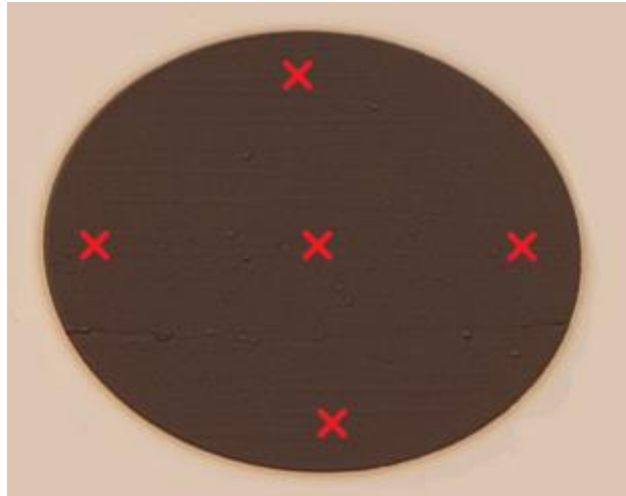

Picture 43: RESMAP measurements on the central structure

The thickness of the copper layer was measured in those points with a mechanical profilometer. Hence, the specific resistivities obtained from measurement on structured wafers should be relatively precise.

b. *Film Thickness / Surface Topology*

It is obvious that the surface topology has a deep impact on the resistivity of the layers. Technically the four-point method (and other methods like the Van-der-Pauw method) requires plane layers in order to deliver correct results. [39], [40] Therefore a closer look at the surface of the samples investigated is necessary.

There are four different methods available at the Infineon site in Villach which are suitable to measure the thickness and surface topology of our samples. Mechanical and optical profilometers are able to measure step heights without having to destroy the sample, SEM and a light microscope can measure the film thickness on broken wafers.

Optical Profilometers

Optical profilometers can measure the surface profile by focusing the objective on one height of the sample, for example the copper seed layer. Then the objective is moved upwards and the areas that can be seen sharp are recorded together with the information, how much the objective has been elevated. The information, which area can be seen sharp is provided by the software. In the confocal mode, the light which is used to illuminate the probe is guided through a beam-splitter and a lens. That way, only a certain point (height) of the sample is illuminated. By moving the objective (on which the light source and the optics are mounted) upwards the different levels of the sample are illuminated depending on their height. By measuring, which area is highlighted and how much the objective has been moved, the software can generate a surface profile. There are also many other methods that can be employed, but these two methods have proven to be the most efficient with our equipment. Depending on the height of the structure and the desired resolution, such a measurement can be done in less than a minute. By recording neighboring areas with overlapping borders, many surface profiles can be stitched together to display a larger area of the sample. That way, three dimensional maps of structures as large as 1cm² and above can be generated. The area that can be measured by one single measurement is depending on the magnification of the objective. Objectives with a low magnification (e.g. 5x) can measure large areas at a time, but the vertical resolution is usually only in the range of 10µm. An objective with 50x magnification can only measure an area of one tenth the size, but with vertical step heights of one micrometer. An example of a structure measured with an optical profilometer can be seen in Picture 44 and Picture 45.

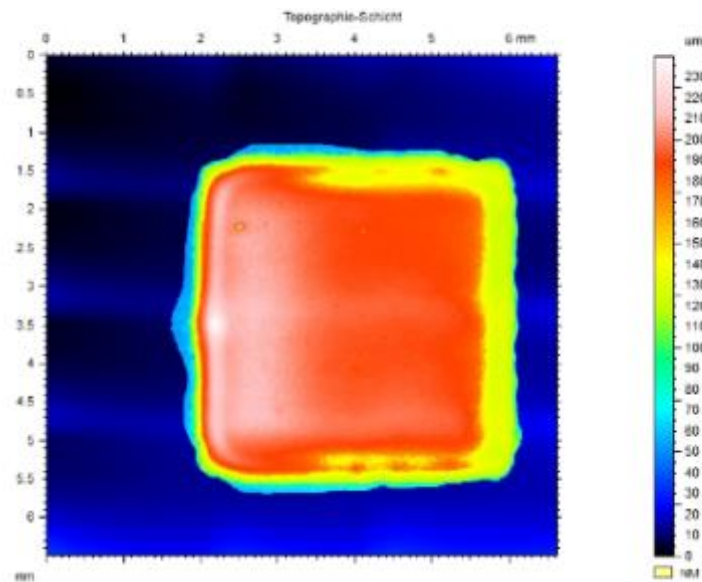

Picture 44: top view of a surface profile acquired with an optical profilometer

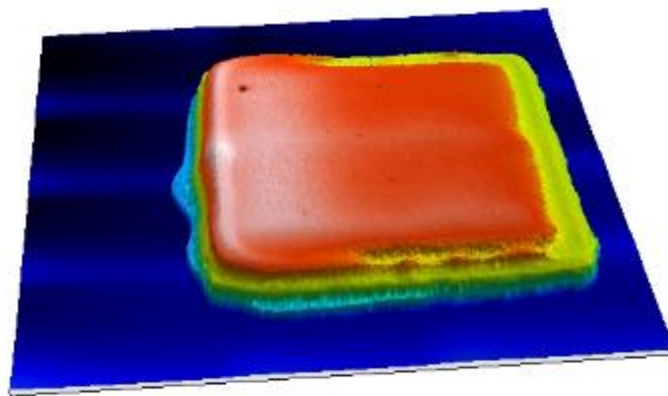

Picture 45: side view of a surface profile acquired with an optical profilometer

These pictures show an about 5x5mm large structure that has been printed through a 200µm stencil. They consist out of several dozens of single measurements which have been stitched together. It can be seen that the base is not completely flat but wavy with height differences of up to 20µm. This is a typical problem of optical profilometers and is due to the highly reflecting nature of the copper-seed layer. After the measurement the data can be analyzed by appropriate software, which can cut out line profiles like it is displayed in Picture 46.

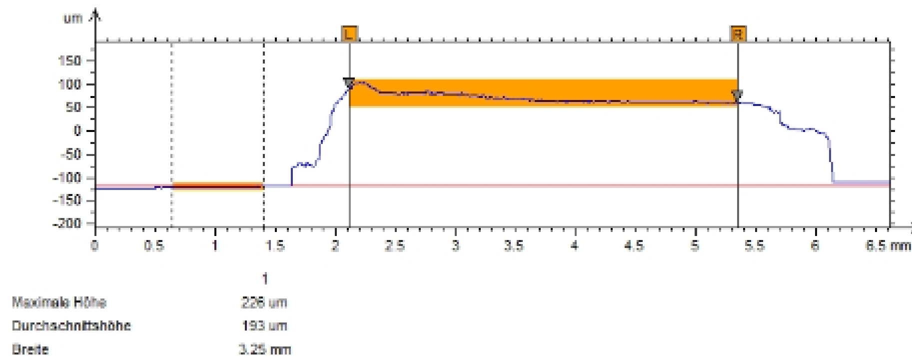

Picture 46: line profile cut out of Picture 45

It can be seen that the average height of the pad is about 190µm, which we believed fitted good to our stencil thickness of 200µm. The hill on one side of the pad indicated the printing direction. We assumed that the squeegee pulled material out of the pad after it had passed the recess in the stencil.

Mechanical Profilometers

Our first clue that the optical profilometer delivered false results came from Intrinsiq Materials, who received samples that had been printed by us in order to cure them with their laser. They measured the sample displayed in the previous subchapter with a mechanical profilometer and found an average height of about 100µm. Mechanical profilometers use a needle-tip consisting of a very hard material, typically tungsten carbide or diamond to move over the surface and measure the vertical displacement of the tip. They are highly accurate and less prone to error than optical profilometers. Optical profilometers can have problems with reflecting surfaces and with color changes (dark/bright). Mechanical profilometers cannot measure soft surfaces that are deformed by contact with the needle. Also, since they do have contact with the sample, they are easily contaminated. Wet and sticky surfaces cannot be measured with them, while this does not pose a problem to optical methods. One huge advantage of optical methods is that they can cover areas and stitch them together to gain larger maps of structures. Mechanical profilometers can only measure line profiles, but do that at much higher rates. The recording of a 20mm line profile by an optical profilometer can take up to 5 minutes or even more, depending on surface roughness and step height, while the measurement with a mechanical one can be done in less than half a minute. The reason for this is that the optical methods will measure every vertical point, while the needle just touches the upper most point of the structure. For example take a structure with a rectangular profile that lies on an even surface. It has a height of 50µm and a length of 2mm as it is displayed schematically in Picture 47.

Picture 47: imaginary test structure

We postulate that the vertical resolution of both profilometers is 10µm in vertical direction and the horizontal resolution shall be also 10µm. Every measurement shall take one second. The mechanical profilometer will need 202 seconds to move over the structure (one point before and after the step). The step height is determined while moving over the step and does not take any extra time. (The measurements are symbolically displayed in Picture 48.

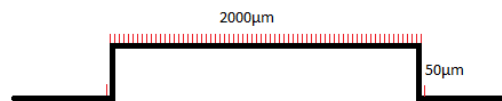

Picture 48: measurement of the test structure with a mechanical profilometer

The optical profilometer moves across every of the indicated 202 points on the surface and measure every possible step height in every single point as indicated by the crossing red lines in Picture 49. This will take 202x5 = 1010 seconds for this structure. This example is actually an understatement since the measurement time of mechanical profilometer is actually much shorter, while one second is a realistic value for optical measurements.

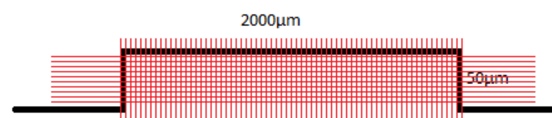

Picture 49: measurement of the test structure with an optical profilometer

At Infineon, contamination of equipment with copper poses an enormous threat. Hence no productive mechanical profilometer could be used for the characterization of our samples. Our samples were measured with a profilometer at the Failure Analysis Department, where copper contamination is no danger for productive wafers. These measurements confirmed that the structure displayed above is actually 100µm high. The reason why the optical profilometer delivered wrong results could not be determined.

Scanning Electron Microscope (SEM)

This established and common method uses an electron beam, which is focused and diverted by magnet coils and scans the surface of a sample. The electrons are emitted by an electron source are accelerated towards and focused on the sample, where they generate secondary electrons through ionization. These secondary electrons are detected and processed to gain a picture of the sample. The voltage used to accelerate the electrons usually lies in the range of 1-30kV, in our case all pictures were taken at 5kV. The distance between the sample and the objective, which focuses the electrons, is called working distance. This distance is displayed on every SEM picture and was typically in the range of 5-10mm. The SEM machines used for our pictures were a Hitachi SU8010 and a Hitachi S4800. Those scanning electron microscopes can resolve structures as small as several nanometers.

We used SEM in order to determine our layer thickness, as well as to evaluate the reduction processes and investigate the sample morphology.

Determination of the Layer-Thickness:

SEM is a very accurate method to determine the layer thickness, but it requires a lot of effort (sample preparation and measurement) and is a destructive method. We used it in the first phase of our investigations as only reliable method, since the optical profilometer delivered wrong results and we had no knowledge of the available mechanical profilometer.

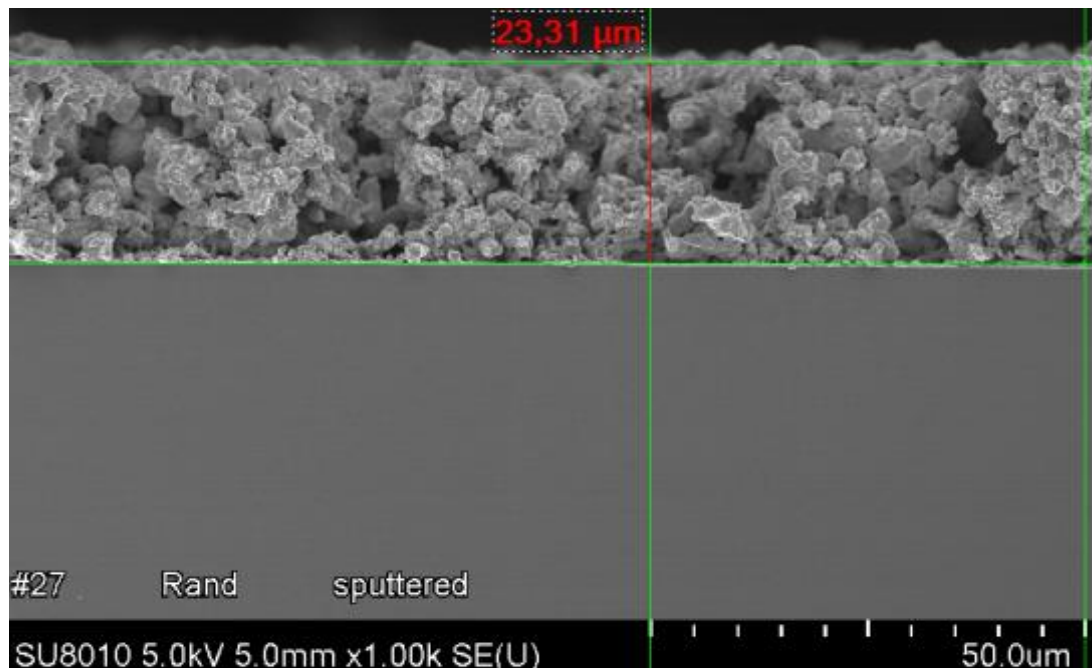

Picture 50: Determination of the sample thickness by SEM

c. *Morphology / Porosity*

SEM is also the method of choice for the characterization of the inner structure of the printed layers. Also the porosity can be estimated from the pictures, although here gravimetric methods deliver better results.

Investigation of the Sample Morphology

Some interesting phenomena are only discovered when the samples are looked upon in SEM. Especially the previously mentioned large spherical structures on the surface of CP-003+ and CP-004 samples are of interest, because their process of the formation is completely unclear. Picture 51 clearly shows that the particle, which is on the top left side, is actually hollow.

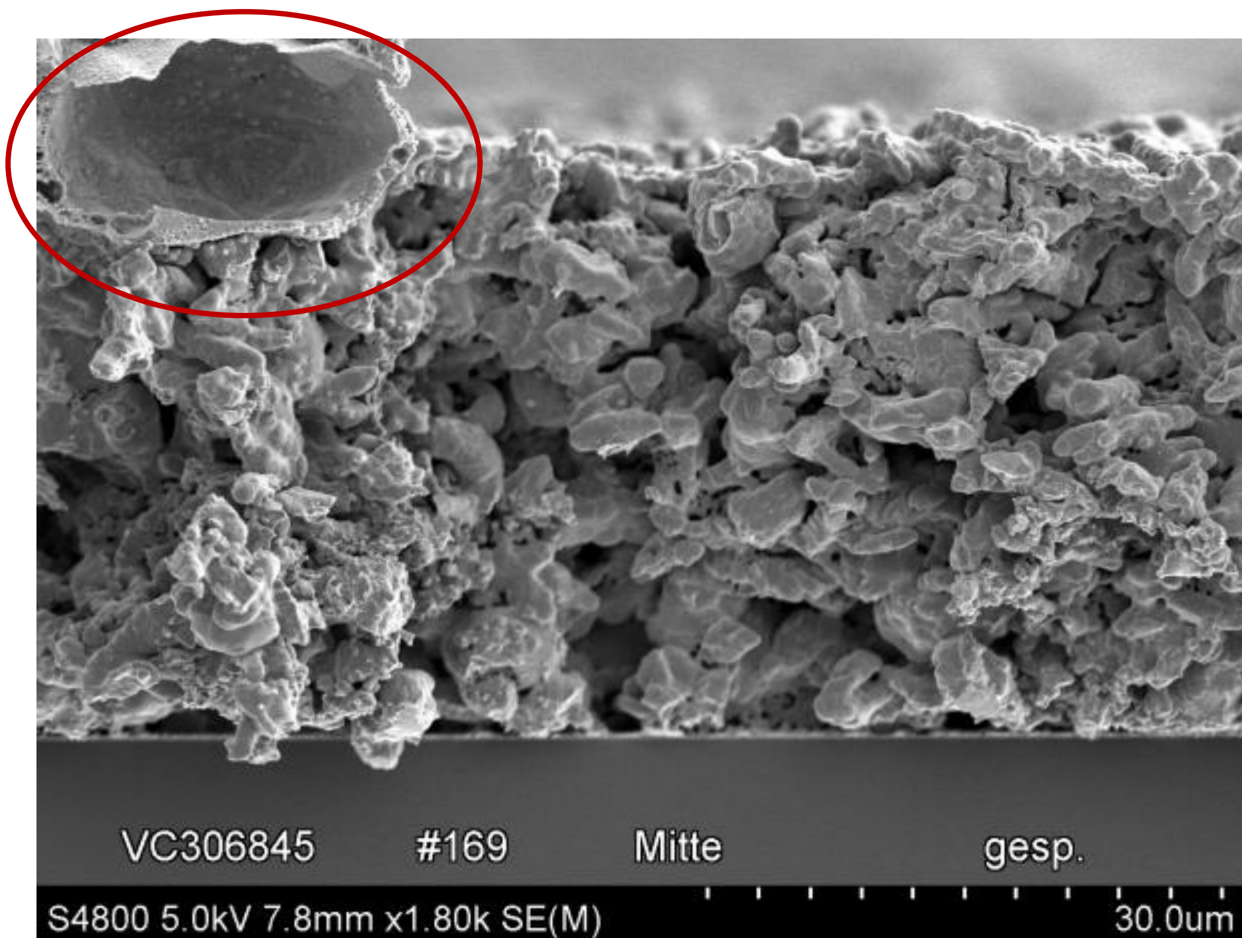

Picture 51: Sample 8Z169 (mag. 1.8k) (Larger version of Picture 16)

These spheres have yet only been discovered on samples with visible holes in the surface, as they have been described in the drying-chapter. Those samples consist of diluted CP-003+ or CP-004. The formation of the visible pores can be observed during the curing process, where the optically continuous layer starts to be disrupted by emerging pores at temperatures of about 350°C. It is

probable that during this process also those spheres displayed in Picture 51 are created. The exact mechanism of their creation will be investigated in further studies.

Evaluation of the Reduction Process

The reduced and annealed samples differ in their morphology from the uncured samples. Uncured samples contain of micro particles that are coated with agglomerates of nanoparticles. These agglomerates vanish upon sintering during the formic acid curing step. Samples which were received by Intrinsiq that have been laser cured also showed these agglomerates (Picture 52), as well as samples which were sintered in forming gas. (Picture 53)

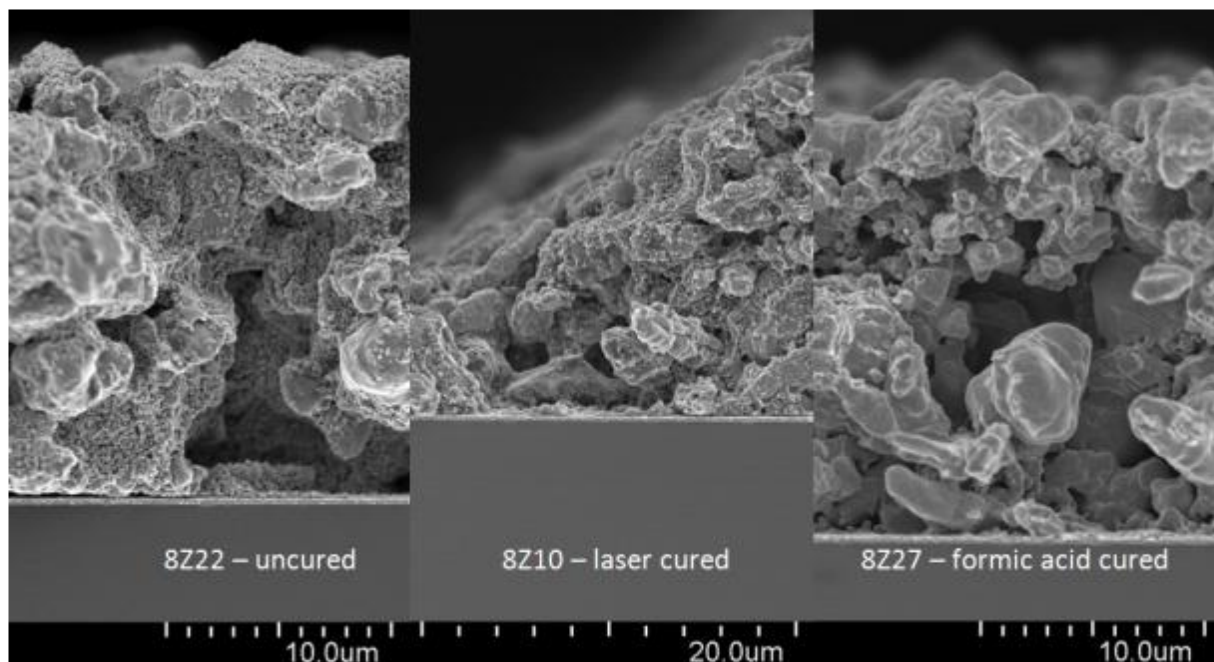

Picture 52: SEM comparison between uncured, laser cured and formic acid cured samples

The density of these agglomerates is decreased during an annealing step, completely reduced wafers do not carry any nanoparticle agglomerates. Hence, it can be seen from the morphology of a sample if the annealing step was complete.

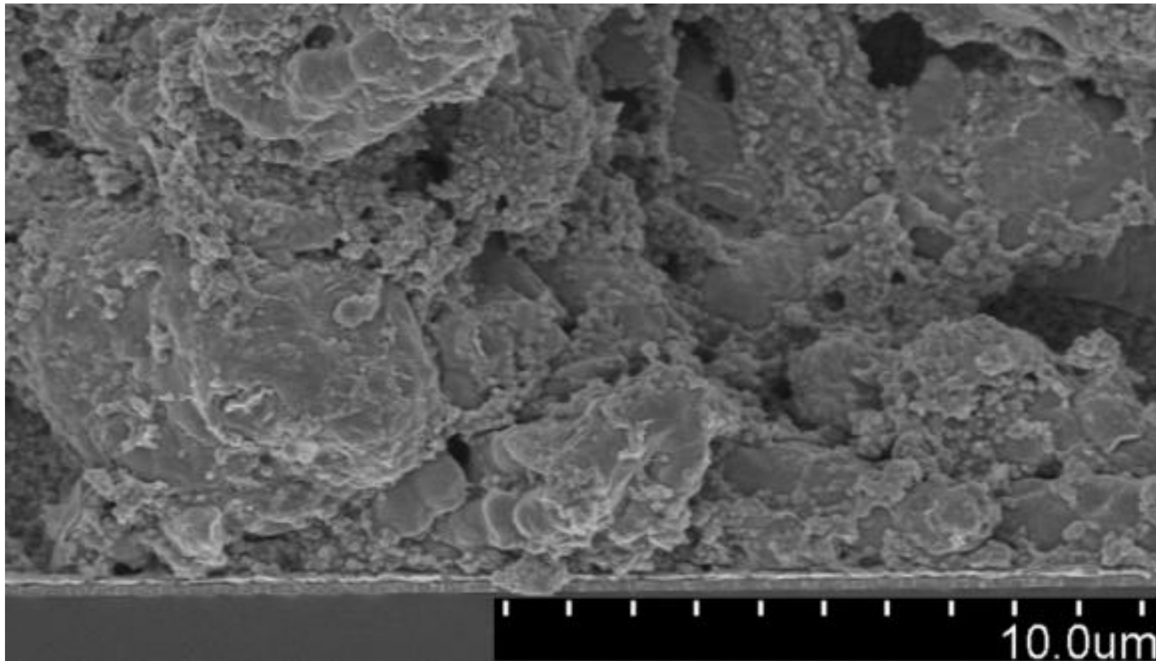

Picture 53: Sample 8Z23, cured for 2.5h at 400°C in forming gas

Determining the porosity

The estimation of the porosity with SEM is difficult, especially at the displayed pictures, because they were obtained through breaking the wafers. In order to see the amount and size of pores, the wafers would have to be cut with a focused ion beam (FIB) which would cut through the micro particles of the paste instead of breaking them.

A better and more low-tech method of determining the porosity is the gravimetric method: By printing a large area with a defined volume of our paste, the porosity can be determined by simply weighing the wafers before the print and after the curing.

We used 8" wafers that were printed with copper paste through a 50µm full-face stencil and weighed them as mentioned. After curing (and weighing), the thickness of our layers was determined by SEM. The printed area was of circular shape with a diameter of 19,6cm. This gives an area of $302cm^2$. Multiplied with the obtained thickness of 21µm we get a volume of $0.633cm^3$. We assume that the paste after the reduction step mainly consists out of copper, and all the other components (residue solvent, organic coating and residue copper oxide) are negligible. The density of solid copper is $8.96g/cm^3$. So, multiplied with the volume of our porous copper, we get a weight of 5.95g. The actual weight of our material is actually 2.8g, which is 49.3% of the weight it would have if it was bulk copper. Hence, our layer has a porosity of about **50%.** This value of course is not exact but more like an estimation, since the homogeneity of the layer on the wafer is not perfect and the 21µm is just a rounded average of the SEM measurements.

d. Elemental composition

The elemental composition of our samples was investigated with EDX (energy-dispersive X-ray spectroscopy). The EDX measurements were performed together with SEM images. The X-ray radiation is generated by accelerating the electron beam from the SEM the sample. The beam strikes out electrons from the inner shells of the metal, which are replaced by electrons from the outer shells. Since the outer shell electrons have higher energy levels than the inner shell ones, the excess of energy is released in form of X-rays upon relaxation.

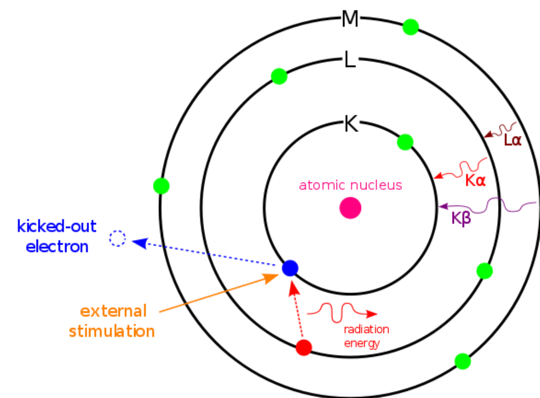

Picture 54: denotation of X-rays

This radiation has a typical wavelength depending on the shell where the relaxing electron came from. An electron that relaxed from the L down to the K shell is denoted Kα, from the M to the K shell Kβ. The X-ray spectrum also includes the so called bremsstrahlung, which is emitted by the accelerated electrons. The different components of the X-ray spectrum are displayed in Picture 55. The X-ray signals emitted by the sample are converted into electrical signals by the detector. The spectrum gained in this measurement consists of the contributions of all the elements in the sample.

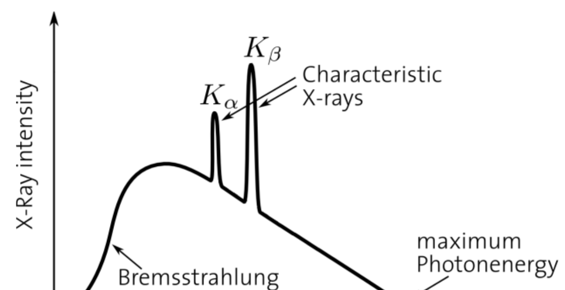

Picture 55: X-ray spectrum

We used EDX to investigate the formic acid reduction process by comparing a wafer reduced with and without formic acid in the nitrogen gas stream. The spectrum displayed in Picture 56 was obtained from a sample which was first laser cured by Intrinsiq Materials and then reduced in formic acid (15 minutes 400°C). The sample was prepared for the measurement by sputtering a thin gold film on it. Picture 57 shows the spectrum of a sample that was processed for 12 minutes at 400°C in nitrogen. The spectra show no significant difference in their shape: Both spectra include a carbon and an oxygen peak indicating the presence of organic residues. The formic acid cured sample was sputtered with gold before the measurement, explaining the peak at 2.2kV. The origin of the lead peak at 2.4kV in the nitrogen annealed spectrum is unclear.

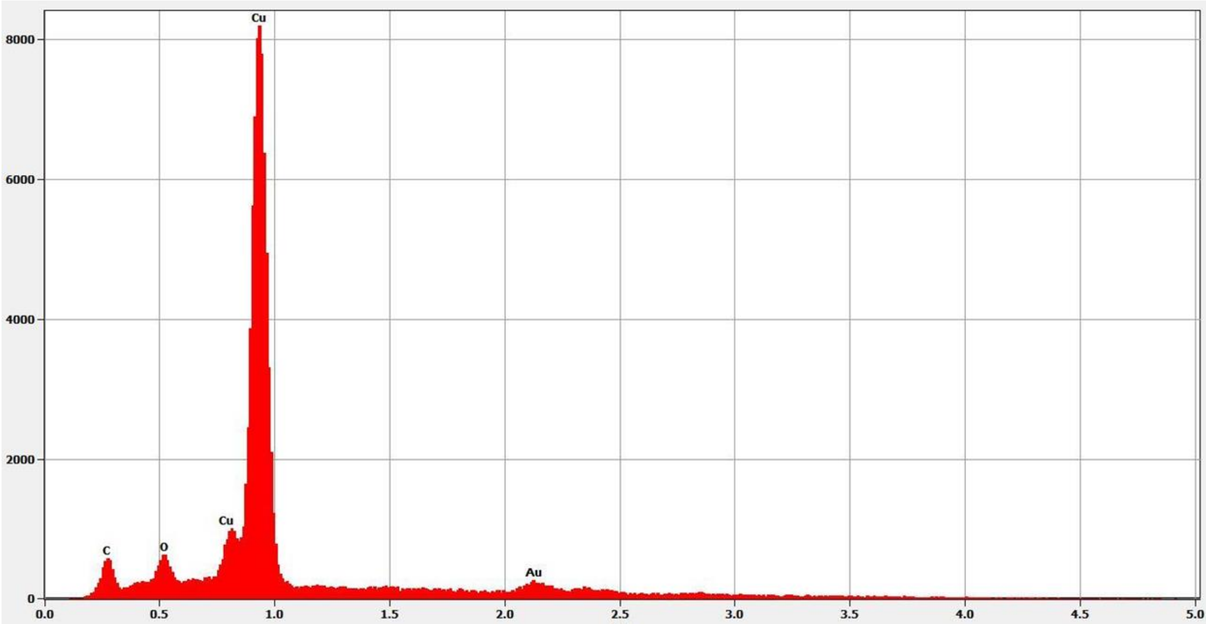

Picture 56: EDX spectrum of a lasercured + formic acid reduced sample

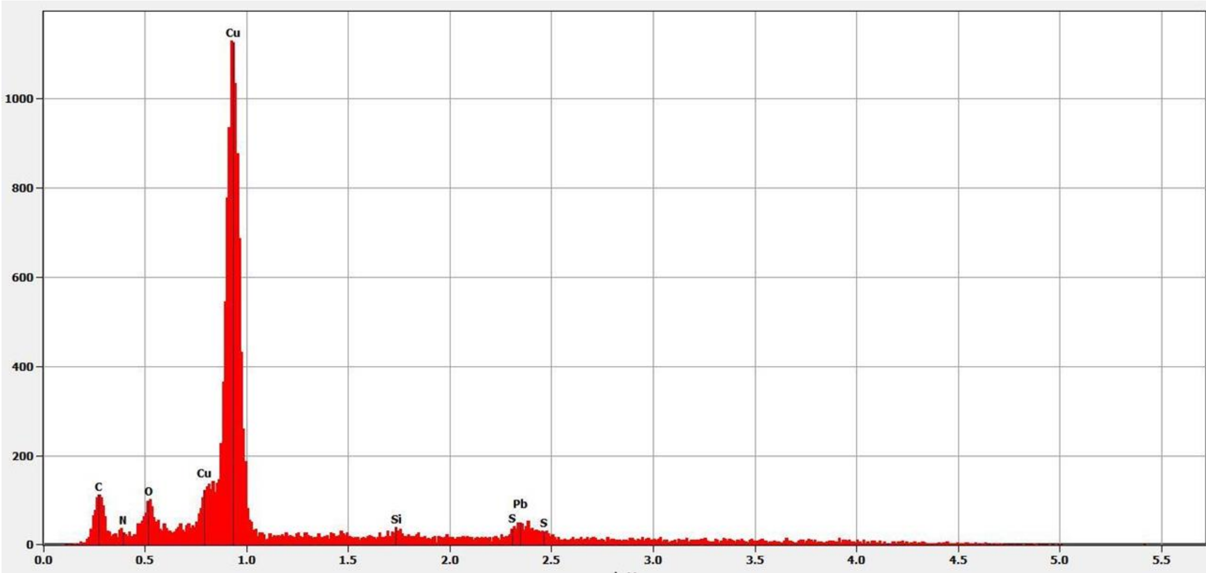

Picture 57: EDX Spectrum of a nitrogen annealed sample

e. Adhesion

The adhesion of the printed copper layers to the substrate (copper seed layer) had been in question due to the low mechanical stress of the copper. In order to disprove these concerns, a pull-test was performed.

The equipment used was a digital “DeFelsco PosiTest AT Adhesion Tester”. The machine uses a steel stamp, which is glued to the sample using a two-component epoxy glue (Araldite 2011) in a 1:1 mixture.

The sample chosen for this test was labeled 8Z50 and was a standard sample (CP-003, Stencil: T9999-050-1D-ST11, pre-dried, vacuum dried, reduced with formic acid for 30 minutes at 400°C). The wafer was broken and five pieces were selected for the test. This stamp has a circular shape and a diameter of 20mm. Hence, the printed copper structures selected for this test were broken and selected in a way that the stamp could be placed on them without any overlapping.

These pieces were glued onto the surface of a ceramic slab with the mentioned two-component glue. The glue was hardened by placing the slab for one hour on a heating plate, which was set to a temperature of 80°C. Then the steel stamps are attached to the copper layers in the same manor. The pull tester applies a vertical tensile force to the stamp, which is increased until the stamp is ripped off. The force needed to rip off the stamp is noted and the site of breakage is examined.

Results

As it can be seen in Picture 59 the breaking occurred in the epoxy-resign, in the central (third) sample in this picture also small parts of our printed copper layer delaminated from the copper seed layer. The tensile strain needed to rip off the stamps was between 12.0 and 14.7MPa, which is a sufficiently good first result.

Picture 60: stamps ready for the pull-test

Picture 59: samples after the pull-test

Picture 58: DeFelsco PosiTest AT Adhesion Tester

f. *Heat dissipation*

The heat dissipation capability is one of the most important properties to determine on printed copper. The corresponding test that our material still has to undergo is called **"polyheater test"**. In Picture 61 a schematic view of this polyheater test setup is displayed. The two large, grey pads on the right and the left side of the picture are copper pads which are contacted with bonded wires. All copper structures in this setup are placed upon a diffusion barrier. They are connected by a thin polysilicon layer displayed in light blue and wine red. The copper layer which is under investigation is the hatched blue area in the middle. The grey pads around it are copper contacts for the measurement equipment. The four pads denoted as TS or TF are used for a four point resistivity measurement between the copper and the polysilicon, from which the temperature can be calculated over the temperature coefficient of the resistance. [41] The pads denoted COP are used for the determination of the electrical resistivity of the investigated copper layer by use of the Van-der-Pauw method. [42] The pads M1 and M2 can be used for other measurements or left unconnected.

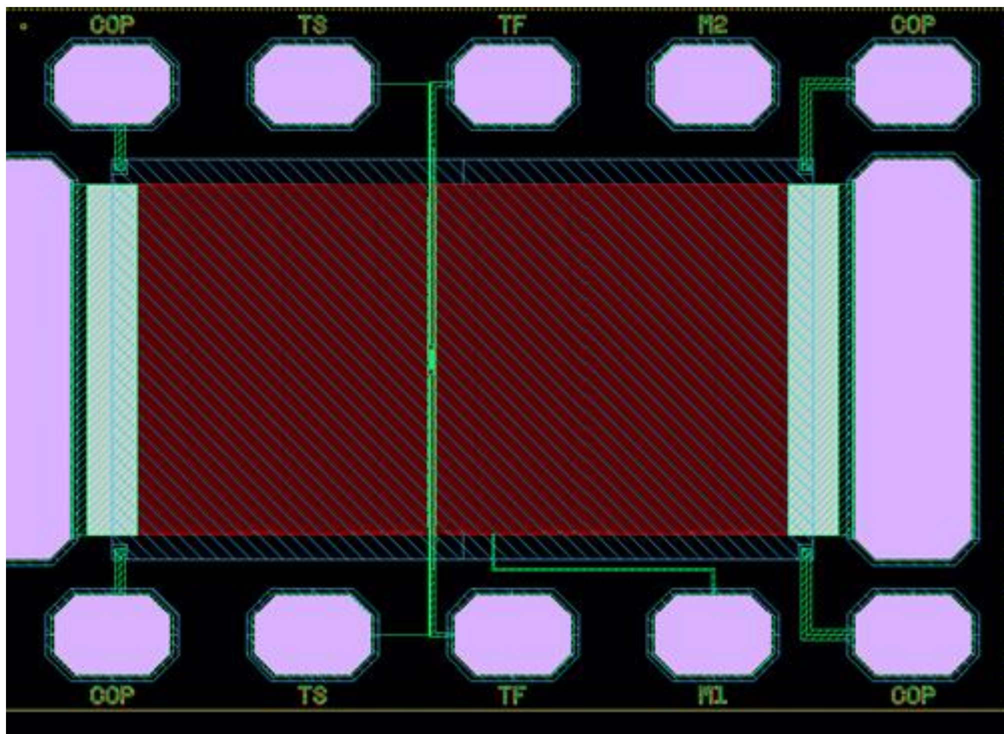

Picture 61: Schematic view of a polyheater device, taken from an internal presentation[10]

The polyheater test is used for fast in-situ heating on wafer level for time-critical reliability monitoring, as well as for more sophisticated research topics. [43] In our case, up to several hundred thousand current pulses of 250-500µs are applied to the contacts which heat up the test assembly. Temperatures of up to 400°C and more can be reached, depending on the material properties and

[10] The picture was taken from an internal report presented by Michael Nelhiebel in January 2013.

the current and voltage of the pulses, as well as their shape and duration. The thermal conductivity of the material can be calculated from the heating phase of the curve, while the cooling phase is largely influenced by the die attach below the polyheater assembly.

This test will be started in the next few months. All the work done in this thesis can be seen as contribution to the feasability of this test with our material.

6. Review and Outlook

The main results of this thesis are summarized in the following Table 7:

Printing process	- Design of a test stencil
	- Development of a stencil printing process for test structures
	- Focus on the paste CP-003
	- Dilution tests with CP-003+
Process flow	- Development of a drying process for crack free layers
	- Development of a reduction process on the basis of formic acid
	- Screening of different reducing agents including H_2 and CO
	- Investigation on the oxidation behavior of the paste
Material characterization	- Layer thickness
	- Conductivity
	- Porosity
	- SEM, EDX
	- Stress (performed by Manfred Schneegans)

Table 7: Achievements of this Work

The printing process was optimized up to the degree where samples for material characterization could be printed reproducibly. A complete DoE (design of experiment) will be necessary to optimize the print results of the standard paste in a first step and then expand this work on the different dilutions. In order to achieve a better aspect ratio photolithography might be necessary, either to print into or to etch through a photolithographic mask. The determination of the oxidation stability of printed copper was one first step in this direction.

The process flow is not yet clear, since the requirements of the corresponding chip technologies are not yet known. Maybe a lithographic step will be inevitable, maybe a wet chemical step will have to remove the particle coating. The reduction with carbon monoxide will be further examined, as well as the reduction with formic acid. More detailed resistivity vs. reduction time/temperature diagrams will have to be made in order to find optimal process conditions.

The possibilities of this new material system seem to be near to endless. It has been stated by the Soviet scientist Genrich S. Altschuller that great inventions are often made by transferring the methods of one branch onto another. [44] By using printing techniques in the semiconductor industry, this statement might prove to be true once again.

7. Acknowledgements

At this point I want to thank all my colleagues, without whom this work could not have been accomplished:

- My supervisor Martin Mischitz, who gave me the opportunity to work on this exiting topic and who supported me in every possible way.
- My fellow colleagues Martin Diestre-Olmos, Thomas Grille, Peter Irsigler, Nikodemus Loman, Walter Make and Thomas Wübben for the constructive discussions.
- Hermann Bidner, Erwin Fritz and Karl-Heinz Gasser for their help with the printing process.
- Gerhard Findenig, Sebastian Helm, Joachim Hirschler, Stefan Krivec, Kurt Pekoll, Herbert Preiml, and Josef Schellander for their support with various experiments in the fab (Koyo, Tepla, Mattson, EKT).
- All the operators at Infineon who helped me prepare and process samples regardless of their own full time schedules.
- The staff of the failure analysis team, who was snowed under with SEM requests and did a remarkable job.

Further I want to express my gratitude to Michael Gobec and the other members of the works council of Cytec Austria GmbH for their efforts to enforce the establishment of a labor foundation. This foundation financed my masters program gave me the opportunity to concentrate on my studies instead of being forced to work part-time, which saved me at least half a year of lifetime.

Also I want to thank the company Infineon Technologies Austria AG for the great working conditions and the supportive attitude of all its employees. It is remarkable that in all these months I never heard a “no” when I asked for support with my work.

In this context I also want to mention my parents, who supported me over the seven years of my studies with funding and motivation.

This work is dedicated to my wife Lisa and my daughters Vivien and Valerie.

8. Bibliography

[1] A. Wintrich, U. Nicolai, W. Tursky, T. Reimann, Application Manual Power Semiconductors, Ilmenau: SEMIKRON International GmbH, 2011.

[2] B. Baliga, "An Overview over Smart Power Technogy," *IEEE Transactions on Electron Devices,* vol. 37, no. 7, pp. 1568-1575, 1991.

[3] V. Authors, "Wikipedia," Wikimedia Foundation Inc., [Online]. Available: http://en.wikipedia.org/wiki/Bipolar_junction_transistor. [Accessed 03 09 2013].

[4] B. Baliga, "Trends in Power Semiconductor Devices," *IEEE Transactions on Electron Devices,* vol. 43, no. 10, pp. 1717-1731, 1996.

[5] R. Weber, "High power semiconductor device with integral heat sink". United States of America Patent 5,057,908, 15 10 1991.

[6] S. Leslie, "Electronics Cooling," 01 11 2006. [Online]. Available: http://www.electronics-cooling.com/2006/11/cooling-options-and-challenges-of-high-power-semiconductor-modules/. [Accessed 03 09 2013].

[7] M. Singh, H. M. Haverinen, . Dhagat, G. E. Jabbour, "Inkjet Printing—Process and Its Applications," *Adv. Mater.,* vol. 22, no. 6, p. 673–685, 2010.

[8] A. Kamyshny, J. Steinke, S. Magdassi, "Metal-based Inkjet Inks for Printed Electronics," *The Open Applied Physics Journal,* vol. 4, pp. 19-36, 2011.

[9] K.F. Teng, R.W. Vest, "Metallization of solar cells with ink jet printing and silver metallo-organic inks," *IEEE Trans Compon Hybrids Manuf Technol,* vol. 11, no. 3, pp. 291 - 297, 1988.

[10] S. Molesa, Shong Yin, R. Farschi, R. ; V. Subramanian, D. Redinger, "An Ink-Jet-Deposited Passive Component Process for RFID," *IEEE Trans on Electron Devices,* vol. 51, no. 12, pp. 1978-1983, 2004.

[11] Sunho Jeong, Kyoohee Woo, Dongjo Kim, Soonkwon Lim, Jang Sub Kim, Hyunjung Shin, Younan Xia, Jooho Moon, "Controlling the Thickness of the Surface Oxide Layer on Cu Nanoparticles for the Fabrication of Conductive," *Adv. Funct. Mater.,* no. 18, p. 679–686, 2008.

[12] M. B. Edwards, *PhD Thesis: Screen and Stencil Print Technologies for Industrial N-Type Silicon Solar Cells,* Sydney: Centre for Photovoltaic Engineering, The University of New South Wales Sydney, 2008.

[13] F. H. K. Lau, V. W. S. Yeung, "A hierarchical evaluation of the solder paste printing process," *Journal of Materials Processing Technology,* vol. 69, no. 1-3, pp. 79-89, 1997.

[14] G. Schubert, *PhD Thesis: Thick Film Metallisation of Crystalline Silicon Solar Cells – Mechanisms,*

Models and Applications, Konstanz: University of Konstanz, 2006.

[15] I. Clark, *Intrinsiq CP-002 Datasheet,* Hampshire, UK: Intrinsiq Materials Ltd., 2012.

[16] Intrinsiq, *CPD-02 Copper Paste Diluent MSDS v1.2,* Hampshire, UK: Intrinsiq Materials Ltd., 2013.

[17] P. Xu, J. Huang and S. Rathi, "Plasma treatment for copper oxide reduction". US Patent 6,734,102 B2.

[18] "Copper Interconnects: The evolution of microprocessors," [Online]. Available: http://www-03.ibm.com/ibm/history/ibm100/us/en/icons/copperchip/. [Accessed 7 April 2013].

[19] A. E. Rakshani, "Preparation, characteristics and photovoltaic properties of cuprous oxide – a review," *Solid-State Electronics Vol. 29, No 1,* pp. 7-17, 1986.

[20] A. Ogwu, "Electrical resistivity of copper oxide thin films prepared by reactive magnetron sputtering," *Journal of Achievements in Materials and Manufacturing Engineering Vol. 24, Issue 1,* pp. 172-177, 2007.

[21] Seiichi Sumikura, Shogo Mori, Sinya Shimizu, Hisanao Usami, Eiji Suzuki, "Photoelectrochemical characteristics of cells with dyed and undyed nanoporous p-type semiconductor CuO electrodes," *Journal of Photochemistry and Photobiology A: Chemistry,* p. 143–147, 2008.

[22] D.E. Diaz-Droguetta, R. Espinozab, V.M. Fuenzalidaa, "Copper nanoparticles grown under hydrogen: Study of the surface oxide," *Applied Surface Science 257,* p. 4597–4602, 2011.

[23] M. Hari Prasad Reddy, J. F. Pierson, S. Uthanna, "Structural, surface morphological, and optical properties of nanocrystalline Cu2O and CuO films formed by RF magnetron sputtering: Oxygen partial pressure effect," *Phys. Status Solidi A,* vol. 209, no. 7, p. 1279–1286, 2012.

[24] S.Y. Lee, N. Mettlach, N. Nguyen, Y.M. Sun, J.M. White, "Copper oxide reduction through vacuum annealing," *Applied Surface Science,* vol. 206, no. 1-4, pp. 102-109, 2003.

[25] Jae Y. Kim, José A. Rodriguez, Jonathan C. Hanson, Anatoly I. Frenkel, Peter L. Lee, "Reduction of CuO and Cu2O with H2: H Embedding and Kinetic Effects in the Formation of Suboxides," *J. Am. Chem. Soc.,* vol. 125, no. 35, pp. 10684-10692, 2003.

[26] M.R. Baklanov, D. G. Shamiryan, Z. Tokei, G.P. Beyer, T. Conard, S. Vanhaelemeersch, K. Maex, "Characterisation of Cu surface cleaning by hydrogen plasma," *J. Vac. Sci. Technol. B,* vol. 19, no. 4, pp. 1201 - 1211 , 2001.

[27] I. Kim, J. Joung and Y. Song, "Reducing agent for low temperature reducing and sintering of copper nanoparticles". US Patent 8,206,609, 26 June 2012.

[28] R. N. Pease, H. S. Taylor, "The reduction of copper oxide by hydrogen," *J. Am. Chem. Soc.,* vol. 43, no. 10, p. 2179–2188, 1921.

[29] W.D. Bond, W.E. Clark, Reduction of Cupric Oxide by Hydrogen: I. Fundamental Kinetics, Oak Ridge, Tennessee: Oak Ridge National Laboratory, 1960.

[30] Sigma-Aldrich, "MSDS of Formic acid," Sigma-Aldrich, [Online]. Available: http://www.sigmaaldrich.com/MSDS/MSDS/DisplayMSDSPage.do?country=DE&language=EN-generic&productNumber=F0507&brand=SIAL&PageToGoToURL=http%3A%2F%2Fwww.sigmaaldrich.com%2Fcatalog%2Fproduct%2Fsial%2FF0507%3Flang%3Dde. [Accessed 7 May 2013].

[31] L.H. Dubois, T.H. Ellis, B.R. Zegarski, S.D. Kevan, "New insights into the kinetics of formic acid decomposition on copper surfaces," *Surface Science,* vol. 172, no. 2, pp. 385-397, 1986.

[32] M. Schmeißer, *Decomposition of formic acid,* Chemnitz: Chemnitz University of Technology, 2011.

[33] M. Schmeißer, *Bachelor Thesis: Reduction of Copper Oxide by Formic Acid - an ab-initio study,* Chemnitz: Chemnitz University of Technology, 2012.

[34] M.R. Columbia, P.A. Thiel, "The interaction of formic acid with transition metal surfaces, studied in ultrahigh vacuum," *Journal of Electroanalytical Chemistry,* vol. 369, no. 1-2, p. 1–14, 1994.

[35] A.K. Galway, D.M. Jamieson, M.E. Brown, "Thermal Decomposition of Three Modifications of Anhydrous Copper(II) Formate," *Journal of Physical Chemistry,* vol. 78, no. 26, pp. 2264-2270, 1974.

[36] C. R. Alder Wright, A. P. Luff, E. H. Rennie, "LII.—Third Report to the Chemical Society on “researches on some points in chemical dynamics.”," *J. Chem. Soc., Trans.,* no. 35, pp. 475-524, 1879.

[37] I.W. Fay, A.F. Seeker, "Reducability of some metal oxides by hydrogen and carbon monoxide," *Journal of the American Chemical Society,* vol. 25, no. 6, pp. 641-647, 1903.

[38] H. A. Jones , H. S. Taylor, "The Reduction of Copper Oxide by Carbon Monoxide and the Catalytic Oxidation of Carbon Monoxide in the Presence of Copper and Copper Oxide," *J. Phys. Chem.,* vol. 27, no. 7, p. 623–651, 1923.

[39] A. Walton, *Microelectronic Test Structures,* Edinburgh Microfabrication Facility Department of Electrical Engineering Kings Buildings University of Edinburgh Edinburgh, EH9 3JL, UK, 2008.

[40] P. Kerschenbauer, *Masters Thesis: Widerstandsbestimmung von metallischen Proben mit der Vier-Punkt-Methode,* Graz: Graz University of Technology, 2008.

[41] W. Muth, W. Walter, "Bias temperature instability assessment of n- and p-channel MOS transistors using a polysilicon resistive heated scribe lane test structure," *Microelectronics Reliability,* vol. 44, no. 8, p. 1251–1262, 2004.

[42] L. v. d. Pauw, "A method of measuring specific resistivity and Hall effect of discs of arbitrary shape," *Philips Research Reports,* vol. 13, no. 1, pp. 1-9, 1958.

[43] T. Aichinger, M. Nelhiebel, S. Einspieler, T. Grasser, "In-Situ Polyheater – A reliable tool for performing fast and defined temperature switches on chip," *Device and Materials Reliability,* vol. 10, no. 1, pp. 3-8, 2010.

[44] G. Altschuller, *Erfinden - Wege zur Lösung technischer Probleme,* Berlin: PI - Planung und Innovation, 1986.

[45] A. Sophie, H. Sprey, P. Soininien and K. Elers, "In situ reduction of copper oxide prior to silicon carbide deposition". US Patent 6,878,628, 12 April 2005.

[46] D. McMonagle, Chemistry: An Illustrated Guide to Science, New York: The Diagram Group, 2006.

[47] C. H. M. B. R. Fogal, "Method and apparatus for wire bonding semiconductor dice to a leadframe". USA Patent 5,322,207, 03 05 1993.

[48] M. I. T. Kikuchi, "Use of a gold alloy wire for wedge bonding". European Union Patent EP 0822264 B1, 28 11 2001.

9. Appendix:

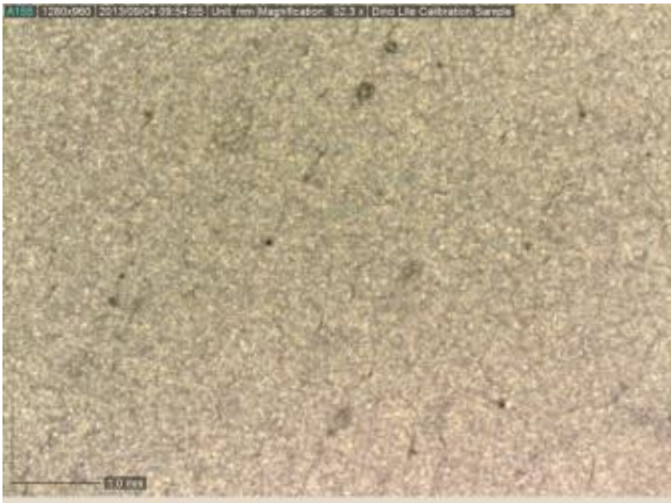

Picture 63: 8Z169 pre-dried (CP-003+ +1% CPD02) 235x

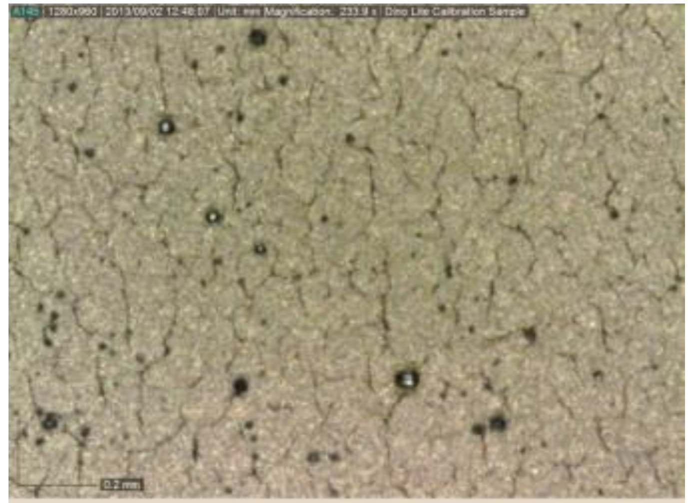

Picture 62: 8Z169 cured (CP-003+ +1% CPD02) 235x

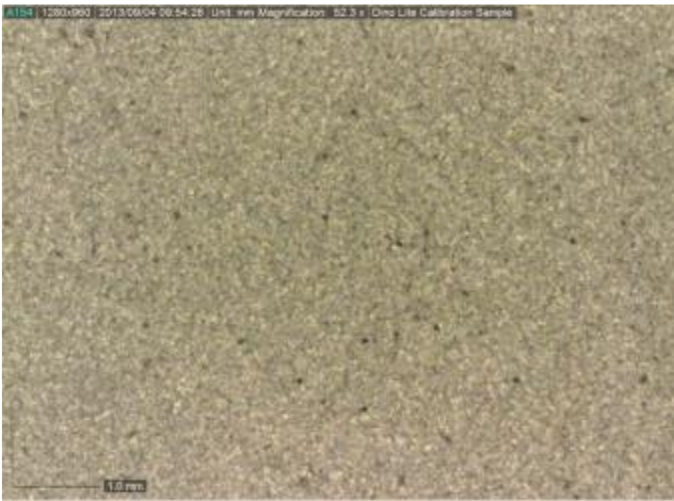

Picture 64: 8Z167 pre-dried (CP-003+ +2.5% CPD02) 235x

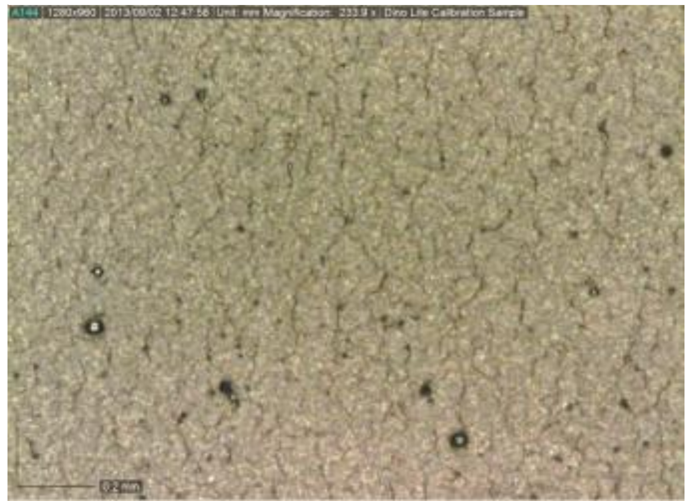

Picture 65: 8Z167 cured (CP-003+ +2.5% CPD02) 235x

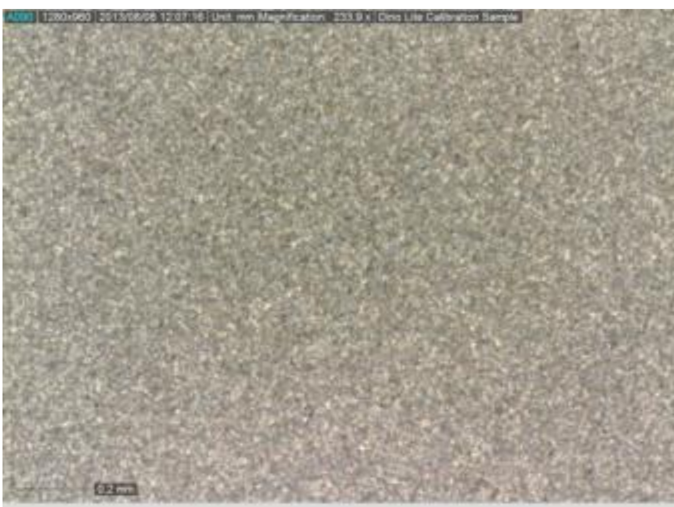

Picture 66: 8Z117 pre-dried (CP-003+ +5% CPD02) 235x

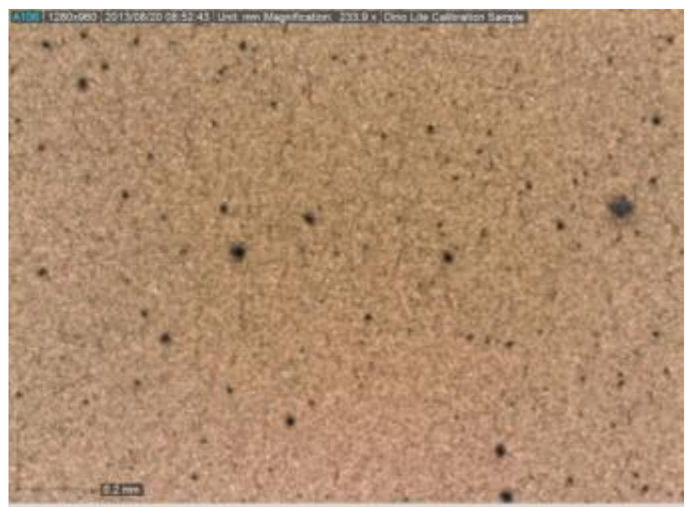

Picture 67: 8Z117 cured (CP-003+ +5% CPD02) 235x

Picture 68: 8Z113 pre-dried (CP-003+ +7.5% CPD02) 235x

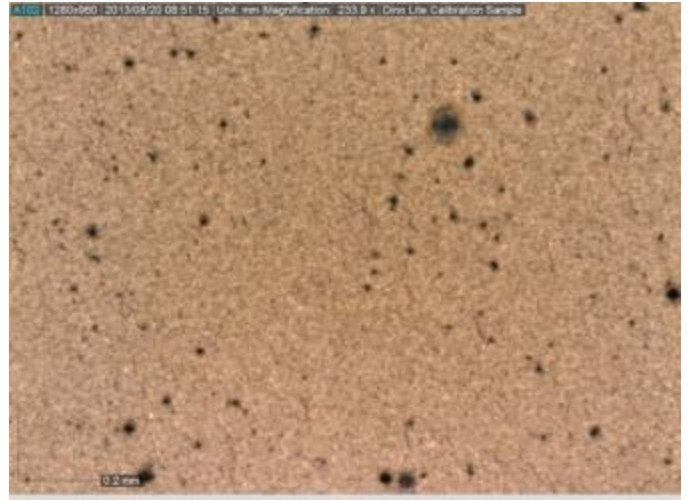

Picture 69: 8Z113 cured (CP-003+ +7.5% CPD02) 235x

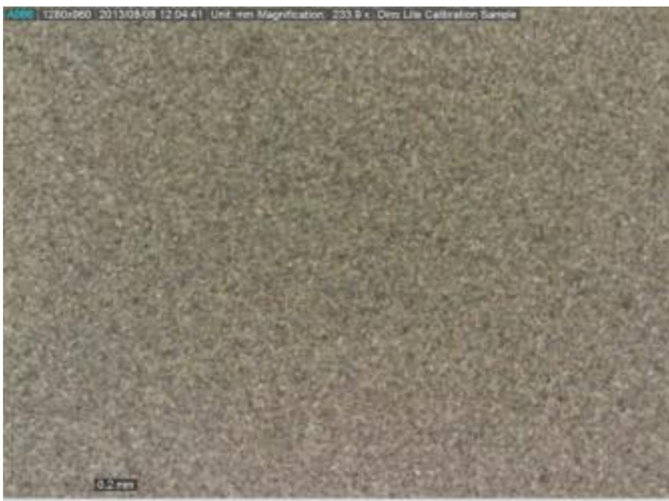

Picture 71: 8Z115 pre-dried (CP-003+ +10% CPD02) 235x

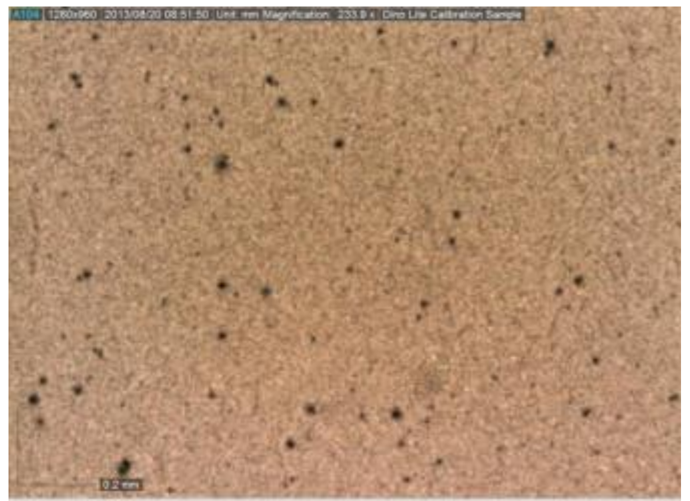

Picture 70: 8Z115 cured (CP-003+ +10% CPD02) 235x

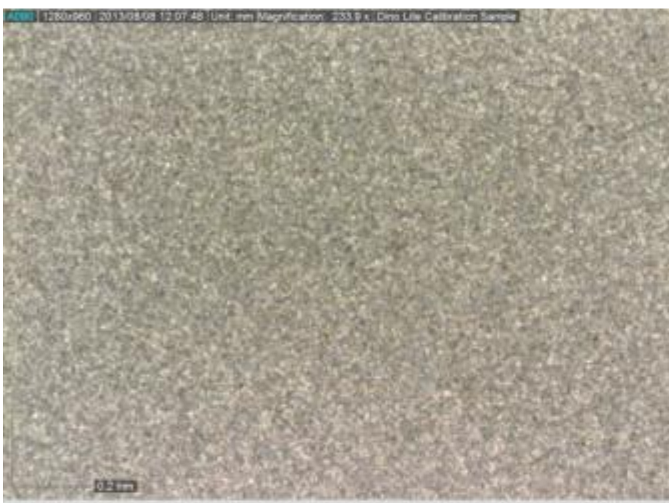

Picture 72: 8Z119 pre-dried (CP-003+ +20% CPD02) 235x

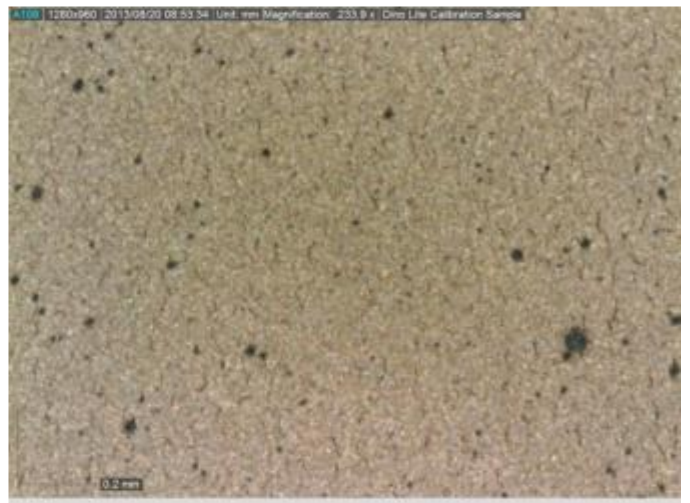

Picture 73: 8Z119 cured (CP-003+ +20% CPD02) 235x

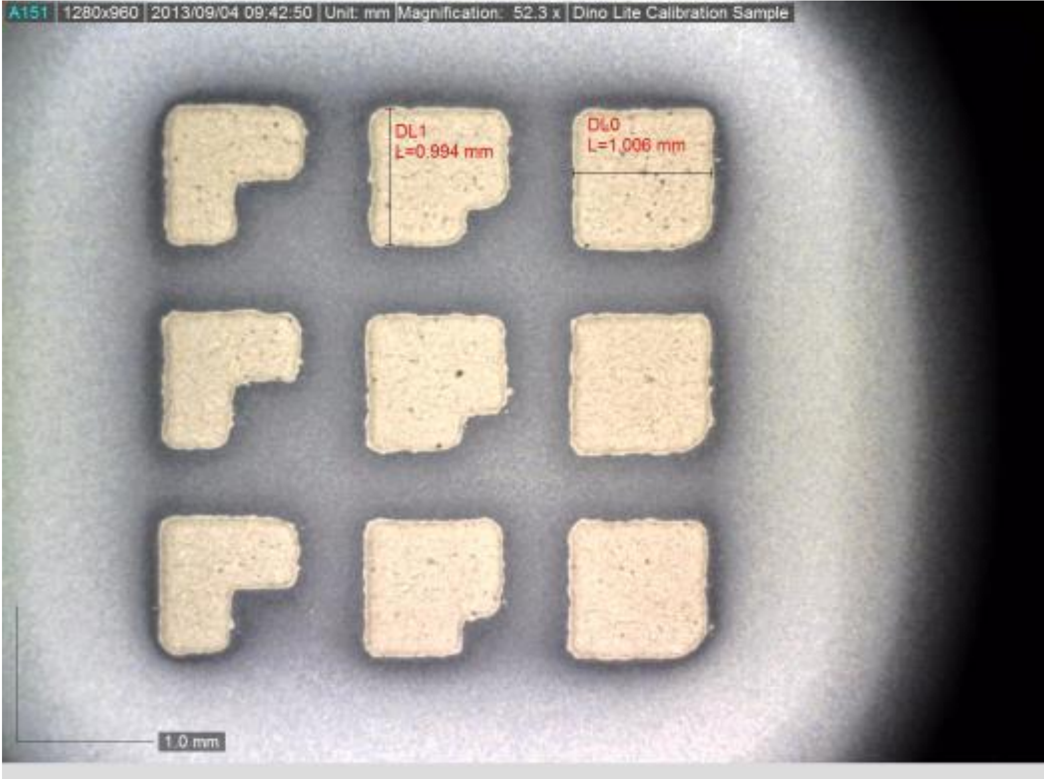

Picture 74: 8Z167 (CP-003+ +2.5% CPD02) 50x

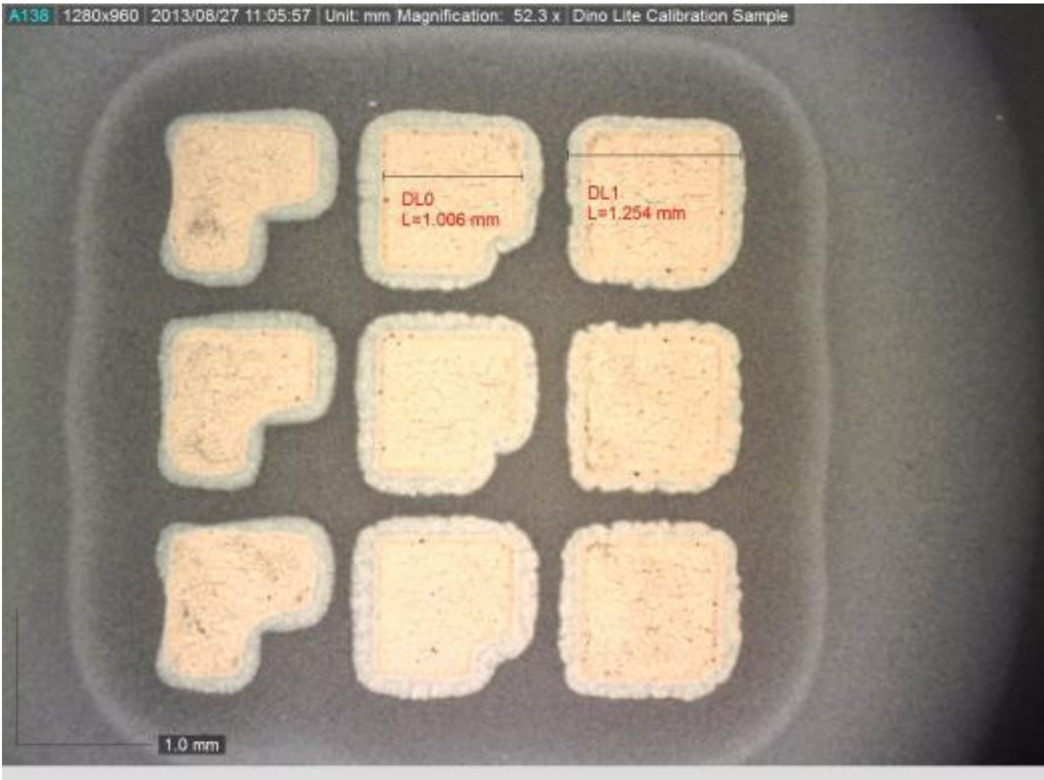

Picture 75: 8Z116 (CP-003+ +5% CPD02) 50x

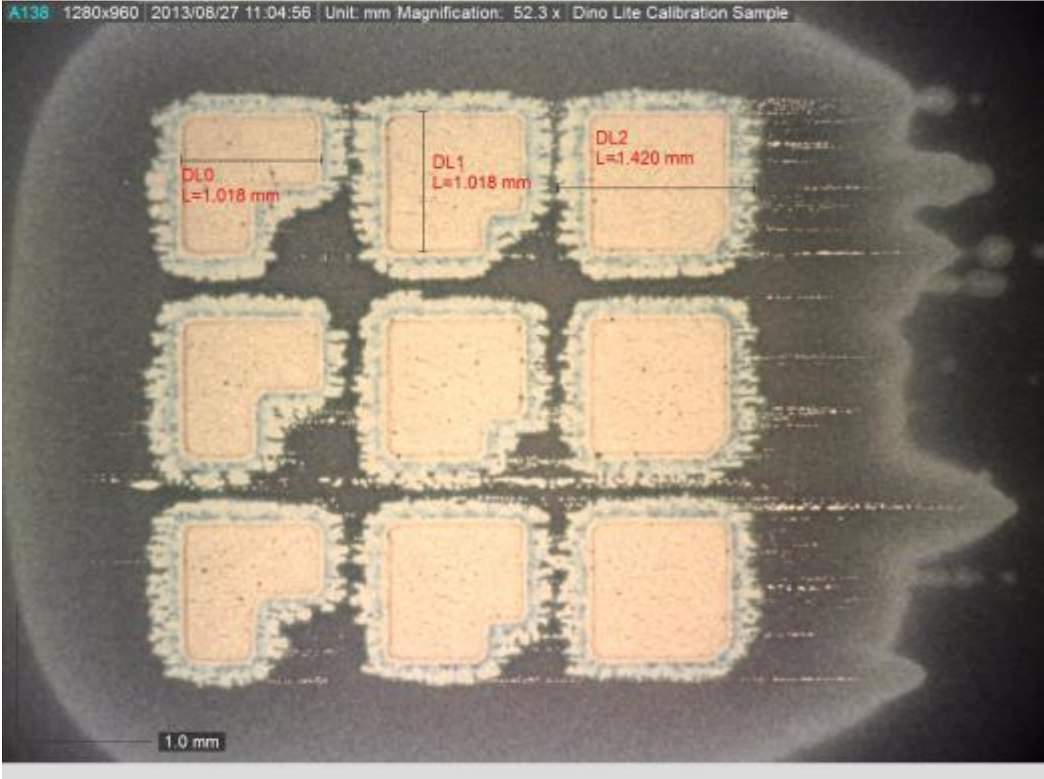

Picture 76: 8Z112 (CP-003+ +7.5% CPD02) 50x

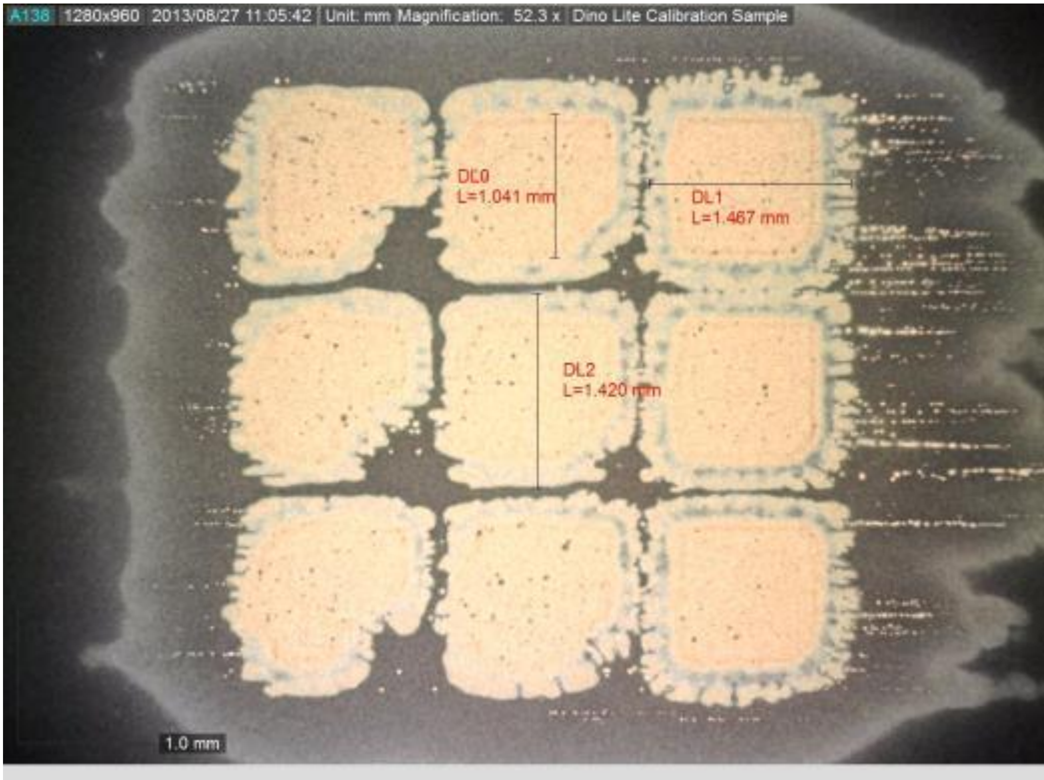

Picture 77: 8Z114 (CP-003+ +10% CPD02) 50x

Intrinsiq CP-002

Nanocopper based Pastes for the Electronics Industry

Product Description

This product is a nanocopper based paste for screen printing that is compatible with low temperature substrates such as paper, PET, polyimide, ceramic and FR4.

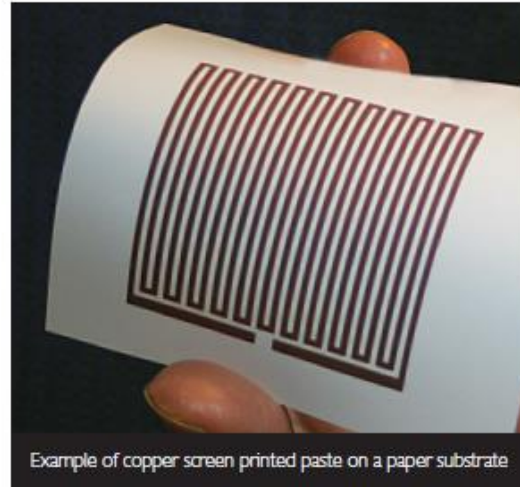

Example of copper screen printed paste on a paper substrate

Product Benefits

- A nanocopper based paste produced using nanoparticles of negligible oxide content resulting in a highly conductive film after sintering.
- The nanocopper component enables room temperature sintering in air.
- Capable of fine line, high resolution printing.

Processing

Property	Specification
Screen Printing Equipment	Reel to reel, semi-automatic, manual
Ink Screen Life	>5 hours - depending on printing process
Screen Types	Polyester and stainless steel
Line Thickness	Typically 20 µm printed thickness using a 325 mesh
Line Widths	Min. 75 µm
Typical Drying Conditions	60°C for 15-30 mins
Typical Sintering Conditions	Xenon flash lamp system, IR laser
Clean Up Solvent	Ethoxy Propanol or Sericol
Substrate	Paper, PET, polyimide, ceramic and FR4
Storage	The product should be kept sealed, in its container, and stored at room temperature (20°C)
Shelf-Life	In a sealed container, stored correctly, the shelf life is minimum 3 months from despatch
Diluent/ Thinner	CP-002-DT

www.intrinsiqmaterials.com

Intrinsiq CP-002

Nanocopper based Pastes for the Electronics Industry

Typical Physical Properties

Property	Value
Solids Content (130°C)[%]	82-90
Viscosity (Bohlin CVO 100 at 50 s^{-1} at 25°C)[Pa.S]	10-30
Coverage [cm^2/g]	110-130

Typical Physical Properties printed on substrates

Property	Value
Sheet resistivity* [mΩ/sq/mil]	8.4
Cured Thickness [µm]	10-30

*Sheet Resistivity measured at 10 µm line thickness

General

Prior to use, please ensure that the paste is mixed thoroughly for a few minutes taking care to avoid introducing air into the paste. If the paste is being stored for longer periods of time it is recommended that periodically, typically once per month, the paste is stirred.

Applications

We can formulate pastes to print on all the commonly used substrate materials found in the electronics industry.

The CP-002 paste formulation is typically used in the following markets:

- Smart Packaging
- Security
- RFID
- Promotional Items
- Photovoltaic Cell Electrodes
- LED systems
- Automotive

Safety and Handling

Please read the Material Safety Data Sheet (MSDS) prior to using this product. These pastes are intended for industrial use by trained personnel. Keep the product container closed when not in use to prevent solvent evaporation and spilling hazard.

Intrinsiq Materials Ltd
Building Y25, Cody Technology Park
Ively Road, Farnborough Ste 2
Hampshire, GU14 0LX
United Kingdom
Sales Tel: +44 (0) 1252 399 792
+44 (0) 7776 457 255
Fax: +44 (0) 1252 397 184
E-mail: ianclark@intrinsiqmaterials.com

www.intrinsiqmaterials.com

The datasheet of the CP-003 is not available, but the paste differs only little from the CP-002.

The CP-004 is no commercial product and hence no datasheet is available.

Deutsche Fassung:
Beschluss der Curricula-Kommission für Bachelor-, Master- und Diplomstudien vom 10.11.2008
Genehmigung des Senates am 1.12.2008

EIDESSTATTLICHE ERKLÄRUNG

Ich erkläre an Eides statt, dass ich die vorliegende Arbeit selbstständig verfasst, andere als die angegebenen Quellen/Hilfsmittel nicht benutzt, und die den benutzten Quellen wörtlich und inhaltlich entnommenen Stellen als solche kenntlich gemacht habe.

Graz, am …………………………… ………………………………………………..
(Unterschrift)

Englische Fassung:

STATUTORY DECLARATION

I declare that I have authored this thesis independently, that I have not used other than the declared sources / resources, and that I have explicitly marked all material which has been quoted either literally or by content from the used sources.

…………………………… ………………………………………………..
date (signature)